

**Bachelor Thesis**  
To obtain the academic title  
Bachelor of Science

**Bachelorarbeit**  
Zur Erlangung des akademischen Grades  
Bachelor of Science

---

**Hazard Assessment for Agricultural Droughts  
In the Spree River Catchment (Brandenburg)  
Based on Open Geodata**

Submitted by / Eingereicht von: Thomas Hoffmann

Supervisors / Gutachter\*Innen: Prof. Dr. Tobia Lakes  
Dr. Fabio Brill

Submitted to the Geography Department of Humboldt University Berlin  
on October 12th, 2022

Eingereicht am Geographischen Institut der Humboldt-Universität zu Berlin  
am 12. Oktober 2022

## Abstract

**Background:** Soil moisture falling below the requirements of vegetation due to a lack of precipitation causes agricultural droughts, resulting in decreased photosynthetic activity and plant productivity, or, in extreme cases, crop failure. Plant characteristics, phenology and soil properties influence agricultural drought intensity. The Spree river catchment in southeastern Brandenburg, Germany, which posits a study area of the CliWaC (Climate and Water under Change) Einstein Research Unit, is a predominantly agricultural area, despite its dry climate and generally poor soils. Indices derived from remote sensing data offer an effective way of drought monitoring over vast areas. The ratio of land surface temperature and the Normalised Difference Vegetation Index is an established way of assessing agricultural droughts, increasing both with high temperatures and low photosynthetic activity. Using exploratory data analysis, potential relations between the LST/NDVI ratio and site-related factors were examined, aiming to provide insight into drought hazards in the study area.

**Data & Methods:** Mid-growing season Landsat-8 LST and NDVI data was extracted to Integrated Administration and Control System agricultural plots for the drought years of 2018 and 2019, as well as the non-drought years of 2016 and 2017 for comparative purposes. Remote sensing data was compiled via Google Earth Engine. Brandenburg state authorities provide IACS plots, including information regarding crop type and/or agricultural practice, as well as soil type and field value (German “*Ackerzahl*”). Seven further sets of hydrological and pedological data were taken from the “soil atlas” (bodenatlas.de) published by the Federal Institute for Geosciences and Natural Resources. Linear regression was performed on the relation between the LST/NDVI ratio and continuous variables, with multivariate regression performed using variables found to exert significant influence on the drought indicator. For categorical variables, absolute and relative shares on all plots and the subset of plots with LST/NDVI ratio values within the upper quartile thereof were compared in each year of interest. Categories exhibiting particularly low and high median LST/NDVI ratios were further investigated. Only data from openly accessible sources and free software was used to enable reproducibility.

**Results & Discussion:** Low field values, high soil water exchange frequencies and percolation rates were found to significantly correlate with high LST/NDVI ratios, potentially posing drought hazards. Specific crop and agricultural land use types, soil types and rooting capacity classes were found to be more common on agricultural plots most affected by drought-like conditions, enabling stratification of drought hazards. Particularly deep, sandy substrate was found to likely posit a drought hazard. The intended scope of this work proved overambitious for a variety of reasons, leading to no results regarding spatial patterns and identifiable processes, albeit highlighting potential for further research. Revisiting this topic after thorough investigation of interdependencies of environmental variables and potential clusters thereof might provide further valuable insight into the topic.

# Table of Contents

Abstract .....	1
Table of Contents .....	2
List of Figures .....	4
List of Tables .....	8
List of Abbreviations .....	12
<b>1. Introduction</b> .....	<b>13</b>
1.1. Motivation & Problem Statement .....	13
1.2. Theoretical Background: Droughts and Remote Sensing Drought Monitoring. ....	13
1.3. Objective .....	15
<b>2. Data &amp; Methods</b> .....	<b>16</b>
2.1. Study Area .....	16
2.2. Data .....	19
2.3. Data Preparation .....	20
2.4. Data Analysis .....	22
2.4.1. Time Series Analysis .....	22
2.4.2. Continuous Data .....	22
2.4.3. Categorical Data .....	23
<b>3. Results &amp; Discussion</b> .....	<b>24</b>
3.1. Time Series Analysis .....	24
3.2. Continuous Data .....	29
3.2.1. LST/NDVI ratio .....	29
3.2.2. Soil Water Exchange Frequency .....	33
3.2.3. Percolation Rate .....	36
3.2.4. Field Value .....	39
3.2.5. Soil Quality Rating .....	42
3.2.6. Field Capacity .....	45
3.2.7. Erosion Potential (Water) .....	48
3.2.8. Multivariate Linear Regression .....	50
3.2.9. UFZ Drought Monitor Data .....	53
3.3. Categorical Data .....	61
3.3.1. Crop and Agricultural Land Use Type .....	61
3.3.2. Soil Type .....	66
3.3.3. Rooting Capacity .....	70
3.3.4. Erosion Potential (Wind) .....	72
3.4. Discussion .....	74
<b>4. Opportunities &amp; Limitations</b> .....	<b>75</b>
<b>5. Conclusions</b> .....	<b>77</b>

Sources .....	78
Software .....	83
Declaration of Authenticity .....	84
Appendix .....	85
Plots .....	85
Code .....	109



## List of Figures

- Figure 1: Map of river catchments (outlined in blue) intersecting with the German federal state of Brandenburg (outlined in black), with catchments subsidiary to the Spree river highlighted (solid blue), parts of the Spree river catchment falling within Brandenburg's borders constitute the study area (hatched)  
 Own diagram: program: QGIS, date: 13.07.2022, CRS: EPSG:25833  
 Sources: Oberirdische Einzugsgebiete des Landes Brandenburg: Landesamt für Umwelt Brandenburg (LfU). URL: <https://geoportal.brandenburg.de/detailansichtdienst/render?url=https://geoportal.brandenburg.de/gs-json/xml?fileid=20636164-EFA9-40D9-BDDF-325E7BBD0F99>  
 [last access on: 06.10.2022]  
 Grenze des Bundeslandes Brandenburg: GeoBasis-DE/LGB. URL: <https://geobroker.geobasis-bb.de/gbss.php?MODE=GetProductPreview&PRODUCTID=ed6ab7a1-7a64-4ceb-8d37-2e156b7f4546> [last access on: 06.10.2022]  
 ..... 16
- Figure 2: 2020 CORINE land cover classification of the study area, superimposed with administrative divisions of Brandenburg  
 Own diagram: program: QGIS, date: 06.10.2022, CRS: EPSG:25833  
 Sources: CORINE Land Cover classification: European Union, Copernicus Land Monitoring Service 2020, European Environment Agency (EEA).  
 URL: <https://land.copernicus.eu/pan-european/corine-land-cover/clc-2000>  
 [last access on: 06.10.2022]  
 Kreisgrenzen des Bundeslandes Brandenburg: GeoBasis-DE/LGB, dl-de/by-2-0. URL: <https://geobroker.geobasis-bb.de/gbss.php?MODE=GetProductPreview&PRODUCTID=ed6ab7a1-7a64-4ceb-8d37-2e156b7f4546> [last access on: 06.10.2022]  
 ..... 17
- Figure 3: Distribution of ALKIS agricultural plots (blue) throughout the study area, superimposed with administrative divisions of Brandenburg  
 Own diagram: program: QGIS, date: 06.10.2022, CRS: EPSG:25833  
 Sources: Amtliches Liegenschaftskatasterinformationssystem (ALKIS-Daten): GeoBasis-DE/LGB, dl-de/by-2-0.  
 URL: <https://data.geobasis-bb.de/geobasis/daten/alkis/Vektordaten/shape/>  
 [last access on: 06.10.2022]  
 Kreisgrenzen des Bundeslandes Brandenburg: GeoBasis-DE/LGB, dl-de/by-2-0. URL: <https://geobroker.geobasis-bb.de/gbss.php?MODE=GetProductPreview&PRODUCTID=ed6ab7a1-7a64-4ceb-8d37-2e156b7f4546> [last access on: 06.10.2022]  
 ..... 18
- Figure 4: Mean LST (left) and greenest pixel NDVI composite (middle) across the study area, and the LST/NDVI ratio calculated on agricultural plot level (right), superimposed with administrative divisions of Brandenburg, 2019 data  
 Own diagram: program: QGIS, date: 06.10.2022, CRS: EPSG:25833  
 Sources: Land Surface Temperature: Landsat-8 imagery, courtesy of U.S. Geological Survey, aggregated via Google Earth Engine. URL: <https://earthengine.google.com>  
 [last access on: 06.10.2022]  
 Normalised Difference Vegetation Index: Landsat-8 imagery, courtesy of U.S. Geological Survey, aggregated via Google Earth Engine. URL: <https://earthengine.google.com>  
 [last access on: 06.10.2022]  
 InVeKoS agricultural plots: MLUK, dl-de/by-2-0, Daten verändert. URL: <https://geobroker.geobasis-bb.de/gbss.php?MODE=GetProductInformation&PRODUCTID=9e95f21f-4ecf-4682-9a44-e5f7609f6fa0> [last access on: 06.10.2022]  
 Kreisgrenzen des Bundeslandes Brandenburg: GeoBasis-DE/LGB, dl-de/by-2-0. URL: <https://geobroker.geobasis-bb.de/gbss.php?MODE=GetProductPreview&PRODUCTID=ed6ab7a1-7a64-4ceb-8d37-2e156b7f4546> [last access on: 06.10.2022]  
 ..... 21

Figure 5:	Plot-level LST/NDVI (greenest pixel) ratio vs. time slope (left) and share of LST/NDVI ratio variance explained by time (right), superimposed with administrative divisions of Brandenburg, 2013 - 2019 Own diagram: program: QGIS, date: 06.10.2022, CRS: EPSG:25833 Sources: Amtliches Liegenschaftskatasterinformationssystem (ALKIS-Daten): GeoBasis-DE/LGB, dl-de/by-2-0. URL: <a href="https://data.geobasis-bb.de/geobasis/daten/alkis/Vektordaten/shape/">https://data.geobasis-bb.de/geobasis/daten/alkis/Vektordaten/shape/</a> [last access on: 06.10.2022] Kreisgrenzen des Bundeslandes Brandenburg: GeoBasis-DE/LGB, dl-de/by-2-0. URL: <a href="https://geobroker.geobasis-bb.de/gbss.php?MODE=GetProductPreview&amp;PRODUCTID=ed6ab7a1-7a64-4ceb-8d37-2e156b7f4546">https://geobroker.geobasis-bb.de/gbss.php?MODE=GetProductPreview&amp;PRODUCTID=ed6ab7a1-7a64-4ceb-8d37-2e156b7f4546</a> [last access on: 06.10.2022]	28
Figure 6:	Boxplots of land surface temperature across all plots 2016-2019 (left to right) Own diagram: program: R, RStudio, date: 03.10.2022	29
Figure 7:	Boxplots of NDVI across all plots 2016-2019 (left to right) Own diagram: program: R, RStudio, date: 03.10.2022	30
Figure 8:	LST / NDVI relation in 2016-2019 (left to right), colours indicating point density ranging from blue (low) via green (medium) to red (high) Own diagram: program: R, RStudio, date: 03.10.2022	30
Figure 9:	Boxplots of LST/NDVI ratio across all plots 2016-2019 (left to right) Own diagram: program: R, RStudio, date: 03.10.2022	31
Figure 10:	Soil water exchange frequency / drought relation in 2016-2019 (left to right), colours indicating point density ranging from blue (low) via green (medium) to red (high) Own diagram: program: R, RStudio, date: 27.09.2022	33
Figure 11:	Boxplots of soil water exchange frequency across all plots (respectively left) and the plots with LST/NDVI ratios in the upper quartile thereof in the given year (respectively right), for 2016-2019 (left to right) Own diagram: program: R, RStudio, date: 27.09.2022	34
Figure 12:	Percolation rate / drought relation in 2016-2019 (left to right), colours indicating point density ranging from blue (low) via green (medium) to red (high) Own diagram: program: R, RStudio, date: 27.09.2022	36
Figure 13:	Boxplots of percolation rates across all plots (respectively left) and the plots with LST/NDVI ratios in the upper quartile thereof in the given year (respectively right), for 2016-2019 (left to right) Own diagram: program: R, RStudio, date: 27.09.2022	37
Figure 14:	Field value / drought relation in 2016-2019 (left to right), colours indicating point density ranging from blue (low) via green (medium) to red (high) Own diagram: program: R, RStudio, date: 28.09.2022	39

Figure 15:	Boxplots of field values across all plots (respectively left) and the plots with LST/NDVI ratios in the upper quartile thereof in the given year (respectively right), for 2016-2019 (left to right) Own diagram: program: R, RStudio, date: 28.09.2022	40
Figure 16:	Soil Quality Rating / drought relation in 2016-2019 (left to right), colours indicating point density ranging from blue (low) via green (medium) to red (high) Own diagram: program: R, RStudio, date: 27.09.2022	42
Figure 17:	Boxplots of SQR scores across all plots (respectively left) and the plots with LST/NDVI ratios in the upper quartile thereof in the given year (respectively right), for 2016-2019 (left to right) Own diagram: program: R, RStudio, date: 27.09.2022	43
Figure 18:	Field capacity / drought relation in 2016-2019 (left to right), colours indicating point density ranging from blue (low) via green (medium) to red (high) Own diagram: program: R, RStudio, date: 27.09.2022	45
Figure 19:	Boxplots of field capacity across all plots (respectively left) and the plots with LST/NDVI ratios in the upper quartile thereof in the given year (respectively right), for 2016-2019 (left to right) Own diagram: program: R, RStudio, date: 27.09.2022	46
Figure 20:	Potential erosion (water) / drought relation in 2016-2019 (left to right), colours indicating point density ranging from blue (low) via green (medium) to red (high) Own diagram: program: R, RStudio, date: 27.09.2022	48
Figure 21:	Boxplots of potential erosion (water) across all plots (respectively left) and the plots with LST/NDVI ratios in the upper quartile thereof in the given year (respectively right), for 2016-2019 (left to right) Own diagram: program: R, RStudio, date: 27.09.2022	48
Figure 22:	Soil Moisture Index (top soil) / drought relation in 2016-2019 (left to right), colours indicating point density ranging from blue (low) via green (medium) to red (high) Own diagram: program: R, RStudio, date: 27.09.2022	53
Figure 23:	Boxplots of topsoil Soil Moisture Index across all plots (respectively left) and the plots with LST/NDVI ratios in the upper quartile thereof in the given year (respectively right), for 2016-2019 (left to right) Own diagram: program: R, RStudio, date: 03.10.2022	54

Figure 24:	Soil Moisture Index (entire soil) / drought relation in 2016-2019 (left to right), colours indicating point density ranging from blue (low) via green (medium) to red (high) Own diagram: program: R, RStudio, date: 27.09.2022	55
Figure 25:	Boxplots of entire soil Soil Moisture Index across all plots (respectively left) and the plots with LST/NDVI ratios in the upper quartile thereof in the given year (respectively right), for 2016-2019 (left to right) Own diagram: program: R, RStudio, date: 03.10.2022	55
Figure 26:	Drought Magnitude (top soil) / drought relation in 2016-2019 (left to right), colours indicating point density ranging from blue (low) via green (medium) to red (high) Own diagram: program: R, RStudio, date: 27.09.2022	56
Figure 27:	Boxplots of topsoil Drought Magnitude across all plots (respectively left) and the plots with LST/NDVI ratios in the upper quartile thereof in the given year (respectively right), for 2016-2019 (left to right) Own diagram: program: R, RStudio, date: 03.10.2022	57
Figure 28:	Drought Magnitude (entire soil) / drought relation in 2016-2019 (left to right), colours indicating point density ranging from blue (low) via green (medium) to red (high) Own diagram: program: R, RStudio, date: 27.09.2022	58
Figure 29:	Boxplots of entire soil Drought Magnitude across all plots (respectively left) and the plots with LST/NDVI ratios in the upper quartile thereof in the given year (respectively right), for 2016-2019 (left to right) Own diagram: program: R, RStudio, date: 03.10.2022	58

Enlarged versions of select figures can be found in the appendix, starting on page 85.

## List of Tables

Table 1:	Mean LST, NDVI (mean and greenest pixel) and LST/NDVI ratio (calculated using mean and greenest pixel NDVI respectively) on a per-plot basis for growing seasons between 2013 and 2021	25
Table 2:	Years ranked with regards to mean LST, NDVI (mean and greenest pixel) and LST/NDVI ratio (calculated using mean and greenest pixel NDVI respectively) on a per-plot basis for growing seasons between 2013 and 2021, including overall rank with regards to drought intensity	25
Table 3:	Mean per-plot slopes and $R^2$ of the linear regressions of LST, NDVI (mean and greenest pixel) and LST/NDVI ratio (calculated using mean and greenest pixel NDVI respectively) in relation to the passage of time	26
Table 4:	Percentiles of slopes of LST, NDVI (mean and greenest pixel) and LST/NDVI ratio (calculated using mean and greenest pixel NDVI respectively) in relation to the passage of time, maxima and minima excluding outliers (outside $1.5 \cdot IQR$ )	26
Table 5:	Percentiles of $R^2$ of LST, NDVI (mean and greenest pixel) and LST/NDVI ratio (calculated using mean and greenest pixel NDVI respectively) in relation to the passage of time, maxima and minima excluding outliers (outside $1.5 \cdot IQR$ )	26
Table 6:	Percentiles of land surface temperature across all plots of the given year, maxima and minima excluding outliers (outside $1.5 \cdot IQR$ )	29
Table 7:	Percentiles of the normalised difference vegetation index across all plots of the given year, maxima and minima excluding outliers (outside $1.5 \cdot IQR$ )	30
Table 8:	Percentiles of the LST/NDVI ratio across all plots of the given year, maxima and minima excluding outliers (outside $1.5 \cdot IQR$ )	31
Table 9:	Percentiles of soil water exchange frequencies across all plots and the plots with LST/NDVI ratios in the upper quartile thereof in the given year, maxima and minima excluding outliers (outside $1.5 \cdot IQR$ )	34
Table 10:	Percentiles of percolation rates across all plots and the plots with LST/NDVI ratios in the upper quartile thereof in the given year, maxima and minima excluding outliers (outside $1.5 \cdot IQR$ )	37

Table 11: Typical soil values exhibited by different soil types Source: Greuner-Pönicke et al., 2014. URL: <a href="https://landkreis-wesermarsch.de/uploads/files/antragsunterlagen_bericht_final_2014-11-15_komplett_teil_1-bericht_und_anlagen.pdf">https://landkreis-wesermarsch.de/uploads/files/antragsunterlagen_bericht_final_2014-11-15_komplett_teil_1-bericht_und_anlagen.pdf</a> [last access on: 06.10.2022]	39
Table 12: Percentiles of field values across all plots and the plots with LST/NDVI ratios in the upper quartile thereof in the given year, maxima and minima excluding outliers (outside 1.5*IQR)	40
Table 13: SQR ranges Source: Bundesanstalt für Geowissenschaften und Rohstoffe, 2014. URL: <a href="https://www.lgi.geographie.uni-kiel.de/de/media/ws_13_14/handzettel-soil-quality-rating-hennings-et-al.pdf">https://www.lgi.geographie.uni-kiel.de/de/media/ws_13_14/handzettel-soil-quality-rating-hennings-et-al.pdf</a> [last access on: 06.10.2022]	42
Table 14: Percentiles of SQR scores across all plots and the plots with LST/NDVI ratios in the upper quartile thereof in the given year, maxima and minima excluding outliers (outside 1.5*IQR)	43
Table 15: Classification of field capacity ranges Source: Bundesanstalt für Geowissenschaften und Rohstoffe, 2014. URL: <a href="https://geoviewer.bgr.de/mapapps4/resources/apps/bodenatlas/index.html">https://geoviewer.bgr.de/mapapps4/resources/apps/bodenatlas/index.html</a> [last access on: 06.10.2022]	45
Table 16: Percentiles of field capacities [mm] across all plots and the plots with LST/NDVI ratios in the upper quartile thereof in the given year, maxima and minima excluding outliers (outside 1.5*IQR)	46
Table 17: Percentiles of potential erosion (water) [t/ha/y] across all plots and the plots with LST/NDVI ratios in the upper quartile thereof in the given year, maxima and minima excluding outliers (outside 1.5*IQR)	49
Table 18: P-values of all continuous data sets when used as predictor variables for multivariate regression of LST/NDVI ratios	50
Table 19: Multivariate regression of LST/NDVI ratios using all continuous data sets as predictor variables, duplicate years marked with an asterisk indicate repetition of the regression without variables previously found to be insignificant	50
Table 20: Beta coefficients and t values of soil water exchange frequency (SWEF), percolation rate (PR), field value (FV), Soil Quality Rating (SQR), field capacity (FC) and water-based erosion potential (EP(W)) when used as predictor variables for multivariate regression of LST/NDVI ratios	51

Table 21: Multivariate regression of LST/NDVI ratios using soil water exchange frequency, percolation rate and field value as predictor variables .....	51
Table 22: Beta coefficients and t values of soil water exchange frequency (SWEF), percolation rate (PR) and field value (FV) when used as predictor variables for multivariate regression of LST/NDVI ratios .....	51
Table 23: Percentiles of topsoil Soil Moisture Index values across all plots and the plots with LST/NDVI ratios in the upper quartile thereof in the given year, maxima and minima excluding outliers (outside 1.5*IQR) .....	54
Table 24: Percentiles of entire soil Soil Moisture Index values across all plots and the plots with LST/NDVI ratios in the upper quartile thereof in the given year, maxima and minima excluding outliers (outside 1.5*IQR) .....	56
Table 25: Percentiles of topsoil Drought Magnitude values across all plots and the plots with LST/NDVI ratios in the upper quartile thereof in the given year, maxima and minima excluding outliers (outside 1.5*IQR) .....	57
Table 26: Percentiles of entire soil Drought Magnitude values across all plots and the plots with LST/NDVI ratios in the upper quartile thereof in the given year, maxima and minima excluding outliers (outside 1.5*IQR) .....	59
Table 27: Ten most common agricultural land use types across all plots and the plots with LST/NDVI ratios in the upper quartile thereof in the given year, underscores indicate types more common in plots with more drought-like conditions, legend to IACS agricultural land use type codes in table 29 .....	61
Table 28: Relative share of ten most common agricultural land use types across all plots and plots with LST/NDVI ratios in the upper quartile thereof in the given year, underscores indicate types more common in plots with more drought-like conditions, legend to IACS agricultural land use type codes in table 29 .....	62
Table 29: Legend to IACS agricultural land use type codes in tables 27 and 28 .....	62
Table 30: Ranks of IACS agricultural land use types with regards to median LST/NDVI ratios, ranging from 1 (lowest ratio) to -1 (highest ratio) due to the unequal amount of categories in every year of interest .....	63

Table 31: Ten most common soil types across all plots and the plots with LST/NDVI ratios in the upper quartile thereof in the given year, underscores indicate types more common in plots with more drought-like conditions, legend to soil type abbreviations in table 33	66
Table 32: Relative share of ten most common soil types across all plots and the plots with LST/NDVI ratios in the upper quartile thereof in the given year, underscores indicate types more common in plots with more drought-like conditions, legend to soil type abbreviations in table 33	67
Table 33: Legend to soil type abbreviations in tables 31 and 32	67
Table 34: Ranks of soil types with regards to median LST/NDVI ratios, ranging from 1 (lowest ratio) to -1 (highest ratio) due to the unequal amount of categories in every year of interest	68
Table 35: Maximum root depth classes across all plots and the plots with LST/NDVI ratios in the upper quartile thereof in the given year, underscores indicate types more common in plots with more drought-like conditions, class names indicate maximum root depth in metres	70
Table 36: Relative share of maximum root depth classes across all plots and the plots with LST/NDVI ratios in the upper quartile thereof in the given year, class names indicate maximum root depth in metres	71
Table 37: BGR wind erosion classes Source: Bundesanstalt für Geowissenschaften und Rohstoffe, 2014. URL: <a href="https://geoviewer.bgr.de/mapapps4/resources/apps/bodenatlas/index.html">https://geoviewer.bgr.de/mapapps4/resources/apps/bodenatlas/index.html</a> [last access on: 06.10.2022]	72
Table 38: Most common wind erosion classes across all plots and the plots with LST/NDVI ratios in the upper quartile thereof in the given year	72
Table 39: Relative share of wind erosion classes across all plots and the plots with LST/NDVI ratios in the upper quartile thereof in the given year	73



## List of Abbreviations

ALKIS:	Amtliches Liegenschaftskatasterinformationssystem
BGR:	Federal Institute for Geosciences and Natural Resources
CIiWaC:	Climate and Water under Change
DM:	Drought Magnitude
DWD:	Deutscher Wetterdienst
EP(W):	Erosion potential (wind)
FC:	Field capacity
FV:	Field value
IACS:	Integrated Administration and Control System
IPCC:	Intergovernmental Panel on Climate Change
IQR:	Interquartile range
LGB:	Landesvermessung und Geobasisinformation Brandenburg
LST:	Land surface temperature
mHM:	Mesoscale Hydrologic Model
NDVI:	Normalised difference vegetation index
NOAA:	National Oceanic and Atmospheric Administration
PR:	Percolation rate
SMI:	Soil Moisture Index
SQR:	Soil Quality Rating
SWEF:	Soil water exchange frequency
UFZ:	Helmholtz Centre for Environmental Research

# 1. Introduction

## 1.1. Motivation & Problem Statement

Extreme weather events, such as droughts, are expected to increase in frequency, severity and duration across the globe as a direct result of anthropogenic climate change (IPCC, 2018). In agriculture, decreased soil moisture levels associated with drought lead to increased vegetation stress, thereby decreasing plant productivity, potentially causing devastating economic effects, including lower production, reduced yield or outright crop failure (Wilhite, Glantz, 1985, p. 115), and societal issues, such as food insecurity (Mishra, Singh, 2010, p. 206).

Attempts to adapt to the increased probability of droughts, particularly in agriculture, include crop selection, irrigation, tillage practice (Wilhelmi, Wilhite, 2002, p. 38), cultivation of more resilient crop varieties (Fukai, Cooper, 1995, p. 1), as well as the introduction of new agricultural practices aimed to mitigate the effects of anthropogenic climate change (Kaye, Quemada, 2017, p. 1). However, drought resilience of vegetation might not be able to explain the impacts of droughts on plant productivity alone. Site-related factors, such as soil properties, might play a role as well (Chukwudi et al., 2021, p. 23). Analysing the interplay of agricultural practices, site factors and drought might contribute to these adaptation attempts by highlighting particularly resilient or vulnerable complexes of site-based variables and by identifying areas where adaptations might be necessary. In association with the CliWaC (Climate and Water under Change) project, an Einstein Research Unit by the Berlin University Alliance, this analysis aims to contribute to the scientific understanding of agricultural drought hazards within the Spree river catchment in southeastern Brandenburg, Germany. Despite being known for its poor soil quality and ranking among the driest federal states of Germany (DWD, 2019b, p. 5), this area exhibits high shares of agricultural use. During the 2018 European heat wave, Germany experienced the driest vegetation period since meteorological record keeping began in 1881 (DWD 2019a, p. 2). The increasing occurrence of unusually long dry periods and heat waves throughout the Spree river catchment (CliWaC, 2022) makes it an ideal study area to analyse various types of potential drought hazards.

A further motivation for conducting this analysis lies within the demonstration of the viability of conducting such analyses using only freely available software and open geodata. Doing so might empower individual actors and stakeholders to assess drought hazards on their agricultural plots and to identify adaptation measures based on practices found to be related to lower drought intensity.

## 1.2. *Theoretical Background: Droughts and Remote Sensing Drought Monitoring*

The root causes of droughts are usually a lack of precipitation, increased atmospheric water demand, or both (Wilhite, Glantz, 1985, p. 111). Furthermore, they are strongly associated with phenomena such as heat waves (Mazdiyasi, AgaKouchak, 2015, p. 11484) and self-intensify via positive feedback loops, such as reduction of evaporative cooling and decrease of precipitation and cloudiness (Miralles et al., 2019, p. 20). Over half of the world

is susceptible to drought each year (Kogan, 1997, p. 622). Depending on the intensity and duration of these conditions, droughts can be classified into one of four categories. Meteorological drought is defined as a lack of precipitation over an area of interest for a period of time. In a hydrological context, a depletion of surface and subsurface water resources might lead to so-called hydrological droughts, whereas in an agricultural context, agricultural droughts usually refer to soil moisture falling low enough to impact the ability of vegetation to photosynthesise, thereby reducing its productivity and potentially leading to crop failure. If a drought affects not only the environment, but also societies and economies within its extent, it can be classified as socio-economic (Wilhite, Glantz, 1985, p. 113). The intensity of agricultural droughts is dependent not only on precipitation, or the lack thereof, itself, but also on biological crop characteristics and phenology, as well as soil properties (Mishra, Singh, 2010, p. 206). Decreases in plant productivity associated with agricultural droughts, such as reduced yield or total crop failure, have devastating economic effects (Wilhite, Glantz, 1985, p. 115). Recent extreme drought events with impacts on agricultural production in Europe include the droughts of 2003 (Rebetez et al., 2006, p. 569), 2006 (Rebetez et al., 2009, p. 1), and 2018 (Buras et al., 2020, p. 1655) and are expected to become increasingly more common (Spinoni et al., 2017, p. 1718).

Before the advent of satellite-based remote sensing techniques in drought monitoring, large-scale approaches were often limited by the availability of in-situ data, such as precipitation, temperature, river discharge or groundwater level measurements. Furthermore, these data sets only served as proxies representing vegetation health indirectly, with the direct and continuous assessment of the latter only being enabled by remote sensing, whose use is well-explored and routinely applied for drought assessment (Crocetti et al., 2020, p. 3). Satellite-based Earth observation data and drought indices derived thereof are an established way of globally monitoring droughts (Bannari et al., 1995, p. 96). The concept of assessing vegetation health via reflected light has been researched since the 1960s (Knipling, 1970, p. 155), with the possibility of satellite-borne sensors gaining traction in the mid 60s (author unknown, Nature, 1968, p. 419). Since the beginning of the new millennium, drought assessment approaches based on remote sensing and geoinformation science have diversified to include a variety of indicators and indices (Mishra, Singh, 2010, p. 207). Commonly used drought indicators are vegetation indices, such as the Normalised Difference Vegetation Index (NDVI), plant biophysical properties, land surface temperature (LST), evapotranspiration, soil moisture, vegetation optical depth, water content or biomass (Crocetti et al., 2020, p. 123). Remote sensing drought monitoring has been applied to diverse study sites around the globe, including Brandenburg (e.g. Ihnegbu, Ogunwumi, 2021).

One particularly well-established drought monitoring index is the ratio of LST and NDVI. It was first pioneered by McVicar and Bierwirth in 2001, to assess the 1997 drought in Papua New Guinea, and has since seen wide-spread application. Its limitations are well-known (Sun, Kafatos, 2007, Karnieli et al., 2010). Both LST and NDVI data is available globally with granularity sufficient to conduct local or plot-based assessment. Similar approaches have been applied to river catchments before, e.g. the Pannonian basin (Crocetti et al., 2020). The analysis of potential relations between the LST/NDVI ratio and site-based variables will form the basis of this thesis.

### **1.3. Objective**

On the example of agricultural plots in the Spree river catchment in Brandenburg, this thesis studies the relation between various local, site-based factors, agricultural practices and drought severity by means of exploratory data analysis, using the recent 2018 European drought for reference. By doing so, this thesis aims to recognise which traits, such as the type of cultivated crops and site-related factors, indicate plots particularly prone or more resilient to drought hazards. To do so, this thesis attempts to answer the following questions:

- Which data sets provide valuable insight into agricultural drought hazards in the study area?
- Which, if any, patterns can be found in the spatial distribution of drought hazards in the study area?
- How is drought hazard intensity distributed and/or stratified across agricultural plots?
- Which, if any, processes and/or phenomena can be identified?

It is expected that remote-sensing-based drought monitoring reveals the most severe drought conditions within the range of available data to appear in 2018 and 2019, resulting from the 2018 European heat wave, reflecting worse vegetation health across the entire study area.

It is further expected that there are clear correlations between drought intensity, i.e. high LST/NDVI ratios, and site-based factors. In the case of continuous data, e.g. the field value (German “*Ackerzahl*”), approximately linear relations are assumed, with more benign local conditions relating to lower drought intensity. In the case of categorical data, such as crop or soil type, it is expected that the presence of certain types on agricultural plots is significantly related to these plots exhibiting higher drought intensity than others in the study area, resulting in clear stratification. Data sets exhibiting such correlations will be assumed to provide valuable insight into agricultural drought hazard in the study area.

Furthermore, it is expected that data sets not showing any signs of mathematical correlation will show clustering effects, indicating anthropogenic processes and/or phenomena, e.g. irrigation.

Lastly, as site-related factors other than agricultural land use and crop type are unlikely to change, plots most and least affected by drought-like conditions are expected to cluster around areas in which the geographical distributions of drought hazard maxima and minima overlap.

## 2. Data & Methods

### 2.1. Study Area

The Spree river catchment constitutes a CliWaC case study and is suitable for wide-area hazard assessment, due to the abundance of agricultural plots and diversity of site-related factors and agricultural practices therein. The study area is constituted by the parts of the Spree river catchment falling within the administrative borders of the German federal state of Brandenburg.

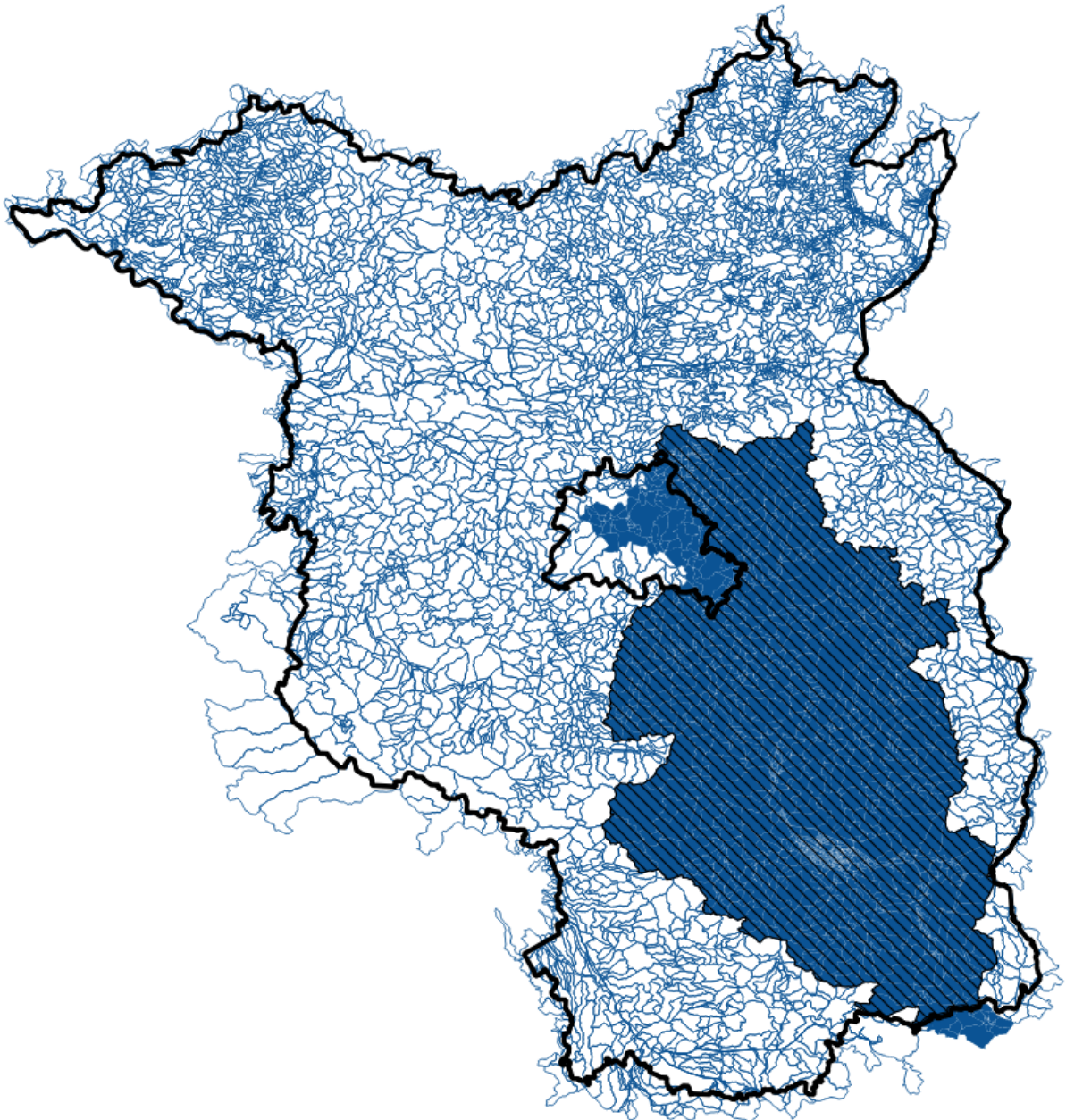


**Figure 1** Map of river catchments (outlined in blue) intersecting with the German federal state of Brandenburg (outlined in black), with catchments subsidiary to the Spree river highlighted (solid blue), parts of the Spree river catchment falling within Brandenburg's borders constitute the study area (hatched)

Brandenburg ranks among the driest federal states in Germany, even without the anthropogenic influence of global climate change, a situation only exacerbated by the latter. Average annual rainfall is about 558 mm, with some areas receiving less than 500 mm and only some areas in the north-west exceeding 600 mm (DWD, 2019a, p. 24). However, the state also experiences broad variability in downpour. Only 390 mm of precipitation were measured during the drought year of 2018, whereas floods caused by excessive rainfall were wide-spread a year prior (average of 721 mm, DWD, 2019a, p. 20). The state government expects both types of extreme weather phenomena to increase in frequency and severity as a result of anthropogenic climate change (DWD, 2019a, p. 20). Whereas mathematically the roughly equivalent increases and decreases in precipitation in 2017 and 2018 seem to balance each other out, extensive drought periods decrease the ability of the soil to absorb water, leading to lower groundwater levels and lowering the agricultural viability of said soils further (DWD, 2019a, p. 21). Both extremes further exacerbate soil erosion, especially on agricultural plots, with extreme rainfall events eroding topsoil directly and extreme droughts increasing vulnerability to wind erosion, effects of which have already been noticed by state authorities (MLUK, 2020 a, p. 3). 95% of Brandenburg's topsoil is composed of loose, quaternary sediments (MLUK, 2020 b, p. 6), with the study area falling within the older parts of the Young Drift and the Old Drift morainic landscapes of Central Europe, whose sandy soils are generally considered to be of poor quality (BGR, 2014, p. 1).

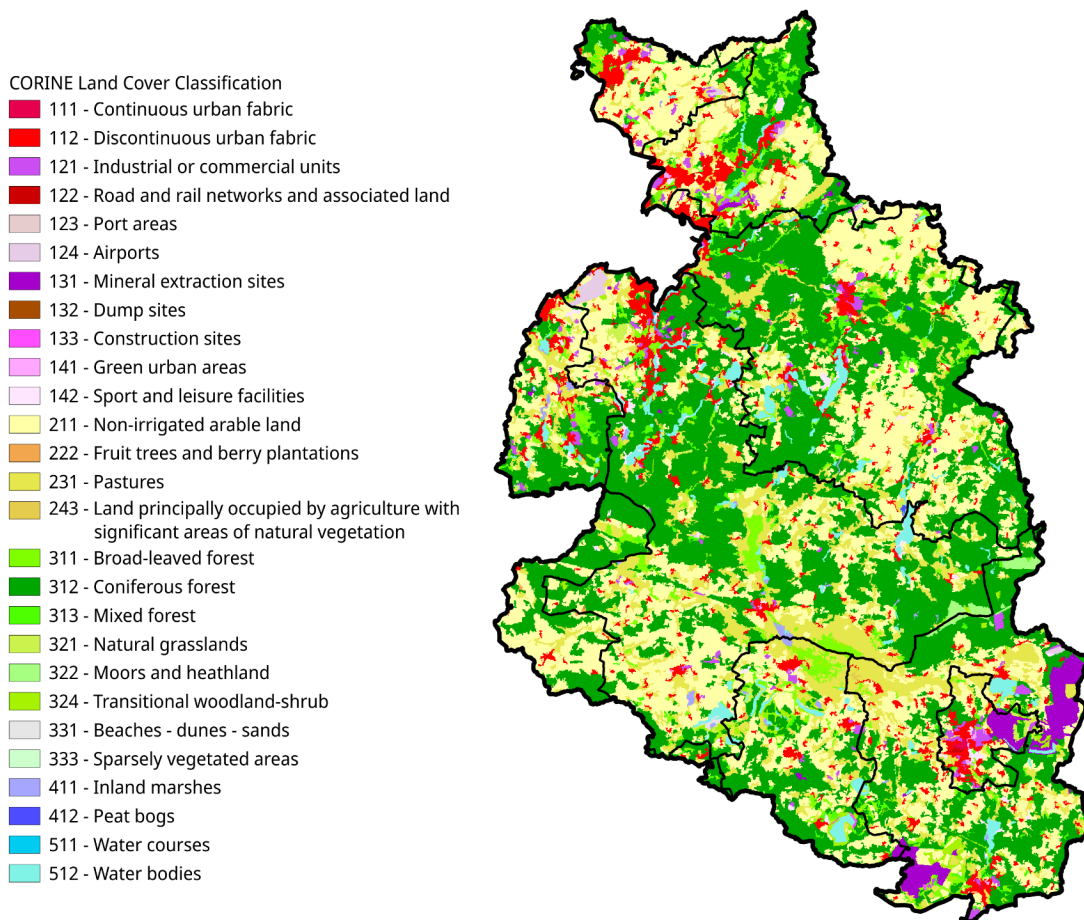


**Figure 2** 2020 CORINE land cover classification of the study area, superimposed with administrative divisions of Brandenburg



Out of the total 10,100 km<sup>2</sup> of the Spree's catchment, 7,155 km<sup>2</sup> fall within the administrative borders of Brandenburg, intersecting the administrative divisions of Barnim, Cottbus, Dahme-Spreewald, Elbe-Elster, Frankfurt (Oder), Märkisch-Oderland, Oberspreewald-Lausitz, Oder-Spree, Spree-Neiße and Teltow-Fläming, in the east and south-east of the federal state. Whilst Brandenburg is a sparsely-populated (85/km<sup>2</sup>), largely rural state, with roughly 49% of its area being used for agriculture, the south-east is slightly more forested than other parts of the state. Within the study area, 45.9% of the land is covered by forestry (largely *fagus sylvatica*, common beech) with only 41.4% being used for agriculture, and the remaining 12.6% comprising mostly of urban areas, open-pit mining, as well as marshes, peat bogs and water bodies, according to 2020 CORINE land cover classification (European Union, Copernicus Land Monitoring Service 2020, European Environment Agency (EEA)). The total number of individual agricultural plots intersecting with the catchment amounts up to roughly 67,000, according to cadaster data provided by the Brandenburg government (ALKIS). The number of plots in use differs from year to year, as shown by Integrated Administration and Control System (IACS) data, provided by the European Commission's INSPIRE directive.

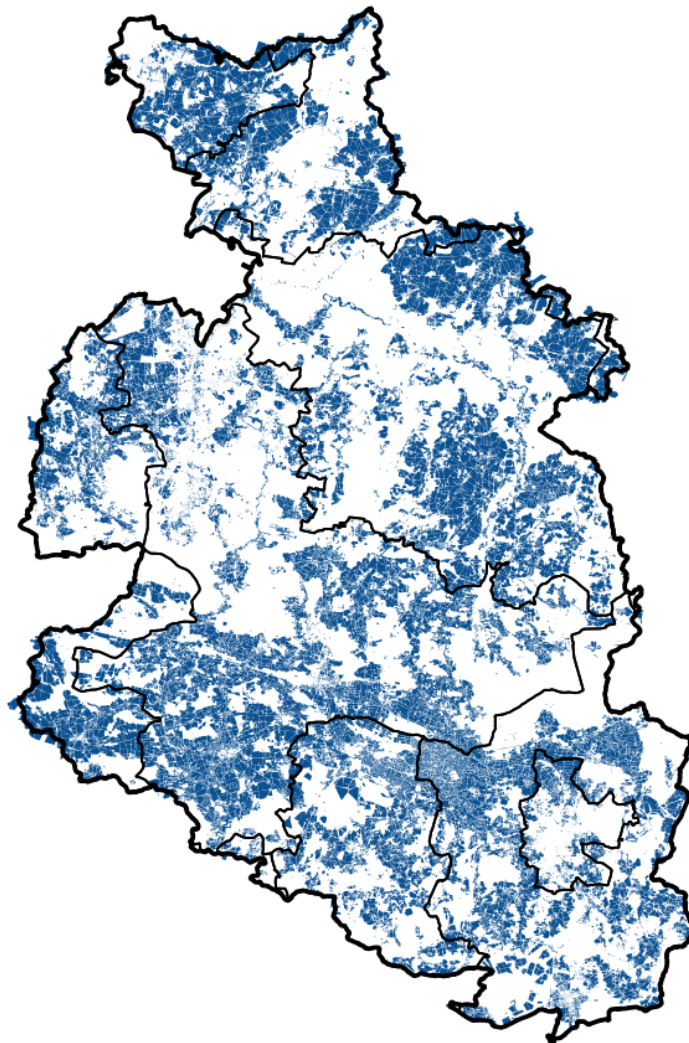


**Figure 3** Distribution of ALKIS agricultural plots (blue) throughout the study area, superimposed with administrative divisions of Brandenburg

## 2.2. Data

The analysis conducted is based on a variety of data sources.

The geometry of the study area was derived from surface catchment area data of Brandenburg's rivers (Oberirdische Einzugsgebiete des Landes Brandenburg) and the state's boundaries, both of which are available via the state's "Geoportal", run by the LGB, a state-owned enterprise.

CORINE Land Cover classification is available via Copernicus, the European Union's Earth observation programme (European Union, Copernicus Land Monitoring Service 2020, European Environment Agency (EEA)).

The primary drought indicator, the LST/NDVI ratio, was calculated from Landsat 8 imagery (U.S. Geological Survey), aggregated via Google Earth Engine (Gorelick et al., 2017).

The initial temporal analyses were conducted on ALKIS plot data, available from the LGB. This data set contains aggregated area-wide geometries of all real estate within the state, including land use information, based on which agricultural plots were selected as the units of this analysis.

For analysis on a year-by-year basis, IACS (Integrated Administration and Control System) data was used. IACS agricultural plot data sets are available throughout the European Union, as they constitute the basis for monitoring agricultural expenses and bestowing agricultural grants. For the federal state of Brandenburg, this data is included in the state's digital agricultural plot cadastre (German "*Digitales Feldblockkataster*"), also available via the LGB. Agricultural plot geometries for the years 2016, 2017, 2018 and 2019, including information regarding precise land use and crop types, were used for the analyses conducted for this thesis. Access to IACS data differs between federal states and some surveyed attributes are subject to a fee, but in this thesis only the crop type data was used, which is open and free for Brandenburg.

Nine sets of auxiliary data were analysed with regards to provision of insight into agricultural drought hazards. Soil water exchange frequency, the mean annual rate of percolation, the Soil Quality Rating, field capacity (water available for plant growth), erosion potential by wind and water (the former classified, the latter continuous in tonnes/ha/year), as well as rooting capacity (maximum root depth) are published by the German Federal Institute for Geosciences and Natural Resources (BGR) on their openly accessible soil atlas (bodenatlas.de), which covers the entirety of German state territory. Soil type and the field value (German "*Ackerzahl*"), are available via the aforementioned LGB ALKIS.

Lastly, for comparative purposes, modelled data from the Helmholtz Centre for Environmental Research (UFZ) Drought Monitor was analysed, which is freely available for download. This includes monthly Soil Moisture Index (SMI) data and the Drought Magnitude (DM), aggregated for growing periods between April and October. Both indices are available for the entire soil and the topsoil, the latter defined as 25 cm depth (Marx et al., 2016, p. 137).



### 2.3. Data Preparation

To generate the geometry of the study area, the catchments of the Spree river and its subsidiaries were selected from the surface catchment area data of Brandenburg's rivers, merged, and clipped to the state's boundaries. This process was conducted in QGIS (QGIS.org, 2022).

To calculate the LST/NDVI drought indicator across the study area, three mosaics were generated from Landsat 8 records (courtesy of the U.S. Geological Survey) for every of the, at the time of writing, nine growing seasons since the satellite's launch in 2013 up until 2021. These included the mean land surface temperature, the mean NDVI and greenest pixel NDVI composites. LST can be directly derived from Landsat 8's Thermal InfraRed Sensor (TIRS) band 10, whereas the NDVI is calculated using the red and near-infrared bands, bands 4 and 5 respectively, of Landsat 8's Operational Land Imager (OLI), using the following formula:

$$NDVI = \frac{(NIR - Red)}{(NIR + Red)}$$

As the factor limiting plant growth towards the edges of the growing season is energy, i.e. lack of solar radiation, with other biophysical variables less relevant during these periods, LST and NDVI correlate positively in early spring and late autumn (Karnieli et al. 2010, p. 618). The LST/NDVI ratio is therefore only applicable for drought monitoring during the mid-growing season, when water is the limiting factor, thus warranting the definition of growing seasons as the periods between May 1st and September 30th of each year for the selection of remote sensing records to aggregate. Cloud masking was applied and the scenes clipped to the study area. A spatial resolution of 30m was maintained for all nine sets of three mosaics, resulting in 27 4,949 by 4,613 pixel scenes. All of these operations were performed using Google Earth Engine (Gorelick et al., 2017).

The ALKIS plots used for the initial time series analysis, based on the analysis conducted by Karnieli et al., 2010, were filtered for agricultural land use and aggregated to the study area using QGIS, amounting to 67,557 polygonal features. For the years between 2016 and 2019, respectively 41,253, 41,880, 42,544 and 42,805 IACS polygonal geometries plots with agricultural use intersected with the study area, which were extracted for detailed analysis. Notably, due to IACS data being prone to faulty topology, erroneous geometries, and parcel overlaps (Jänicke et al., 2022), such issues were corrected for the plots within the study area. Notably, a separate workaround to fix apparently faulty geometries, consisting of generating geometries "buffered" with a width of 0, had to be applied during subsequent operations using the R (R Core Team, 2022) "terra" package (Hijmans et al., 2022), as documented in the code (see appendix).

To extract precise LST and NDVI (mean and greenest pixel) values onto the aggregated ALKIS plots, an R script was written using RStudio (RStudio Team, 2022), as well as the "sf" (Pebesma, 2018) and the aforementioned "terra" packages. The LST/NDVI ratio was calculated twice for each plot in each year, once using the mean NDVI values, and once using the greenest pixel composite. Analogously, LST and greenest pixel NDVI were extracted to the plots of the yearly IACS data sets, as well their ratio calculated.

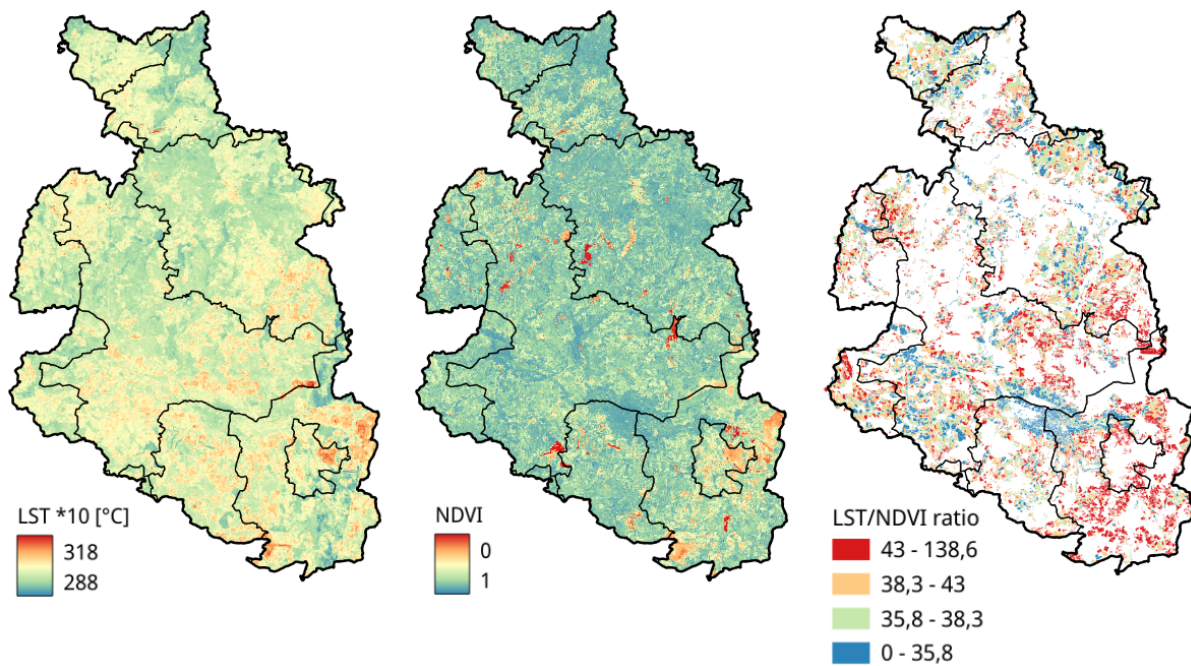


**Figure 4** Mean LST (left) and greenest pixel NDVI composite (middle) across the study area, and the LST/NDVI ratio calculated on agricultural plot level (right), superimposed with administrative divisions of Brandenburg, 2019 data

The extraction of mean soil water exchange frequency, percolation rate, field value (German “*Ackerzahl*”), SQR, field capacity, water erosion potential, UFZ SMI data for the relevant months and DM data for the relevant growing seasons, as well as the most common soil type, rooting potential class and wind erosion potential class onto each plot in the yearly IACS data sets was executed in QGIS, using the “zonal statistics” tool.

All cartographic depictions were created using QGIS.

## **2.4. Data Analysis**

All statistical analyses were conducted using base R (R Core Team, 2022) in RStudio (RStudio Team, 2022).

### **2.4.1. Time Series Analysis**

The primary goal of conducting basic time series analysis of the LST/NDVI ratio across the study area was to establish a frame of reference from which to study the effect of the selected auxiliary variables on drought hazard. Whilst the severity of the 2018 European heat wave and its long-term effects already warranted the detailed analysis of 2018 and 2019 data, non-drought years were necessary for comparative purposes. To facilitate this, the year with the overall “healthiest” indicators, i.e. the year least affected by drought, and the year with the most average conditions within the range of available data were to be determined.

To do so, LST, the NDVI (both mean and greenest pixel), as well as the LST/NDVI ratios of each plot calculated using either of the NDVI rasters, were aggregated into yearly means for all, at the time of writing, nine complete growing periods since the launch of Landsat 8 in 2013. These yearly means were then ranked according to their severity, with a rank of 1 indicating the year with the mildest conditions in any given indicator, e.g. the lowest LST or highest NDVI, and a rank of 9 indicating the most severe conditions, e.g. the highest LST or lowest NDVI. The median rank of 5 indicates the most average conditions within the range of available data. The average rank of each year across the indicators was used to rank how much any given year was affected by drought, facilitating the selection of the other two years of interest.

Furthermore, the availability of per-plot data for all values and indices enabled the calculation of plot-level time series. Linear regression was performed for all 67,557 ALKIS plots with regards to LST, mean NDVI, greenest pixel NDVI, as well as the LST/NDVI ratio calculated both using the mean and the greenest pixel NDVI. These results were aggregated into per-value or per-indicator means to get an overview of how these values and indices tend to behave over time and how much of their variation can be explained by the passage of time alone, as a proxy for the compound effects of anthropogenic climate change. Percentiles were also calculated to assess the range of behaviours exhibited by these values and indices throughout the study area.

### **2.4.2. Continuous Data**

First, to gain an understanding for the potential relationships between the LST/NDVI ratio and continuous, site-related variables, the ranges of the component variables of the drought indicator, i.e. LST and NDVI exhibited by agricultural plots in each year of interest, were analysed by comparing yearly percentiles. Furthermore, the relationship between the indicator components was investigated using linear regression. Lastly, to conclude familiarisation with the drought indicator’s behaviour throughout agricultural plots in the study area, the ranges of the LST/NDVI ratio in each year of interest were investigated by comparing yearly percentiles.

Relationships between the LST/NDVI ratio and continuous, site-related variables, i.e. soil water exchange frequency, percolation rate, field value, Soil Quality Rating, field capacity and water-based erosion potential, were investigated using linear regression. To confirm or specify the behaviour of potential patterns or the absence thereof, the ranges of the continuous variables were compared between all agricultural plots and the subset of plots exhibiting NDVI ratios within the upper quartile thereof in each year of interest.

The initial null hypothesis would always assume no relation between the independent site-related predictor variable and the LST/NDVI ratio. The discovery of relationships between the predictor variable and the LST/NDVI ratio would disprove this null hypothesis, enabling the assumption that analysis of said variable would provide insight into drought hazard. The lack of any discernible patterns would prevent disproving this null hypothesis, i.e. not disproving that a respective variable does not pose a drought hazard.

In a last step, multivariate linear regression was performed using all variables found to correlate with the LST/NDVI ratio and the subset of variables appearing most likely to pose drought hazards. The intention behind doing so was the assessment of how much of the variance in LST/NDVI ratio values can be explained using aforementioned variables and to ascertain whether particular variables appear more insightful into drought hazard than others.

For comparison, the UFZ's Soil Moisture Index and Drought Magnitude indices were investigated for potential relations with the LST/NDVI ratio, analogous to the process described above. As both are modelled drought indices, derived from the hydrological model system mHM (Samaniego et al., 2010; Kumar et al., 2013), rather than environmental, site-related factors, they cannot be considered drought hazards themselves, and were not used as predictor variables for multivariate regression. Identifiable relations between the two drought indices would serve as mutual validation of the drought indices, whereas a lack thereof would warrant discussion.

### **2.4.3. Categorical data**

To investigate the influence of categorical variables, i.e. crop and agricultural land use type, soil type, rooting capacity and wind-based erosion potential, the types or classes overall most common in each year of interest were compared to those most common on the the subset of plots exhibiting NDVI ratios within the upper quartile thereof in each year of interest. These comparisons were conducted both on the level of absolute occurrences and relative shares, as the former might provide little insight into the behaviour of statistically more common classes, e.g. soil types dominating the study area. Should individual classes be more common on plots exhibiting high LST/NDVI ratios, these classes could then be assumed to pose drought hazards.

In the case of data sets with high numbers of distinct classes, i.e. crop and agricultural land use type, as well as soil type, only the ten most common classes were investigated as described above. In such cases, the classes whose plots exhibited the highest and lowest median LST/NDVI ratios in each year were further analysed.

## **3. Results & Discussion**

### **3.1. Time Series Analysis**

Land surface temperature (LST) is a fundamental parameter for assessing surface energy and water balance (Crocetti et al., 2020, p. 122) indicating soil moisture deficit and serving as a drought indicator. The NDVI, the ratio of the difference of red and infrared radiance over their sum, has been applied to identify aboveground green biomass for over fifty years (Rouse et al., 1973). The NDVI ranges from -1 to 1. Negative values typically correspond to inanimate matter, bare soil usually exhibits NDVI values between 0.1 and 0.2, and values between 0.2 and 1 usually imply vegetation. Healthy vegetation usually exhibits NDVI values above 0.5, barring phenological effects (Cherlinka, 2019). Towards the beginning and the end of growing seasons, LST and NDVI are positively correlated, with higher land surface suggesting high amounts of solar energy available for plant growth. In the mid-growing season, when vegetation growth is not limited by solar radiation but by available water resources, LST, as a proxy for evapotranspiration, vegetation water stress, soil moisture and thermal inertia, and the NDVI are negatively correlated (Karnieli et al. 2010, p. 618). Both LST and NDVI values were therefore aggregated for the periods between May 1st and September 30th of each year.

The ranking of each growing season between 2013 and 2021 with regards to LST, mean NDVI, greenest pixel NDVI, ratio of LST and mean NDVI, and ratio of LST and greenest pixel NDVI aggregated to the mean of all ALKIS plots within the study area served to facilitate an overview of the drought conditions in each growing season within the range of available data. For each variable or index, each growing season was ranked from 1 to 9, with a rank of 1 indicating the year with the mildest conditions in any given indicator, e.g. the lowest LST or highest NDVI, and a rank of 9 indicating the most severe conditions, e.g. the highest LST or lowest NDVI. The mean rank of each growing season served to rank the growing seasons with regards to their drought intensity.

The attempted prediction of each value and indicator using time as a proxy for the compound effects of anthropogenic climate change as the independent variable in linear regression served to facilitate an overview of the range of developments therein across agricultural plots in the study area. Analogous analyses have been conducted by Karnieli et al., 2010, albeit on the level of individual pixels instead of plots.

## Results

**Table 1** Mean LST, NDVI (mean and greenest pixel) and LST/NDVI ratio (calculated using mean and greenest pixel NDVI respectively) on a per-plot basis for growing seasons between 2013 and 2021

Year	2013	2014	2015	2016	2017	2018	2019	2020	2021
LST	30.196	29.755	30.248	30.371	29.998	30.522	30.177	30.145	30.029
Mean NDVI	0.685	0.689	0.664	0.672	0.687	0.632	0.633	0.642	0.681
Gr. px. NDVI	0.784	0.767	0.772	0.778	0.797	0.776	0.746	0.751	0.769
Mean ratio	45.312	44.527	47.322	46.561	44.988	50.196	49.850	48.649	45.504
Gr. px. ratio	39.226	39.609	39.991	39.726	38.266	40.138	41.573	41.109	39.782

**Table 2** Years ranked with regards to mean LST, NDVI (mean and greenest pixel) and LST/NDVI ratio (calculated using mean and greenest pixel NDVI respectively) on a per-plot basis for growing seasons between 2013 and 2021, including overall rank with regards to drought intensity

Year	2013	2014	2015	2016	2017	2018	2019	2020	2021
LST	6	1	7	8	2	9	5	4	3
Mean NDVI	3	1	6	5	2	9	8	7	4
Gr. px. NDVI	2	7	5	3	1	4	9	8	6
Mean ratio	3	1	6	5	2	9	8	7	4
Gr. px. ratio	2	3	6	4	1	7	9	8	5
Rank	3	2	6	5	1	8	9	7	4

**Table 3** Mean per-plot slopes and R<sup>2</sup> of the linear regressions of LST, NDVI (mean and greenest pixel) and LST/NDVI ratio (calculated using mean and greenest pixel NDVI respectively) in relation to the passage of time

Data	slope	R <sup>2</sup>
LST	0.008	0.086
Mean NDVI	-0.004	0.197
Greenest pixel NDVI	-0.003	0.184
Mean LST/NDVI ratio	0.364	0.182
Greenest pixel LST/NDVI ratio	0.171	0.185

**Table 4** Percentiles of slopes of LST, NDVI (mean and greenest pixel) and LST/NDVI ratio (calculated using mean and greenest pixel NDVI respectively) in relation to the passage of time, maxima and minima excluding outliers (outside 1.5\*IQR)

Percentile	LST	Mean NDVI	Gr. px. NDVI	Mean ratio	Gr. px. ratio
Maximum	0.087	0.012	0.012	1.523	0.962
75th	0.029	-0.000	0.001	0.618	0.356
Median	0.010	-0.004	-0.002	0.253	0.120
25th	-0.010	-0.008	-0.006	0.015	-0.049
Minimum	-0.069	-0.020	-0.017	-0.890	-0.654

**Table 5** Percentiles of R<sup>2</sup> of LST, NDVI (mean and greenest pixel) and LST/NDVI ratio (calculated using mean and greenest pixel NDVI respectively) in relation to the passage of time, maxima and minima excluding outliers (outside 1.5\*IQR)

Percentile	LST	Mean NDVI	Gr. px. NDVI	Mean ratio	Gr. px. ratio
Maximum	28.83%	71.01%	67.89%	64.40%	67.92%
75th	12.22%	30.57%	28.93%	27.80%	29.04%
Median	4.71%	13.67%	11.95%	12.54%	12.19%
25th	1.14%	3.61%	2.94%	3.39%	3.12%
Minimum	0.00%	0.00%	0.00%	0.00%	0.00%

## Discussion

As expected, the most extreme conditions with regards to drought intensity have been detected in 2018 and 2019, albeit the study area had appeared to have suffered worse conditions in 2019 than 2018 (tables 1, 2). This contradicts findings of other studies, such as Kowalski et al., 2022, albeit this might result from the selection of the study area. Long-term effects of the sustained meteorological drought conditions might provide a further explanation approach. 2017 appeared to have been the mildest year, matching the reportedly anomalously rainy conditions reported by Brandenburg authorities (DWD, 2019a, p. 20). The most average conditions throughout the range of available data were found in 2016, albeit it must be noted that this year also exhibited the overall second-highest LST values found throughout the range of available data. These results warranted the selection of 2016, 2017, 2018 and 2019 for detailed analysis.

Linear regression of the data points (table 3) yielded plausible results. Mean LST on average appeared to increase by 0.008 K per year across all plots, with the passage of time on average explaining roughly 8.6% of the variance in the data. For reference, Europe's annual temperature has increased at an average rate of 0.015 K per year since 1910, albeit this has more than tripled to 0.047 K per year since 1981 (NOAA, 2021). NDVI appeared to decrease at an average rate of -0.004 and -0.003 per year for mean and greenest pixel NDVI respectively, with the passage of time respectively explaining roughly 19.7% and 18.4% of the variance.

The LST/NDVI ratio calculated using the mean NDVI increased at an average rate of 0.364 per year, with the passage of time explaining roughly 18.2% of the variance in the data, whereas the ratio calculated using greenest pixel NDVI increases at a slower pace of 0.171 per year on average, with the passage of time explaining roughly 18.5% of the variance in the data. The average temporal behaviour of these values and indices matches expectations with regards to anthropogenic climate change (IPCC, 2018), with LST increasing and NDVI decreasing from year to year, also resulting in an increasing LST/NDVI ratio. Furthermore, the difference between the behaviour of LST/NDVI ratios calculated using mean and greenest pixel NDVI was also expected. Mean NDVI pixels more likely include signals from temporarily barren agricultural plots, plots with vegetation in early growth stages or suffer from the mixed pixel problem, i.e. containing signals from both photosynthetically active vegetation and soil or not photosynthetically active vegetation (Kowalski et al., 2021, p. 5). The purpose of greenest pixel components is to maximise the chance of a pixel reflecting the state of photosynthetically active vegetation by selecting the highest NDVI value of each pixel encountered per growing season. The latter, therefore, is a scientifically more robust choice for ascertaining vegetation state, wherefore, in further analyses, only the greenest pixel NDVI will be considered for LST/NDVI ratio calculation. However, the aggregation of composites of greenest pixels from individual satellite records might mask potentially worse drought conditions present over longer periods of time.

It is further noteworthy that, as shown in table 4, not all plots exhibited behaviour congruent with expectations resulting from climate change predictions. The lowest quartile of LST slopes was negative, implying these plots to exhibit generally decreasing temperatures, the upper quartile of NDVI slopes was either close to or above zero, implying either inconsistent behaviour or even improving conditions with regards to the NDVI, with the same being true



for the lower quartile of ratio values also suggesting either inconsistent or improving conditions within parts of the study area. This is reflected in the temporal slopes of the resulting LST/NDVI ratio, as shown in figure 5 (left).

Equally as surprising was the share of data variance seemingly explained by the passage of time alone (table 3). On the average plot, the passage of time explained between 8.6% of variance shown (LST) and 19.7% of variance (mean NDVI). As shown in table 5, however, the ranges of variance explained by the passage of time for each indicator were quite wide, with maxima ranging from up to 28.83% in the case of LST to up to 71.01% in the case of mean NDVI. However, the distributions were bottom-heavy with median shares of variance explained ranging from 4.71% in the case of LST to 13.67% in the case of mean NDVI. Nonetheless, the percentiles show that a significant share of the 67,557 ALKIS plots have exhibited fairly linear behaviour with regards to the drought variables and indicators, implicitly reinforcing the applicability of the LST/NDVI ratio for monitoring agricultural droughts.

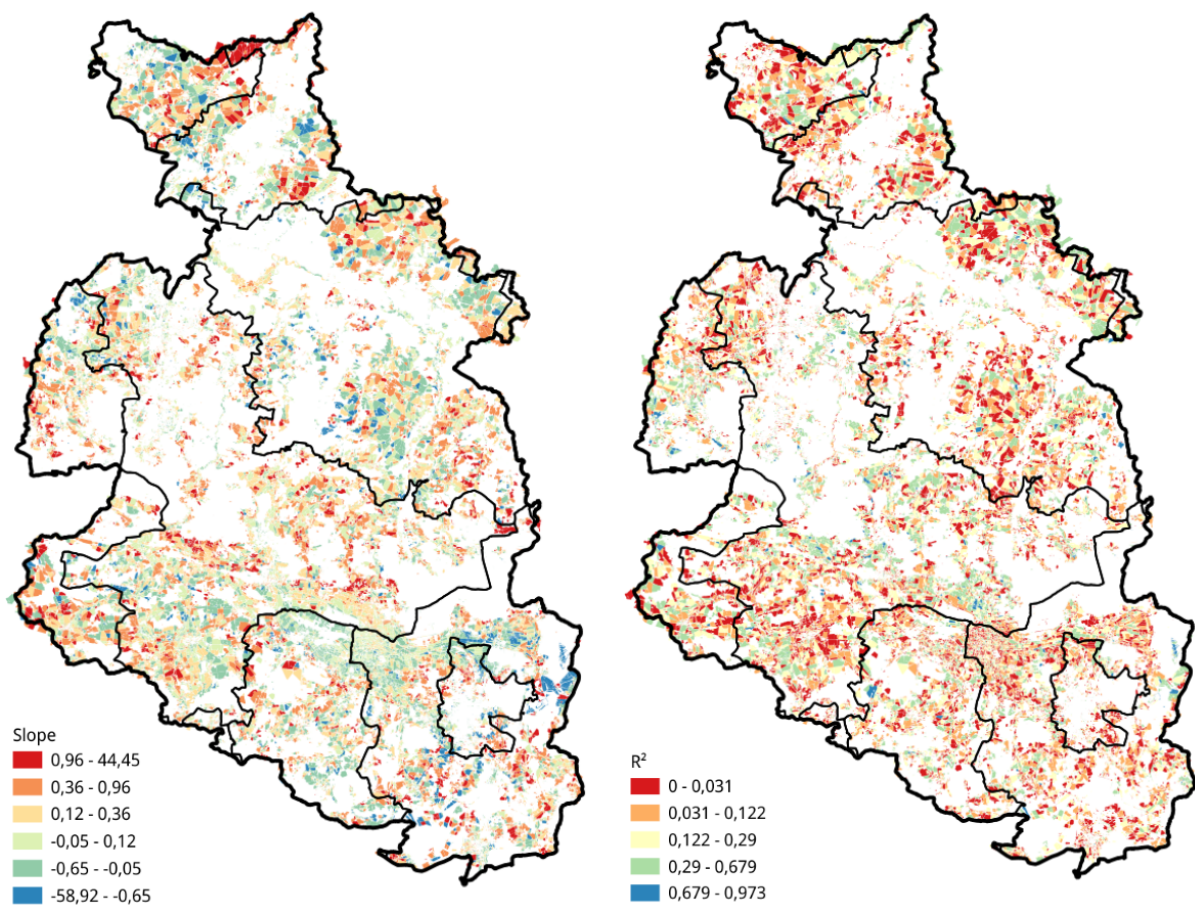


**Figure 5** Plot-level LST/NDVI (greenest pixel) ratio vs. time slope (left) and share of LST/NDVI ratio variance explained by time (right), superimposed with administrative divisions of Brandenburg, 2013 - 2019

## 3.2. Continuous Data

### 3.2.1. LST/NDVI Ratio

The distribution of LST/NDVI ratio values is mathematically dependent on its two components, the land surface temperature and the Normalised Difference Vegetation Index. The analysis of the overall ranges of the LST/NDVI ratio and its components exhibited by agricultural plots in the study area for each of the years of interest serves to foster better understanding of the patterns of potential relations between the drought indicator and site-related variables.

## Results

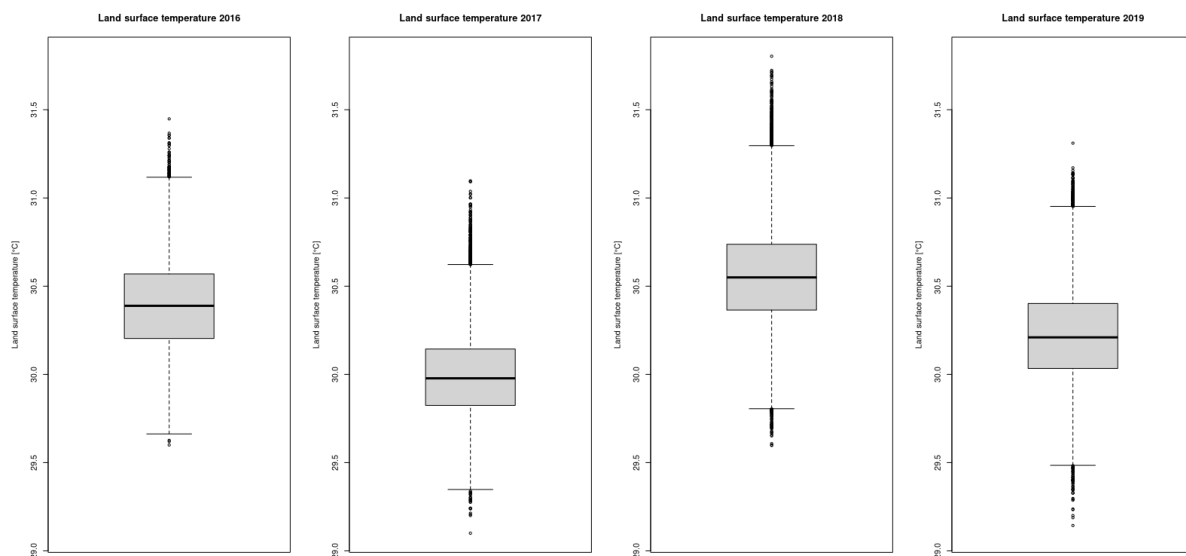


**Figure 6** Boxplots of land surface temperature across all plots 2016-2019 (left to right)

**Table 6** Percentiles of land surface temperature across all plots of the given year, maxima and minima excluding outliers (outside  $1.5 \cdot \text{IQR}$ )

Percentile	2016	2017	2018	2019
Maximum	31.12	30.62	31.30	30.95
75th	30.57	30.14	30.74	30.40
Median	30.39	29.98	30.55	30.21
25th	30.20	29.83	30.36	30.03
Minimum	29.66	29.35	29.81	29.49

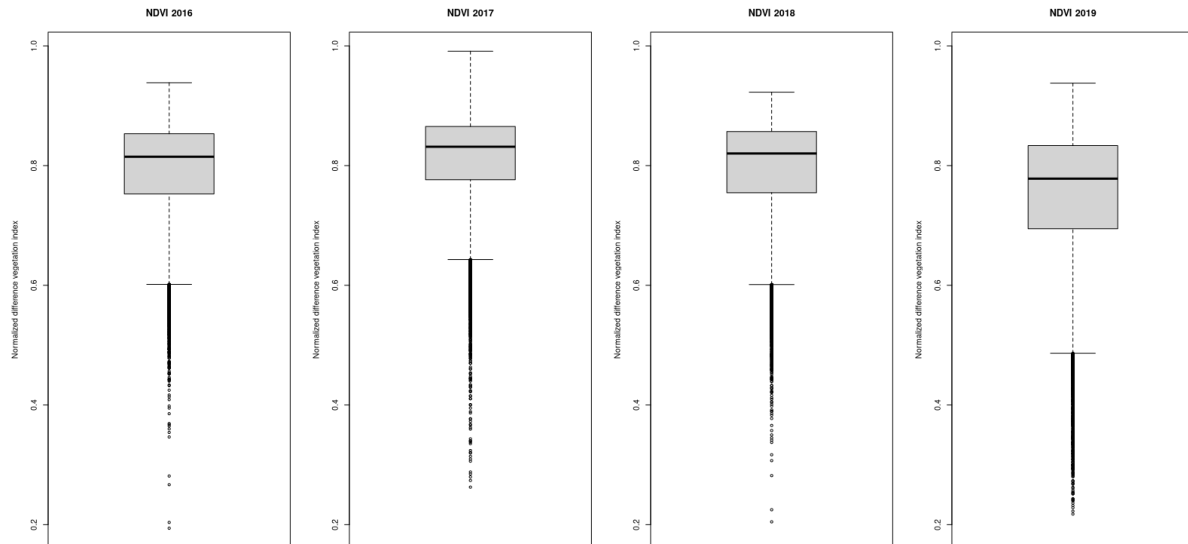


**Figure 7** Boxplots of NDVI across all plots 2016-2019 (left to right)

**Table 7** Percentiles of the normalised difference vegetation index across all plots of the given year, maxima and minima excluding outliers (outside 1.5\*IQR)

Percentile	2016	2017	2018	2019
Maximum	0.94	0.99	0.92	0.94
75th	0.85	0.87	0.86	0.83
Median	0.82	0.83	0.82	0.78
25th	0.75	0.78	0.76	0.70
Minimum	0.60	0.64	0.60	0.49

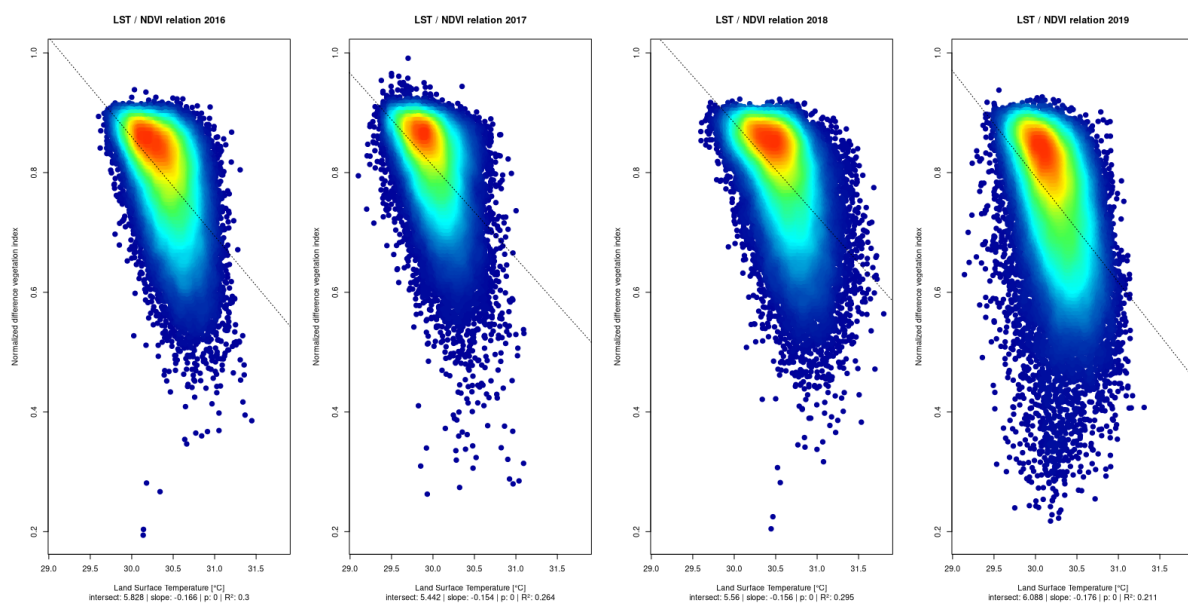


**Figure 8** LST / NDVI relation in 2016-2019 (left to right), colours indicating point density ranging from blue (low) via green (medium) to red (high)

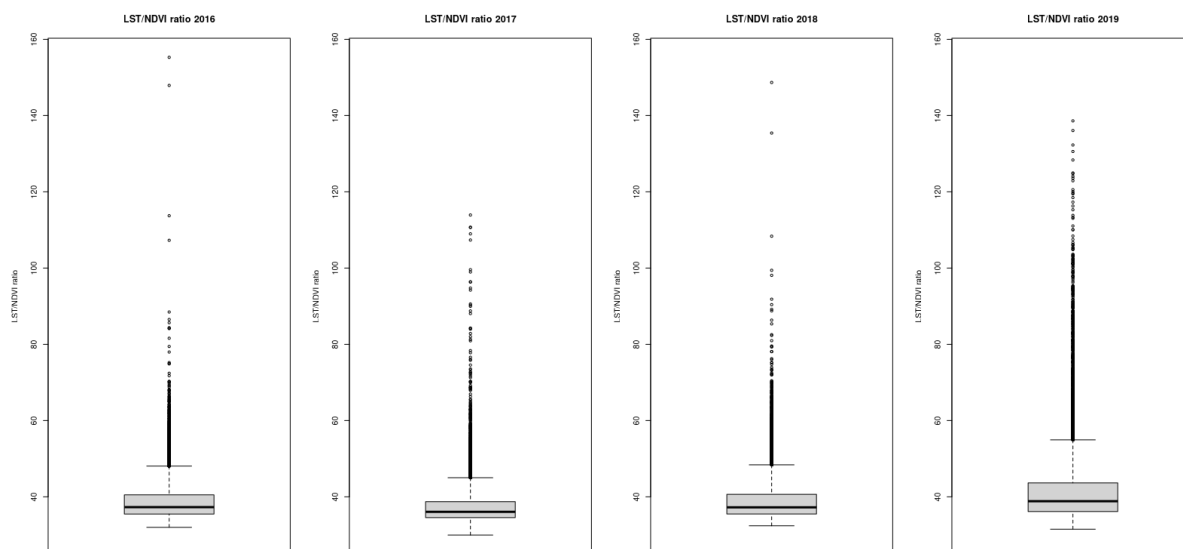


**Figure 9** Boxplots of LST/NDVI ratio across all plots 2016-2019 (left to right)

**Table 8** Percentiles of the LST/NDVI ratio across all plots of the given year, maxima and minima excluding outliers (outside  $1.5 \cdot \text{IQR}$ )

Percentile	2016	2017	2018	2019
Maximum	48.07	45.02	48.40	54.94
75th	40.52	38.74	40.66	43.67
Median	37.30	36.07	37.25	38.86
25th	35.49	34.55	35.50	36.15
Minimum	32.00	29.97	32.40	31.52

## Discussion

The differences in LST and NDVI ranges (figures 6 and 7, corresponding percentile values provided in tables 6 and 7), for 2017 and 2018 match government reports regarding the weather conditions in these years (DWD, 2019a, p. 20). For the extraordinarily wet 2017, LST values are overall lower than in the other years of interest, matching a cooling effect expected of higher soil moisture resulting from more intense rainfall. LST values are overall highest for the drought year of 2018, albeit they are notably lower in 2019. A similar pattern can be seen when examining NDVI over the years of interest, with the highest values encountered in the wet 2017, but the overall distribution gradually shifting downwards over the drought years of 2018 and 2019. The interquartile range was widest in 2019, indicating the most heterogeneous NDVI values throughout all years of interest. Notably, the NDVI values of 2018 are only slightly lower than in 2016, indicating that with regards to NDVI, the drought had its strongest effects in 2019. Nonetheless, the quartiles of NDVI values of all years of interest indicate the presence of vegetation generally classifiable as healthy, albeit these values are derived from greenest pixel composites, thereby reflecting the healthiest

vegetation conditions encountered on each plot throughout the respective growing period, whereas overall conditions might have been worse. Greenest pixel components might also be influenced by irrigation. Furthermore, it is notable that each year contained NDVI outliers (defined as falling outside 1.5 times the interquartile range) well below 0.3.

Matching the expectations for the relation between LST and NDVI set by Karnieli et al., 2010, NDVI is negatively correlated to LST on agricultural plots within the study area, as shown in figure 8. The correlation between LST and NDVI was significant in all years of interest ( $p$ -value  $< 2.2e-16$ ). Linear regression reveals distinct negative slopes in all four examined years, with an increase in LST of 1 K decreasing NDVI by -0.166 in 2016, -0.154 in 2017, -0.156 in 2018 and -0.176 in 2018, indicating a significant decrease in vegetation health associated with higher land surface temperatures. Predicting the NDVI as a proxy for vegetation health using LST as the independent variable explains between 30% of the variance in NDVI values in 2016 and 21.1% in 2019, thus reinforcing the suitability of the LST/NDVI ratio as a drought indicator.

As most LST values range from ca. 29°C to below 32°C and most NDVI values range from upwards of 0.6 to upwards of 0.9, the division of these components most commonly results in values between upwards of 29 and ca. 50 (see figure 9, table 8). The distribution of LST/NDVI values is therefore strongly concentrated around the lower bounds of the spectrum. As the LST/NDVI value mathematically responds particularly strong to decreases in the NDVI, truly drought-like conditions are likely to only be found on plots with LST/NDVI ratio values in the upper quartile thereof, albeit under the consideration of the previously mentioned effects of using greenest pixel composites. Nonetheless, facilitating better recognition of influence of site-related factors as potential drought hazards on the LST/NDVI ratio warrants the separate examination of plots exhibiting LST/NDVI values within the upper quartile values encountered in the respective year.

### 3.2.2. Soil Water Exchange Frequency

Soil water exchange frequency describes how often water and the substances dissolved therein can be replaced in a soil layer during the annual leachate flow. It is defined as field capacity divided by the amount of percolate water. For the BGR data set, the latter was calculated by subtracting evaporation and surface runoff from rainfall, corrected for different types of land use, e.g. agricultural land. Soils with lower water storage capacity exhibit higher exchange frequencies than soils with high water storage capacity, assuming equal amounts of percolate water. The risk of discharge of easily detachable materials like nitrate into the groundwater rises with higher soil water exchange frequencies (Stegger, 2016). The loss of nutrients available for plant growth via the leachate flow negatively affects vegetation health and thereby diminishing its drought resilience, the investigation of a potential relation between soil water exchange frequency and drought severity was warranted.

### Results

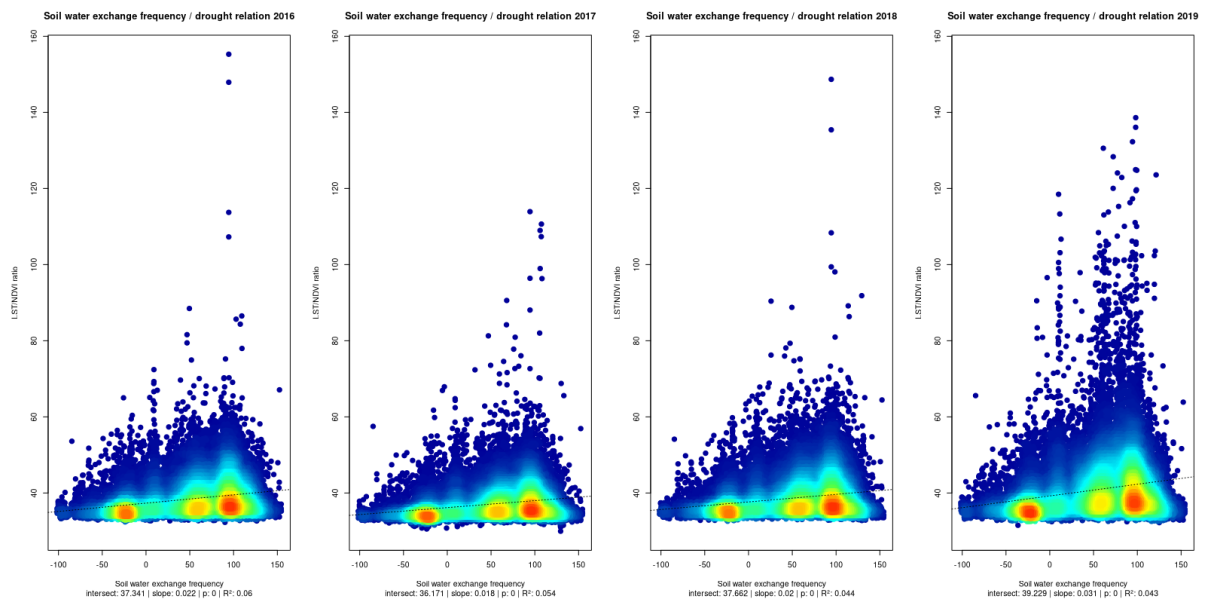


**Figure 10** Soil water exchange frequency / drought relation in 2016-2019 (left to right), colours indicating point density ranging from blue (low) via green (medium) to red (high)

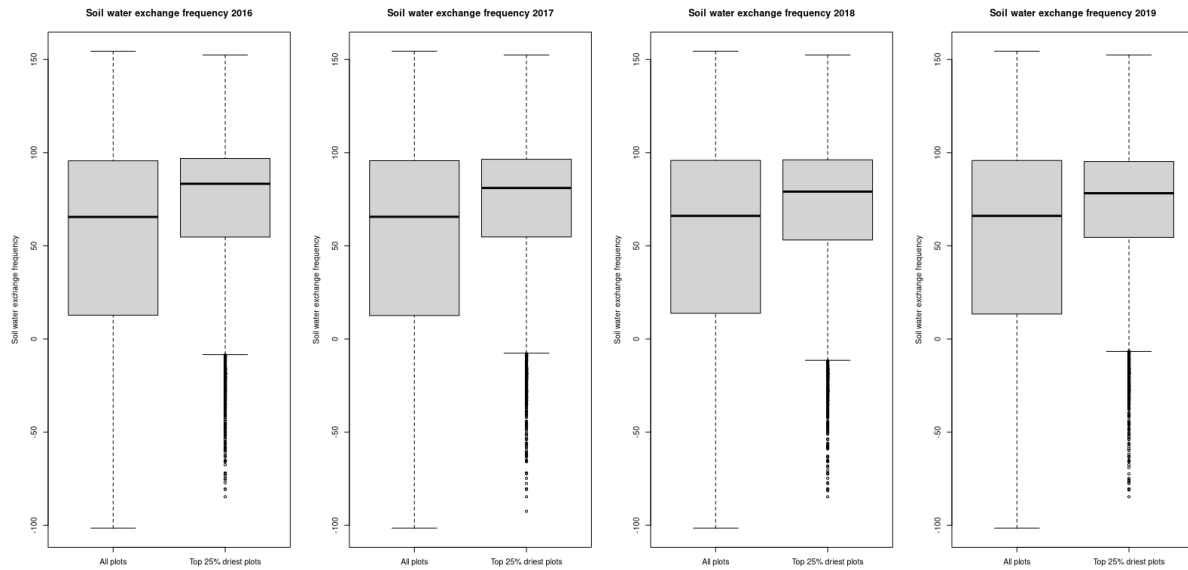


**Figure 11** Boxplots of soil water exchange frequency across all plots (respectively left) and the plots with LST/NDVI ratios in the upper quartile thereof in the given year (respectively right), for 2016-2019 (left to right)

**Table 9** Percentiles of soil water exchange frequencies across all plots and the plots with LST/NDVI ratios in the upper quartile thereof in the given year, maxima and minima excluding outliers (outside  $1.5 \cdot IQR$ )

	2016		2017		2018		2019	
Percentile	All plots	Top 25%	All plots	Top 25%	All plots	Top 25%	All plots	Top 25%
Maximum	154.44	152.45	154.44	152.45	154.44	152.45	154.44	152.45
75th	95.64	96.90	95.69	96.46	95.85	96.14	95.80	95.26
Median	65.51	83.30	65.58	81.03	66.08	79.11	66.08	78.23
25th	12.78	54.69	12.60	54.75	13.789	53.12	13.40	54.48
Minimum	-101.56	-8.35	-101.56	-7.64	-101.56	-11.41	-101.56	-6.66

## Discussion

Whilst the general distribution of LST/NDVI values causes clustering along the lower bound of its range, particularly at specific soil water exchange frequency values, likely caused by the discrete values of the source raster and its spatial resolution, linear effects are discernible in all four examined years (figure 10). Plots with low soil water exchange frequencies and thereby higher nutrient retention, appear to exhibit smaller ranges of LST/NDVI ratios, whereas plots with high exchange frequencies exhibit a wider range within LST/NDVI ratio values, creating conical patterns. This results in linear regression approximating upwards slopes for the LST/NDVI ratio in relation to soil water exchange frequency between 0.018 for 2017 and 0.031 for 2019, mirroring the respective yearly ranges of LST/NDVI ratio values. However, the range of LST/NDVI ratios widening with increasing soil water exchange frequency results in low percentages of explained variance,

ranging from 4.3% in 2019 to 6% in 2016. Nonetheless, the correlation was found to be significant in all years of interest ( $p$ -value  $< 2.2e-16$ ).

The assumption that high soil water exchange frequency implies higher LST/NDVI ratios is reinforced by the comparison of the ranges of soil water exchange frequency across all plots and across plots within the upper quartile of LST/NDVI ratio values (figure 11, table 9). The median soil water exchange frequency of plots with high LST/NDVI ratios is, on average, 15 units higher than the median of the entire sample. Likewise, the minimum soil water exchange frequency (excluding outliers) encountered in high LST/NDVI ratio plots, appears to be, on average, 93 units higher than the sample minimum (excluding outliers). In general, the 25th percentile of soil water exchange frequencies strongly affected by drought-like conditions appears to be approach the median soil water exchange frequency of the entire sample, meaning that roughly three quarters of soil water exchange frequencies of high LST/NDVI ratio plots fall within the upper half of soil water exchange frequencies of the entire sample.

This distinct behaviour contradicts the null hypothesis of no relation between soil water exchange rates and the LST/NDVI ratio, leading to the assumption that analysing soil water exchange frequencies might provide some insight into drought hazard.

However, it has to be noted that soil water exchange frequency might form complex interdependencies with other site-based variables, such as soil type (Knoblauch et al., 1999, p. 1, Kunkel, Wendland, 2003, p. 348). Furthermore, due to its mathematical nature, it is intertwined with field capacity and percolation rates, which can both be measured independently. Such interdependencies would warrant their own investigations in the study area, potential clusters of plots exhibiting certain configurations of hydrological variables positing a basis for the investigation of the influence of hydrology on the LST/NDVI ratio.



### 3.2.3. Percolation Rate

The percolation rate, measured in mm/a, is defined as the amount of water that leaves the soil after consideration of capillary rise, i.e. water exceeding the soil's field capacity, contributing to recharging the groundwater or being discharged into surface water bodies (Duijnsveld, 2016a). Similarly to the soil water exchange frequency, it provides insight into the leaching of nutrients and pollutants, albeit under consideration of the total amount of percolate water as opposed to the ratio of field capacity and percolate water, thereby warranting the investigation of potential relations between percolation rates and the LST/NDVI ratio.

### Results

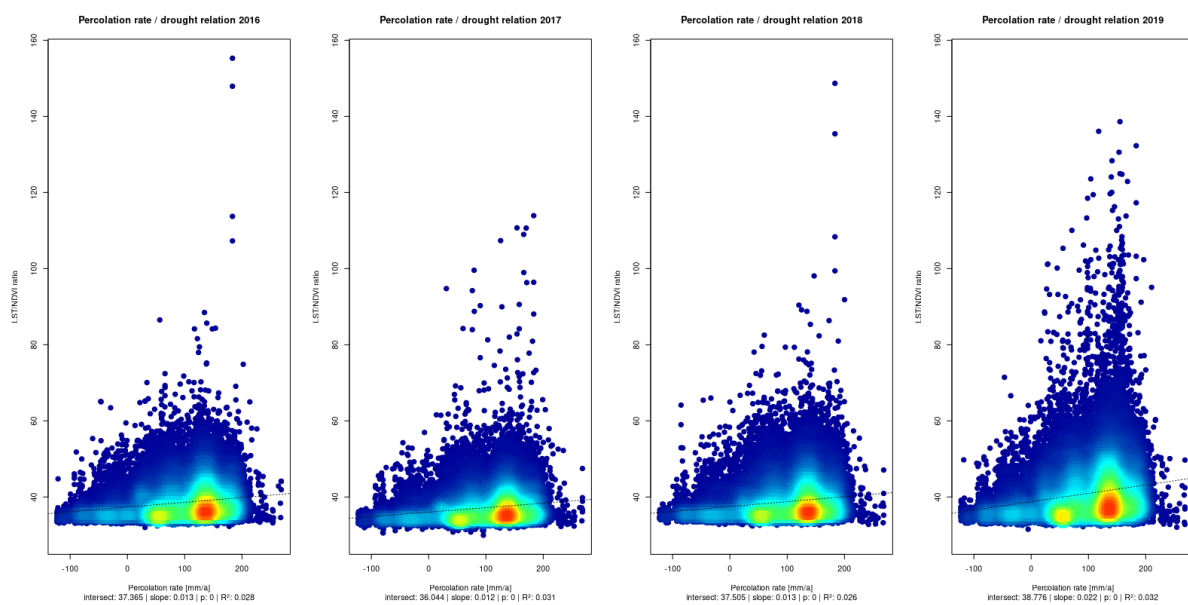


**Figure 12** Percolation rate / drought relation in 2016-2019 (left to right), colours indicating point density ranging from blue (low) via green (medium) to red (high)

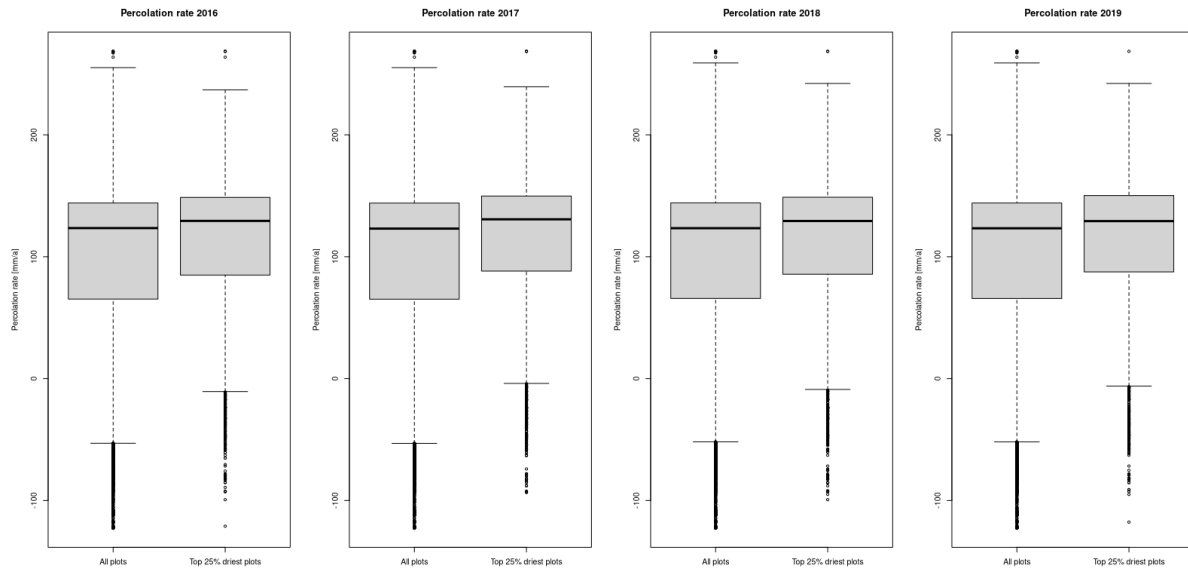


**Figure 13** Boxplots of percolation rates across all plots (respectively left) and the plots with LST/NDVI ratios in the upper quartile thereof in the given year (respectively right), for 2016-2019 (left to right)

**Table 10** Percentiles of percolation rates across all plots and the plots with LST/NDVI ratios in the upper quartile thereof in the given year, maxima and minima excluding outliers (outside 1.5\*IQR)

	2016		2017		2018		2019	
Percentile	All plots	Top 25%	All plots	Top 25%	All plots	Top 25%	All plots	Top 25%
Maximum	255.13	236.83	255.13	239.38	258.93	242.13	258.93	242.13
75th	144.07	148.64	144.00	149.78	144.16	148.77	144.08	150.23
Median	123.46	129.38	123.06	130.70	123.38	129.31	123.31	129.21
25th	65.23	84.95	65.17	88.20	65.75	85.61	65.67	87.53
Minimum	-52.98	-10.56	-53.08	-3.93	-51.87	-8.87	-51.93	-6.12

## Discussion

As percolation rates and soil water exchange frequencies are related, the investigation of relationships to LST/NDVI ratio produces similar results. Plots with low percolation rates, i.e. where almost all water is subject to capillary rise, retained via sufficient field capacity and/or absorbed by vegetation, exhibit generally low LST/NDVI ratios (figure 12). The range of LST/NDVI ratios exhibited by agricultural plots widens with increasing percolation rates, as more water leaves the soil vertically, leaching out nutrients necessary for healthy vegetation, thus contributing to drought characteristics. This results in a conical pattern, with linear regression using the percolation rate as the independent variable seemingly reflecting this behaviour, approximating upwards slopes of LST/NDVI ratio in relation to percolation rates between 0.012 in 2017 and 0.022 in 2019. However, due to the widening range of LST/NDVI values with increasing percolation rates, the share of variance explained by these

regressions remains between 2.6% (2018) and 3.2% (2019). Nonetheless, the relation was found to be significant in all years of interest ( $p$ -value  $< 2.2e-16$ ).

Furthermore, the assumption that high percolation rates imply higher LST/NDVI ratios is reinforced by the comparison of the ranges of percolation rates across all plots and across plots within the upper quartile of LST/NDVI ratio values (figure 13, table 10). Albeit less pronounced than in the case of soil water exchange frequency, plots with high LST/NDVI ratios generally experience higher percolation rates than the total samples, there is still significant overlap between the quartiles. The median percolation rate of the plots most affected by drought-like conditions is, on average, 6 units higher than the median of the respective entire sample. The upper 75th percentile is slightly higher in the plots most affected by drought-like conditions, being roughly 5 units higher than the 75th percentile of the total samples. More pronounced differences are exhibited in the 25th percentiles and the minima, which are, on average, respectively 21 and 45 units above their counterparts in the total sample of the given year.

Whilst overall less pronounced than the relation between soil water exchange frequency and the LST/NDVI ratio, plots strongly affected by drought-like conditions tend to have higher percolation rates. The null hypothesis of no relation between percolation rates and the LST/NDVI ratio can be rejected, indicating the potential of high percolation rates potentially posing a drought hazard.

Furthermore, as previously stated, percolation rates are interdependent with other hydrological variables, such as field capacity. Soil type also influences percolation rates (Köhn et al., 2019), thus positing an interdependence with other site-based variables. These interdependencies, both with hydrological and pedological site-based variables would warrant separate investigations. Potential thematic clusters would posit a basis for further investigation of the influence of these interdependent variables on the LST/NDVI ratio.

### 3.2.4. Field Value

The field value (German “*Ackerzahl*”) is an index assessing soil quality, commonly used in Germany. It is based on the soil value (German “*Bodenwertzahl*”), an assessment of soil type, condition, development and parent material (Hüwe, Roubitschek, 2004, p. 29). The soil value ranks soils on a scale from 1 (very low) to 100 (very high) with regards to their agricultural yield potential and profitability under normal and proper management conditions. The soils found in the study area, mostly sand and moderately loamy soils, usually fall within the lower bounds and middle of the spectrum respectively.

**Table 11** Typical soil values exhibited by different soil types

Type	Lower bound	Upper bound
Sand	0	11
Sandy loam	11	30
Heavy to clayey loam	31	50
Loam partially covered by loess	51	70
Loam covered by loess	71	90
Loess	91	100

The field value further refines the soil value, incorporating site-related factors, such as terrain and climate, e.g. average annual temperature, slope, forest shade, etc. (Ratzke, Mohr, 2005, p. 28). The resulting index ranks soil quality on a scale from 1 (very poor) to 120 (excellent).

## Results

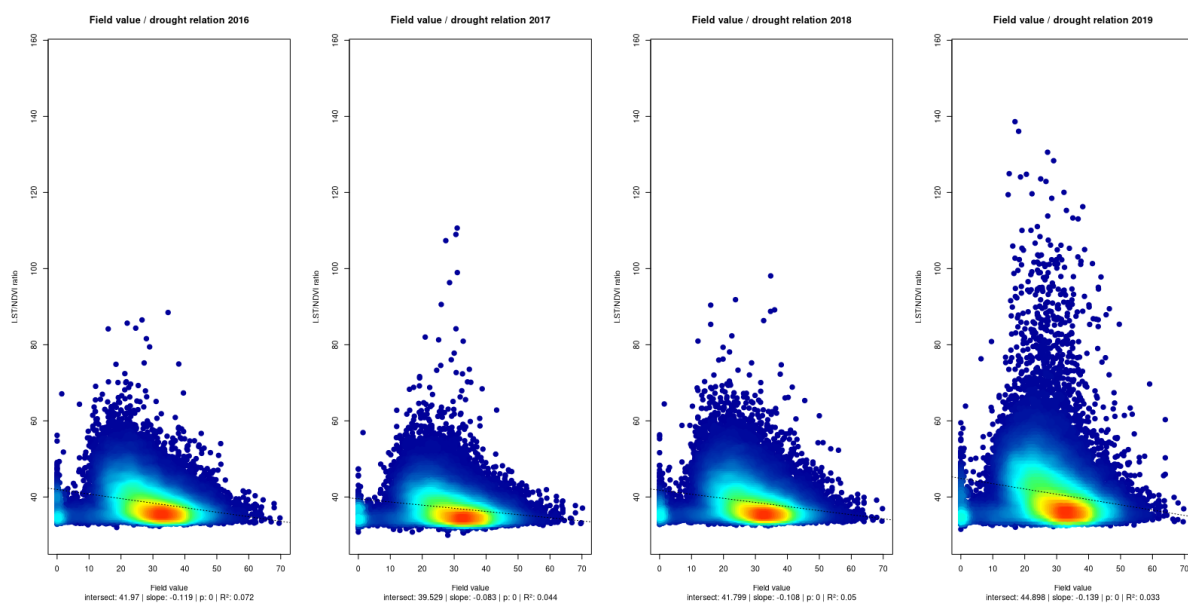


**Figure 14** Field value / drought relation in 2016-2019 (left to right), colours indicating point density ranging from blue (low) via green (medium) to red (high)

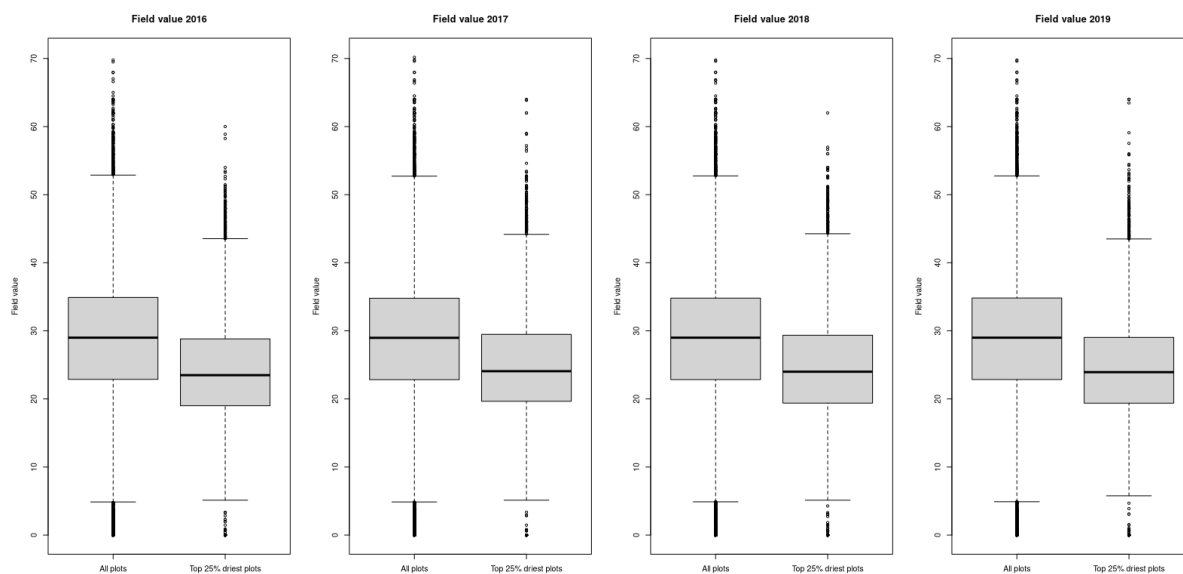


**Figure 15** Boxplots of field values across all plots (respectively left) and the plots with LST/NDVI ratios in the upper quartile thereof in the given year (respectively right), for 2016-2019 (left to right)

**Table 12** Percentiles of field values across all plots and the plots with LST/NDVI ratios in the upper quartile thereof in the given year, maxima and minima excluding outliers (outside  $1.5 \cdot IQR$ )

	2016		2017		2018		2019	
Percentile	All plots	Top 25%	All plots	Top 25%	All plots	Top 25%	All plots	Top 25%
Maximum	52.87	43.53	52.73	44.17	52.76	44.26	52.76	43.49
75th	34.90	28.82	34.79	29.48	34.80	29.36	34.82	29.03
Median	29.00	23.49	28.97	24.08	29.00	24.00	29.00	23.94
25th	22.88	19.00	22.82	19.65	22.83	19.38	22.85	19.38
Minimum	4.87	5.13	4.87	5.13	4.89	5.13	4.90	5.78

## Discussion

When plotting the LST/NDVI ratio against field value (figure 14), the resulting point cloud consistently forms a triangular cluster regardless of the year, with its bottom, horizontal edge delimited by the lower bounds of LST/NDVI ratio values. Throughout all observed years, the general distribution of LST/NDVI values appears to cause the cluster's highest density to form close to the lower LST/NDVI ratio bound, centred on the mean of field values recorded in the study area. Notably, from its densest parts to the periphery, the triangular clusters are slanted, forming slopes, indicating plots exhibiting decreasing ranges of LST/NDVI ratios the higher their mean field value. This leads to the assumption of linear effects and to the implication of more stable conditions on better soils. Linear regression reveals this slope to be most pronounced in 2019 at  $-0.139$ , and least pronounced in 2017 at  $-0.083$ , matching

the respective yearly ranges of LST/NDVI ratio values. However, this converging pattern causes the results of linear regression using field value as the independent variable to seemingly only explain low percentages of variance in LST/NDVI ratio. Out of the four years of interest, the most LST/NDVI ratio variance was explained by the field value in 2016, at 7.2%, and the least in 2019 at 3.3%. Nonetheless, the relation between field value and the LST/NDVI ratio was found to be significant in all years of interest (p-value < 2.2e-16).

The comparison of the distribution of field values across all plots and across plots within the upper quartile of LST/NDVI ratio values (figure 15, table 12) further reinforces the theory that plots more strongly affected by drought-like conditions tend to have lower field values. The median field value of plots with high LST/NDVI ratios is, on average, 5 units lower than the median of the entire sample. Likewise, the maximum field value encountered in high LST/NDVI ratio plots, appears to be, on average, 9 units lower than the sample maximum. In general, the 75th percentile of field values strongly affected by drought-like conditions appears to be roughly equal to median field value of the entire sample, meaning that 75% of field values of high LST/NDVI ratio plots fall within the lower half of field values of the entire sample.

The null hypothesis of no relation between field value and the LST/NDVI ratio can be rejected, leading to the assumption that analysing field values might provide some insight into drought hazard.

Of interest for further investigation might be whether individual soil types throughout the study area exhibit wide ranges of field values, or whether the former stratifies the latter. Should individual soil types exhibit multiple distinct clusters of field values, respective soils could be treated as separate categories for further investigation with regards to influence on the LST/NDVI ratio or potential processes or phenomena.

### 3.2.5. Soil Quality Rating

The Soil Quality Rating (SQR) was developed by the Leibniz Centre for Agricultural Landscape Research (ZALF) to globally classify soil suitability for agricultural use and yield potential. It is based on multiple indicators, such as soil type and maximum root depth, which are weighted and aggregated into a score under consideration of the severity of the local factor limiting agricultural potential the most (BGR, 2014, p. 2). The resulting score ranges from 0 for poor soils to 102 for excellent soils, with quality ranges shown in table 13. Most plots within the study area exhibit SQR scores between the lower 40s and upper 50s, indicating very low to medium soil quality, with outliers ranging from the mid 30s to the upper 70s, thus including soils of extremely low and high soil quality, according to the SQR index.

**Table 13** SQR ranges

Yield potential	Lower SQR bound	Upper SQR bound
Extremely low	0	<35
Very low	35	<50
Low	50	<60
Medium	60	<70
High	70	85
Very high	91	

### Results

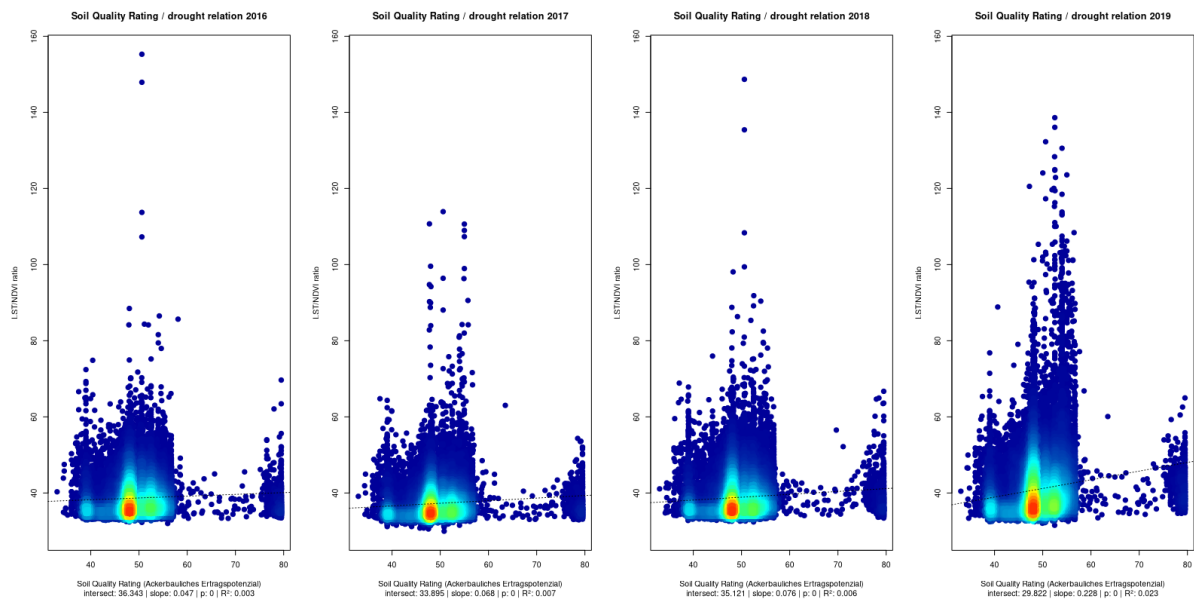


**Figure 16** Soil Quality Rating / drought relation in 2016-2019 (left to right), colours indicating point density ranging from blue (low) via green (medium) to red (high)

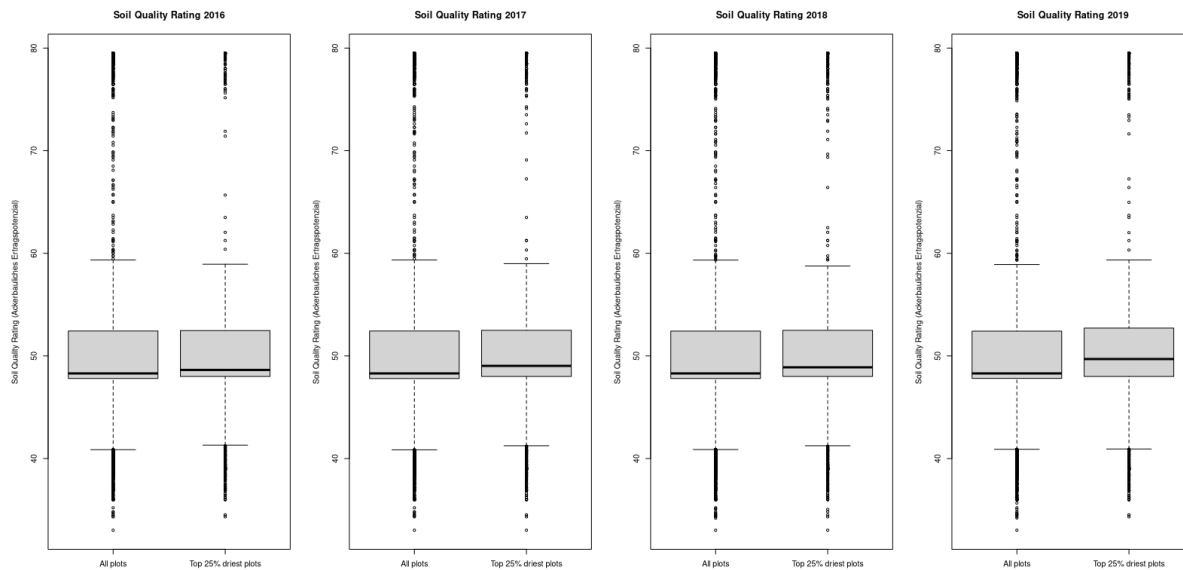


**Figure 17** Boxplots of SQR scores across all plots (respectively left) and the plots with LST/NDVI ratios in the upper quartile thereof in the given year (respectively right), for 2016-2019 (left to right)

**Table 14** Percentiles of SQR scores across all plots and the plots with LST/NDVI ratios in the upper quartile thereof in the given year, maxima and minima excluding outliers (outside  $1.5 \cdot IQR$ )

	2016		2017		2018		2019	
Percentile	All plots	Top 25%	All plots	Top 25%	All plots	Top 25%	All plots	Top 25%
Maximum	59.35	58.94	59.35	58.99	59.34	58.76	58.91	59.35
75th	52.43	52.47	52.43	52.50	52.42	52.50	52.42	52.72
Median	48.30	48.64	48.30	49.03	48.30	48.89	48.30	49.70
25th	47.80	48.00	47.80	48.00	47.81	48.00	47.81	48.00
Minimum	40.86	41.309	40.85	41.25	40.88	41.25	40.90	40.93

## Discussion

In comparison to the field value, the distribution of SQR values is visibly more disjunct, with a gap ranging from the upper 50s to the upper 70s clearly visible in all four examined years (figure 16). This is likely a result of the discrete values of the source raster, with the data points in-between resulting from the calculation of the average score of fields containing source raster pixels with different SQR scores. Linear regression implies a significant relation between SQR and the LST/NDVI ratio ( $p\text{-value} < 2.2e\text{-}16$ ), albeit this relationship is inconsistent. First, the positive slopes calculated counterintuitively imply rising LST/NDVI ratios with increasing soil quality. Second, only a small share of variance in LST/NDVI ratios was explainable using SQR as the independent variable. The highest share of variance in LST/NDVI ratio values explained by the SQR amounted to 2.3% in 2019 with the other years examined falling well below even 1%.



This inconsistent relation between SQR and the LST/NDVI ratio is further exacerbated by the apparent lack of differences in SQR distribution between the entirety of each year's sample and the subset of plots exhibiting LST/NDVI ratios within the upper quartile thereof (figure 17, table 14). Whereas p-values would enable the rejection of the null hypothesis, its inconsistent nature does not exclude the possibility that SQR provides no insight into drought hazard. Comparison with other predictor variables in multivariate linear regression will provide further insight into this apparent inconsistency.

Likely causes for this behaviour include the previously mentioned methodology of the SQR's aggregation, which always only involves the factor inhibiting crop growth the most (BGR, 2014). Approaches involving either analysing individual factors limiting crop growth, e.g. soil type, rooting potential, etc., or aggregate indices including all relevant inhibiting factors, such as in the case of the field value, are likely to provide more insight into drought hazard.

### 3.2.6. Field Capacity

Field capacity describes how much water soils can hold, thereby providing a measure for water available for plant growth. It is dependent on soil type, density, depth and humus content. The method used by the BGR to calculate it contains corrections for land use categories, derived from CORINE land cover classes (Duijnsveld, 2016b).

**Table 15** Classification of field capacity ranges

Class	Lower bound [mm]	Upper bound [mm]
Very low	0	<50
Low	50	<90
Medium	90	<140
High	140	<200
Very high	200	<270
Extremely high	$\geq 270$	

The definition of agricultural droughts is based on low soil moisture levels, thus warranting the analysis of the relation between field capacity and LST/NDVI ratio.

### Results

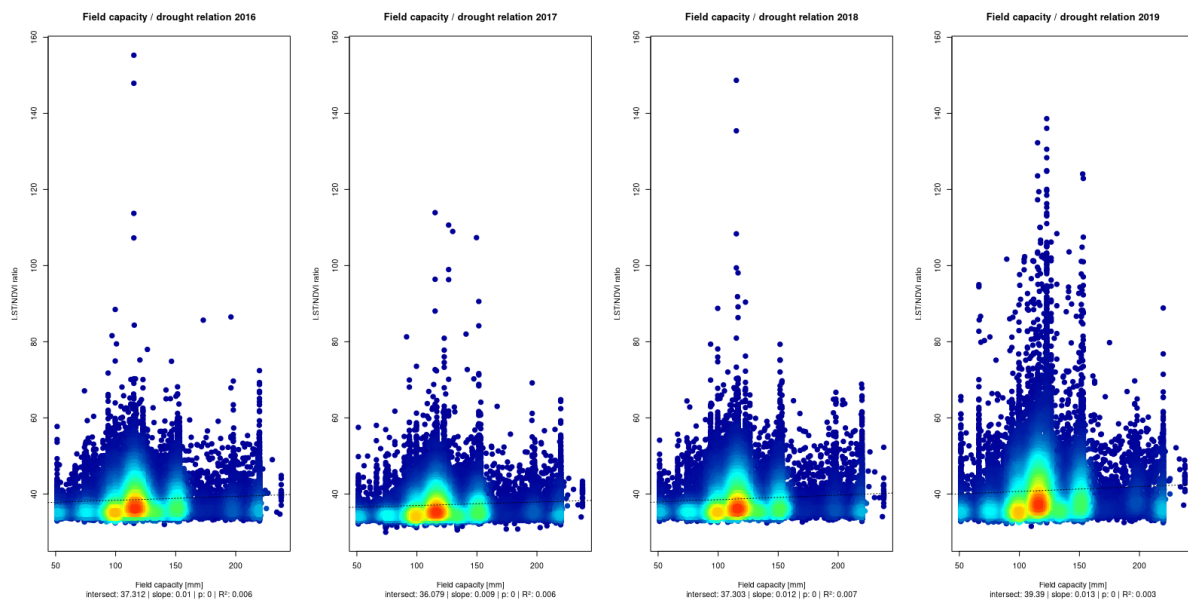


**Figure 18** Field capacity / drought relation in 2016-2019 (left to right), colours indicating point density ranging from blue (low) via green (medium) to red (high)

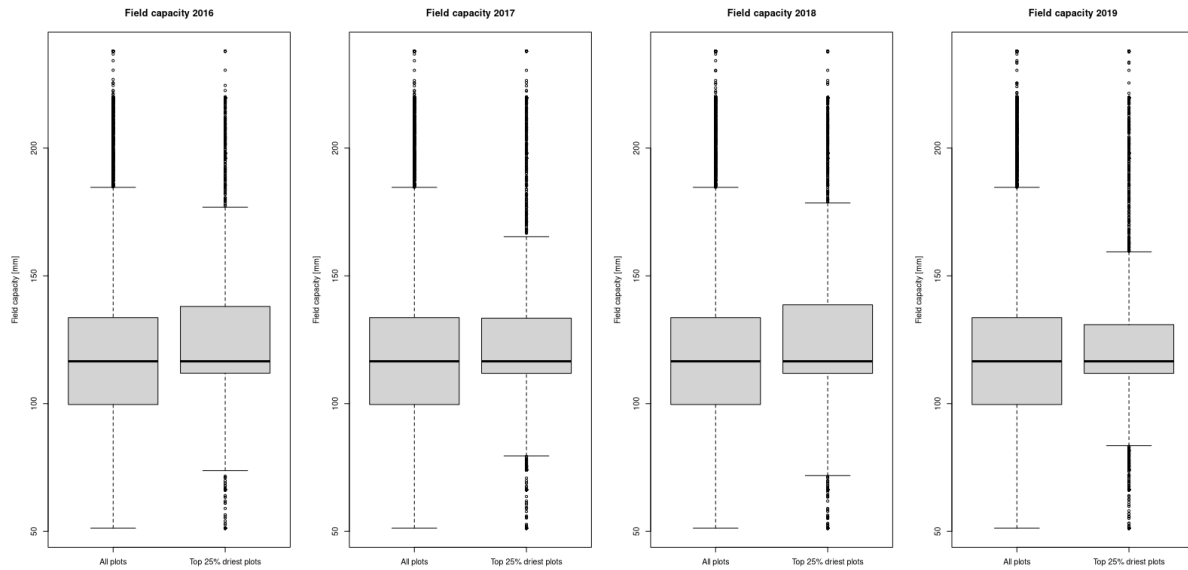


**Figure 19** Boxplots of field capacity across all plots (respectively left) and the plots with LST/NDVI ratios in the upper quartile thereof in the given year (respectively right), for 2016-2019 (left to right)

**Table 16** Percentiles of field capacities [mm] across all plots and the plots with LST/NDVI ratios in the upper quartile thereof in the given year, maxima and minima excluding outliers (outside 1.5\*IQR)

	2016		2017		2018		2019	
Percentile	All plots	Top 25%	All plots	Top 25%	All plots	Top 25%	All plots	Top 25%
Maximum	184.64	176.87	184.64	165.31	184.64	178.52	184.64	159.39
75th	133.65	138.04	133.65	133.44	133.65	138.66	133.65	130.91
Median	116.56	116.56	116.56	116.56	116.56	116.56	116.56	116.56
25th	99.64	111.92	99.64	111.86	99.64	111.86	99.64	111.86
Minimum	51.23	73.77	51.23	79.53	51.23	71.82	51.23	83.50

## Discussion

The behaviour of the LST/NDVI ratio with regards to field capacity, as depicted in figure 18, appears to resemble a Gaussian distribution, rather than a linear relationship. The highest range of LST/NDVI values appears around a median field capacity of 116 mm, with the range of LST/NDVI values diminishing towards both extremes of field capacities found in the study area. Secondary hotspots in point density and spikes can be found at distinct values of the source field capacity raster. The amplitude of the bell-shaped distribution increases with drought severity. Linear regression nonetheless returns significant correlation between the two values ( $p$ -value <  $2.2e-16$ ).

The behaviour described is also reflected in the comparison between field capacities of all plots and those exhibiting LST/NDVI ratios within the respective year's upper quartile thereof

(figure 19, table 16). The field capacities of the plots most affected by drought-like conditions in each year appear to centre around the overall median value, with the median field capacity of both the global and the limited sample being equal. However, the field capacity ranges of plots with high LST/NDVI ratios are smaller than those of the global samples, with higher minima and lower maxima. Notably, whilst the difference between the 75th percentile of LST/NDVI ratios of both the global and the limited sample is small, the 25th percentile of the ratio exhibited by plots highly affected by droughts distinctly approaches the median value, resulting in somewhat top-heavy distributions. Furthermore, despite differing numbers of active plots in each given year, the quartiles of recorded field capacities in all global samples are congruent (see table 16), whereas other continuous data displays some variance, further reinforcing the fundamentally analogous distribution of LST/NDVI values regardless of drought conditions.

The distribution of the data appears to suggest that there is a range of mid to high field capacity values which is related to high LST/NDVI ratios, whereas plots outside this range experience less drought-like conditions. Potential causes for these patterns might be interdependencies with e.g. soil depth or rooting capacity, with soil water reserves potentially inaccessible to the vegetation above, which, however, would warrant its own investigation. Even though linear regression would suggest the possibility of rejecting the initial null hypothesis of no relations between field capacity and LST/NDVI, its likely nonlinearity complicates the matter, warranting further investigation. Multivariate regression might provide further insight.

Furthermore, how much of the field capacity is actually used, i.e. containing water available for vegetation growth, might provide better insight into drought hazard (Samarah, 2005). This, however, would likely depend on precipitation, whose erratic behaviour (DWD, 2019a, p. 20) would make soil moisture indices derived from periodically aggregated remote-sensing data better candidates for the discovery of relations to drought indicators, such as the LST/NDVI ratio. An alternative would be posited by investigating which soil types and/or depths (potentially also in conjunction with hydrological variables, such as percolation rates or relative soil water exchange frequencies) are particularly prone to have depleted field capacities, which then could be interpreted as a potential drought hazard and investigated for relations to drought indices, such as the LST/NDVI ratio.

### 3.2.7. Erosion Potential (Water)

Water-based erosion potential is measured in tonnes per hectare per year.

#### Results

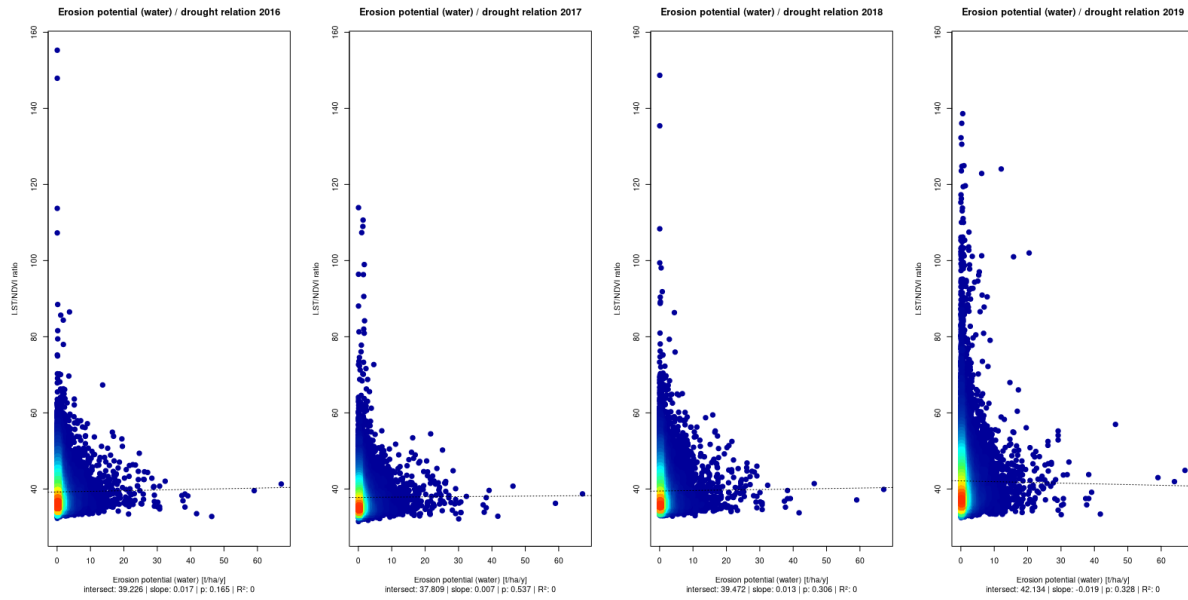


**Figure 20** Potential erosion (water) / drought relation in 2016-2019 (left to right), colours indicating point density ranging from blue (low) via green (medium) to red (high)

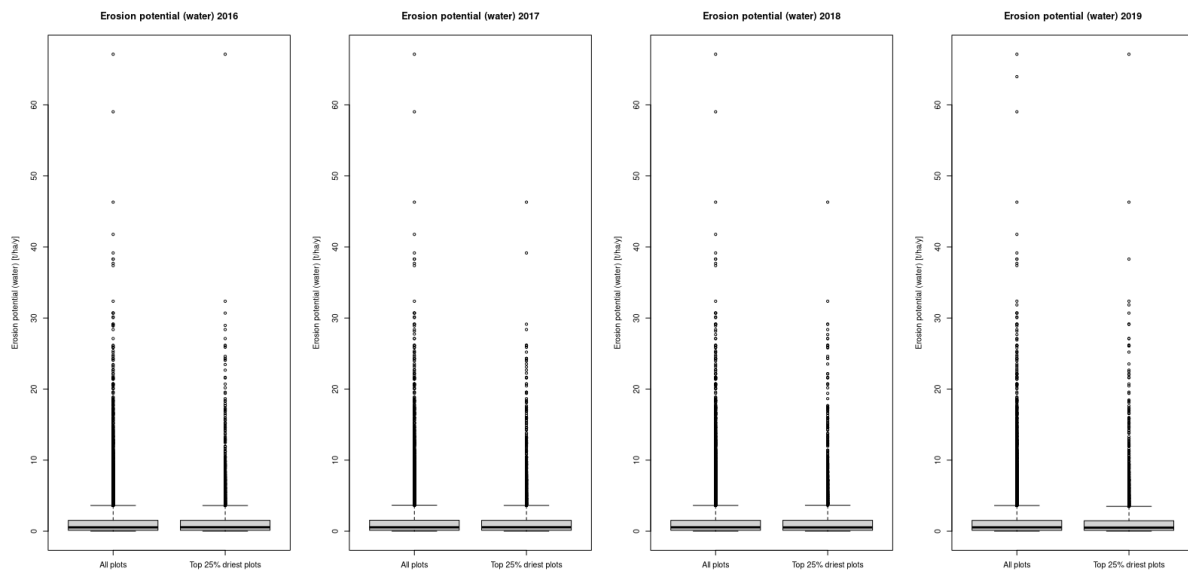


**Figure 21** Boxplots of potential erosion (water) across all plots (respectively left) and the plots with LST/NDVI ratios in the upper quartile thereof in the given year (respectively right), for 2016-2019 (left to right)

**Table 17** Percentiles of potential erosion (water) [t/ha/y] across all plots and the plots with LST/NDVI ratios in the upper quartile thereof in the given year, maxima and minima excluding outliers (outside 1.5\*IQR)

Percentile	2016		2017		2018		2019	
	All plots	Top 25%	All plots	Top 25%	All plots	Top 25%	All plots	Top 25%
Maximum	3.63	3.62	3.66	3.63	3.63	3.65	3.62	3.49
75th	1.53	1.53	1.54	1.53	1.53	1.54	1.52	1.47
Median	0.54	0.55	0.55	0.56	0.54	0.53	0.54	0.51
25th	0.12	0.13	0.13	0.13	0.13	0.13	0.13	0.12
Minimum	0	0	0	0	0	0	0	0

## Discussion

Most plots within the study area exhibit no or very low potential for water-based erosion, causing the widest ranges of the LST/NDVI ratio to form at the erosion potential minimum (figure 20). Linear regression reveals no significant relationship between water erosion potential and the LST/NDVI ratio (p-values 0.165, 0.537, 0.306, 0.328 for 2016-2019). The distribution of water erosion potential values is equal between the entire sample and the plots exhibiting LST/NDVI values within the upper quartile thereof in all years of interest (figure 21, table 17). The analysis was repeated for the upper quartile of water erosion potential values, resulting in nearly identical patterns, with clustering near the absolute minimum of values and the distribution of potential water erosion values not changing between the upper quartile sample and the 25% of plots most affected by drought-like conditions therein. Therefore, the null hypothesis of no relation between water-based erosion potential and the LST/NDVI ratio could not be disproven. Likewise, it could not be disproven that the examination of water-based erosion potential provides no insight into drought hazard.

Furthermore, as surface erosion and drought are interdependent (Thurow, Taylor, 1999, p. 1), with prolonged droughts accelerating erosion, ambiguous categories such as “erosion potential” are unlikely to provide insight into drought hazard. Perhaps it would be more insightful to investigate potential correlations between erosion empirically measured, rather than predicted, and drought indicators. This would likely also relate to other site-based variables, particularly soil type and horizontal water runoff and be dependent on the amount of rainfall during the study period (MLUK, 2020a, p. 3), opening the potential of investigating respective thematic clusters and drought hazard.

### 3.2.8. Multivariate Linear Regression

Mathematically, the null hypothesis of no relation to LST/NDVI ratios across the study area was disproven for all continuous variables except for water-based erosion potential. However, plausible linear relations were only discovered for three out of the six variables, i.e. soil water exchange frequency, percolation rate, and field value. To ascertain the nature of these presumed relations and their ability to identify potential drought hazards, multivariate linear regression was performed using all variables as predictor variables and only those with presumed implications on the LST/NDVI ratio. In the former case, variables the algorithm found to be insignificant ( $p$ -value  $> 0.05$ ) in a given year were iteratively removed and the respective regression repeated.

#### Results

**Table 18** P-values of all continuous data sets when used as predictor variables for multivariate regression of LST/NDVI ratios

Predictor	2016	2017	2018	2019
Soil water exchange frequency	$< 2.2e-16$	$< 2.2e-16$	$6.6e-11$	0.004
Percolation rate	$3.6e-4$	$1.7e-8$	$2.1e-6$	$1.2e-7$
Field value	$< 2.2e-16$	$< 2.2e-16$	$< 2.2e-16$	$< 2.2e-16$
Soil Quality Rating	$1.1e-13$	0.016	0.275	$< 2.2e-16$
Field capacity	$< 2.2e-16$	$< 2.2e-16$	$< 2.2e-16$	$1.7e-4$
EP(W)	$6.8e-9$	$3.0e-7$	$6.1e-7$	$3.7e-7$

**Table 19** Multivariate regression of LST/NDVI ratios using all continuous data sets as predictor variables, duplicate years marked with an asterisk indicate repetition of the regression without variables previously found to be insignificant

Year	Adjusted R <sup>2</sup>	Residual Standard Error	Error Rate	p-value	Insignificant variables
2016	14.12%	4.272	11.05%	$< 2.2e-16$	
2017	10.05%	3.943	10.58%	$< 2.2e-16$	
2018	11.08%	4.737	12.19%	$< 2.2e-16$	Soil Quality Rating
2018*	11.08%	4.737	12.19%	$< 2.2e-16$	
2019	8.19%	7.646	18.62%	$< 2.2e-16$	

**Table 20** Beta coefficients and t values of soil water exchange frequency (SWEF), percolation rate (PR), field value (FV), Soil Quality Rating (SQR), field capacity (FC) and water-based erosion potential (EP(W)) when used as predictor variables for multivariate regression of LST/NDVI ratios

Predictor	2016		2017		2018		2019		Mean	
	Beta coeff.	t value	Beta coeff.	t value	Beta coeff.	t value	Beta coeff.	t value	Beta coeff.	t value
SWEF	0.012	12.51	0.008	8.57	0.007	6.53	0.005	2.87	0.008	7.62
PR	0.003	3.57	0.004	5.64	0.004	4.74	0.007	5.30	0.005	4.81
FV	-0.184	-58.91	-0.142	-49.49	-0.184	-54.05	-0.251	-45.75	-0.190	-52.05
SQR	-0.048	-7.43	-0.015	-2.41	-0.008	-1.09	0.109	9.30	0.010	-0.41
FC	0.018	12.72	0.012	9.51	0.015	9.73	0.010	3.75	0.014	8.93
EP(W)	-0.067	-5.80	-0.053	-5.12	-0.062	-4.99	-0.099	-5.08	-0.070	-5.25

**Table 21** Multivariate regression of LST/NDVI ratios using soil water exchange frequency, percolation rate and field value as predictor variables

Year	Adjusted R <sup>2</sup>	Residual Standard Error	Error Rate	p-value
2016	13.63%	4.140	10.71%	< 2.2e-16
2017	11.09%	3.756	10.08%	< 2.2e-16
2018	10.86%	4.533	11.67%	< 2.2e-16
2019	8.81%	7.286	17.74%	< 2.2e-16

**Table 22** Beta coefficients and t values of soil water exchange frequency (SWEF), percolation rate (PR) and field value (FV) when used as predictor variables for multivariate regression of LST/NDVI ratios

Predictor	2016		2017		2018		2019		Mean	
	Beta coeff.	t value	Beta coeff.	t value	Beta coeff.	t value	Beta coeff.	t value	Beta coeff.	t value
SWEF	0.014	24.52	0.010	20.62	0.011	17.85	0.014	14.83	0.012	19.46
PR	0.008	17.93	0.008	20.47	0.010	19.44	0.018	22.92	0.011	20.19
FV	-0.127	-54.36	-0.096	-45.44	-0.125	-49.56	-0.158	-39.19	-0.127	-47.14

## Discussion

Whereas single linear regression only rejected water-based erosion potential as a predictor variable for the LST/NDVI ratio, the results of multivariate regressions using all continuous variables covered in this analysis as predictor variables for the LST/NDVI ratio are



inconsistent with this conclusion. When using all analysed continuous variables as predictor variables for the LST/NDVI ratio (table 18), all of them were identified to significantly influence the latter, with the exception of the Soil Quality Rating in 2018 (p-value 0.275). All predictors achieved p-values below 0.05, although in 2017, the SQR's p-value was only 0.016, which could have been classified as statistically insignificant were one to use a different threshold for significance. Whereas field value consistently displayed statistically significant influence on the LST/NDVI ratio (p-value < 2.2e-16), soil water exchange frequency and percolation rates performed less consistently, albeit still being statistically significant. Notably, in 2019, the p-value of SWEF was only 0.004.

However, inconsistent patterns emerge when observing the nature of the influence of each indicator on the LST/NDVI ratio. As seen in table 20, the SQR's presumed influence on the LST/NDVI ratio fluctuates, with its beta coefficients being negative from 2016 to 2018, but positive in 2019, further casting doubt on the ability of the SQR to provide insight into drought hazard. The beta coefficients of field capacity and water-based erosion potential appear more consistent, although previous findings contend with these regression results. In the case of the relationship between LST/NDVI ratios and field capacity, the suspicion of nonlinearity and interdependencies, see section 3.2.6., suggests that the latter is not a suitable predictor variable for linear regressions. Furthermore, as discussed in section 3.2.7., the generally low water erosion potential throughout the study area causes high LST/NDVI ratio values to be more likely to appear in the lower bounds of the former, likely resulting in negative beta coefficients, wrongly suggesting that higher erosion potential correlates to lower LST/NDVI ratios. Aside from that, due to feedback loops between droughts and erosion potential (Thurow, Taylor, 1999, p. 1), the latter cannot be considered an independent variable used to predict the former.

The performance of regressions using all available continuous data sets as predictor variables (table 19) varies when compared to the regressions performed using only soil water exchange frequency, percolation rate and field value as predictor variables (table 21). The use of all continuous data sets as predictor variables leads to higher rates of LST/NDVI ratio variance explained in 2016 and 2018, whilst explaining less in 2017 and 2019. The error rate of the models using all continuous data sets as predictor variables however, is higher in all years of interest, suggesting the models using only soil water exchange frequency, percolation rate and field value as predictor variables to be more accurate.

The investigation of the beta coefficients and their associated t-test values reveals field value to exert the greatest influence on the outcome of the LST/NDVI ratio prediction (table 20, 22) and does so consistently (table 18). Higher field values are therefore strongly related to lower LST/NDVI ratios. Regression results further support the assumption that higher soil water exchange frequencies and percolation rates statistically significantly contribute to high LST/NDVI ratios.

Out of the continuous variables investigated in this thesis, field value, soil water exchange frequency and percolation rate can therefore be assumed to provide the most insight into drought hazard. Nonetheless, it has to be noted that, as previously stated, multiple of the predictor variables used are likely interdependent, thereby not positing independent variables as necessitated for regression.

### 3.2.9. UFZ Drought Monitor Data

The Soil Moisture Index ranges between 0 and 1, with its value indicating the commonness of comparable soil moisture in a reference period between 1951 and 2015. For example, an SMI of 0.2 would indicate that such dryness only occurs in 20% of months in the reference period (Marx et al., 2016, p. 136). The SMI is available for the entire soil and the topsoil, the latter defined as 25 cm depth (Marx et al., 2016, p. 137). The Drought Magnitude is an index increasing with prolonged negative divergence from the 20th percentile of the SMI, aggregated for growing periods between April and October. It is calculated both using the topsoil SMI and the SMI for the entire soil. Both indices are calculated using the hydrological model system mHM (Samaniego et al., 2010; Kumar et al., 2013).

### Results

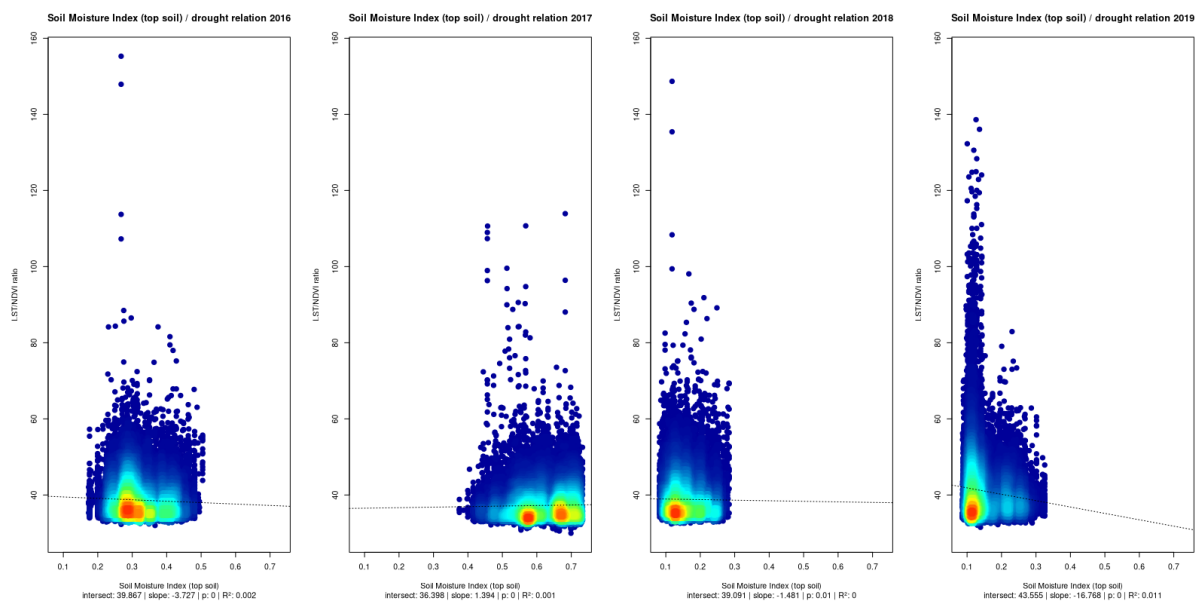


**Figure 22** Soil Moisture Index (top soil) / drought relation in 2016-2019 (left to right), colours indicating point density ranging from blue (low) via green (medium) to red (high)

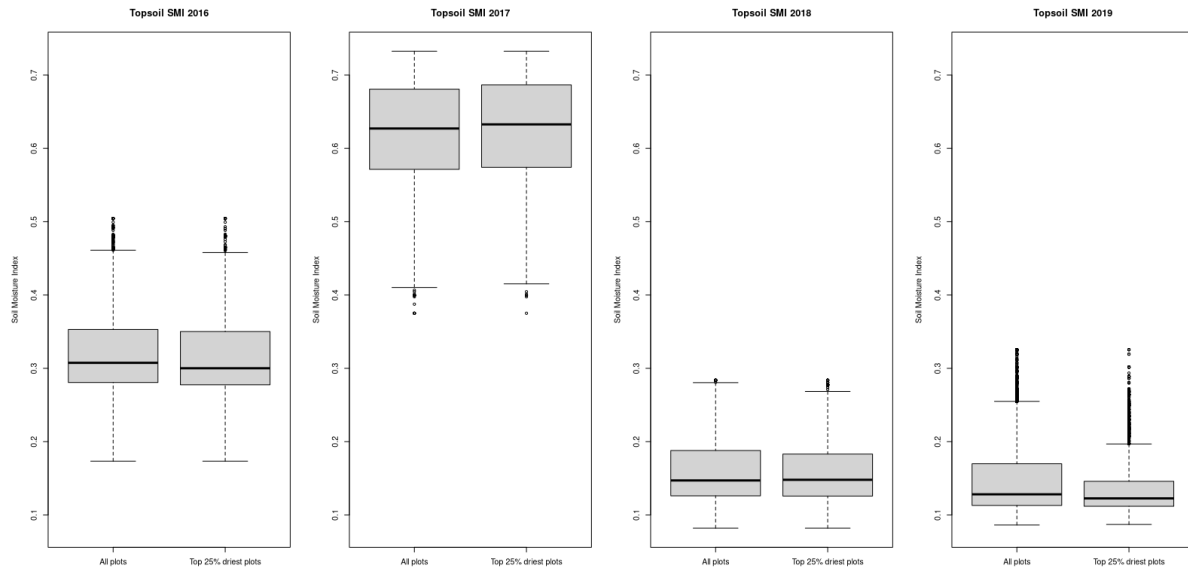


**Figure 23** Boxplots of topsoil Soil Moisture Index across all plots (respectively left) and the plots with LST/NDVI ratios in the upper quartile thereof in the given year (respectively right), for 2016-2019 (left to right)

**Table 23** Percentiles of topsoil Soil Moisture Index values across all plots and the plots with LST/NDVI ratios in the upper quartile thereof in the given year, maxima and minima excluding outliers (outside 1.5\*IQR)

	2016		2017		2018		2019	
Percentile	All plots	Top 25%	All plots	Top 25%	All plots	Top 25%	All plots	Top 25%
Maximum	0.46	0.46	0.73	0.73	0.28	0.27	0.26	0.20
75th	0.35	0.35	0.68	0.69	0.19	0.18	0.17	0.16
Median	0.31	0.30	0.63	0.63	0.15	0.15	0.13	0.12
25th	0.28	0.28	0.57	0.57	0.13	0.13	0.11	0.11
Minimum	0.17	0.17	0.41	0.42	0.08	0.08	0.09	0.09

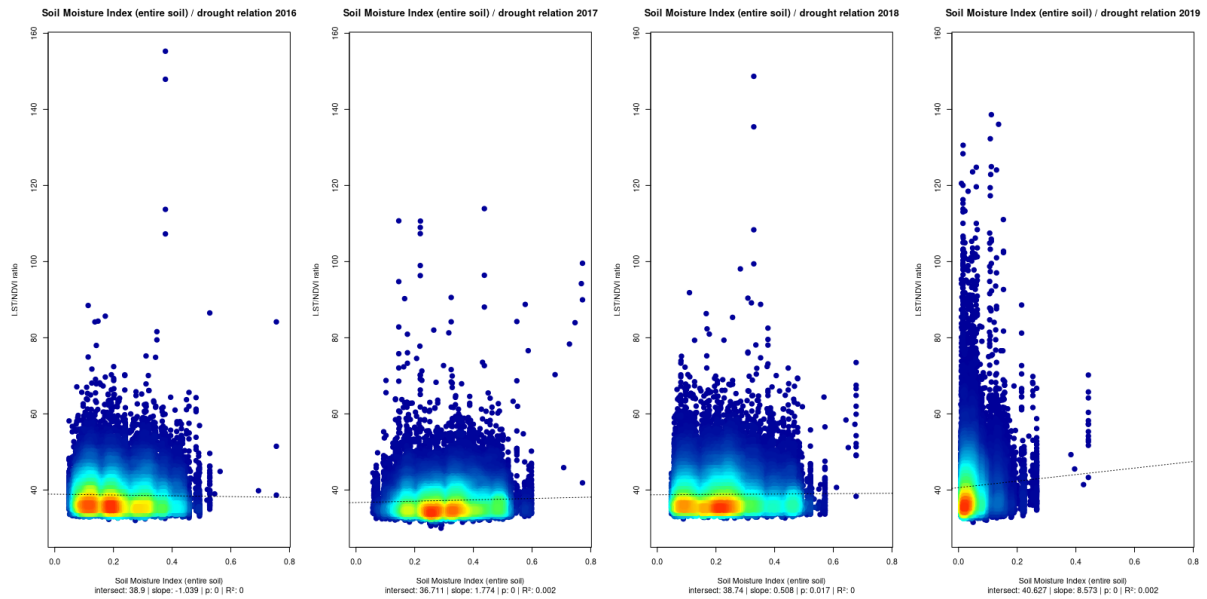


**Figure 24** Soil Moisture Index (entire soil) / drought relation in 2016-2019 (left to right), colours indicating point density ranging from blue (low) via green (medium) to red (high)

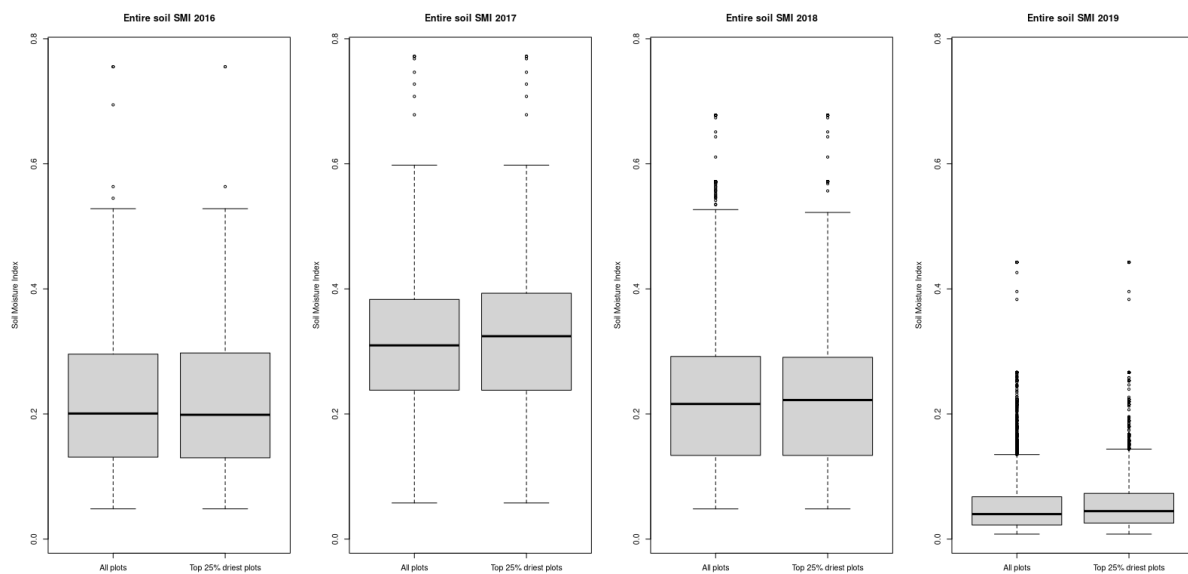


**Figure 25** Boxplots of entire soil Soil Moisture Index across all plots (respectively left) and the plots with LST/NDVI ratios in the upper quartile thereof in the given year (respectively right), for 2016-2019 (left to right)

**Table 24** Percentiles of entire soil Soil Moisture Index values across all plots and the plots with LST/NDVI ratios in the upper quartile thereof in the given year, maxima and minima excluding outliers (outside 1.5\*IQR)

	2016		2017		2018		2019	
Percentile	All plots	Top 25%	All plots	Top 25%	All plots	Top 25%	All plots	Top 25%
Maximum	0.53	0.53	0.60	0.60	0.53	0.52	0.14	0.14
75th	0.30	0.30	0.38	0.39	0.29	0.29	0.07	0.07
Median	0.20	0.20	0.31	0.32	0.22	0.22	0.04	0.05
25th	0.13	0.13	0.24	0.24	0.13	0.13	0.02	0.03
Minimum	0.05	0.05	0.06	0.06	0.05	0.05	0.01	0.01

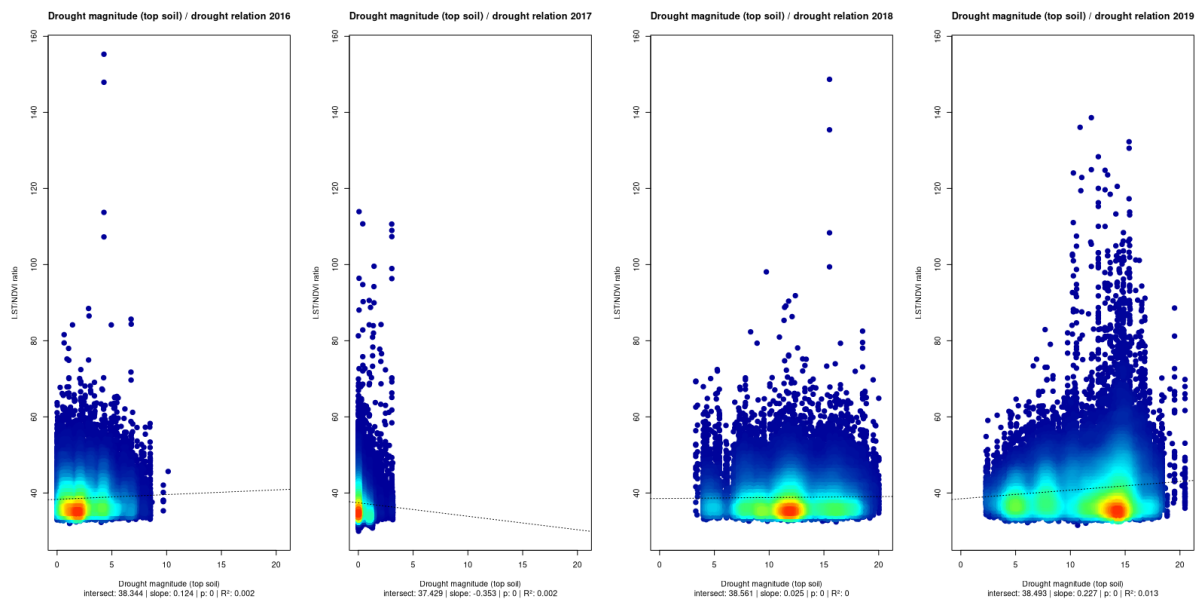


**Figure 26** Drought Magnitude (top soil) / drought relation in 2016–2019 (left to right), colours indicating point density ranging from blue (low) via green (medium) to red (high)

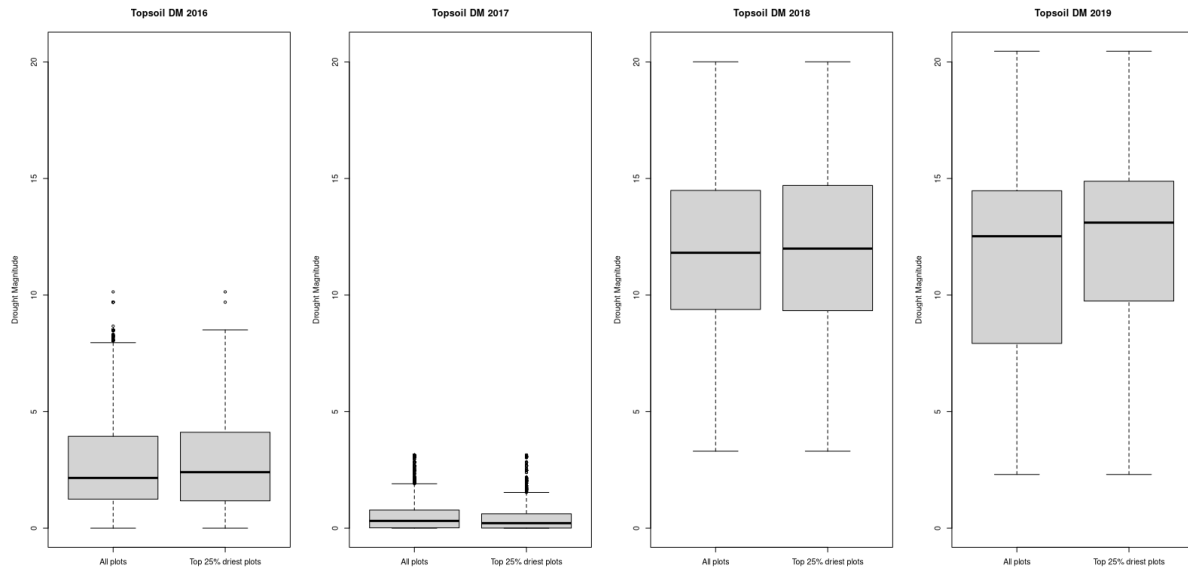


**Figure 27** Boxplots of topsoil Drought Magnitude across all plots (respectively left) and the plots with LST/NDVI ratios in the upper quartile thereof in the given year (respectively right), for 2016-2019 (left to right)

**Table 25** Percentiles of topsoil Drought Magnitude values across all plots and the plots with LST/NDVI ratios in the upper quartile thereof in the given year, maxima and minima excluding outliers (outside  $1.5 \cdot IQR$ )

	2016		2017		2018		2019	
Percentile	All plots	Top 25%	All plots	Top 25%	All plots	Top 25%	All plots	Top 25%
Maximum	7.96	8.51	1.91	1.54	20.01	20.01	20.46	20.46
75th	3.94	4.12	0.78	0.62	14.49	14.70	14.48	14.88
Median	2.16	2.41	0.31	0.22	11.81	11.99	12.53	13.11
25th	1.25	1.18	0.02	0.00	9.38	9.33	7.93	9.74
Minimum	0.00	0.00	0.00	0.00	3.30	3.30	2.31	2.31

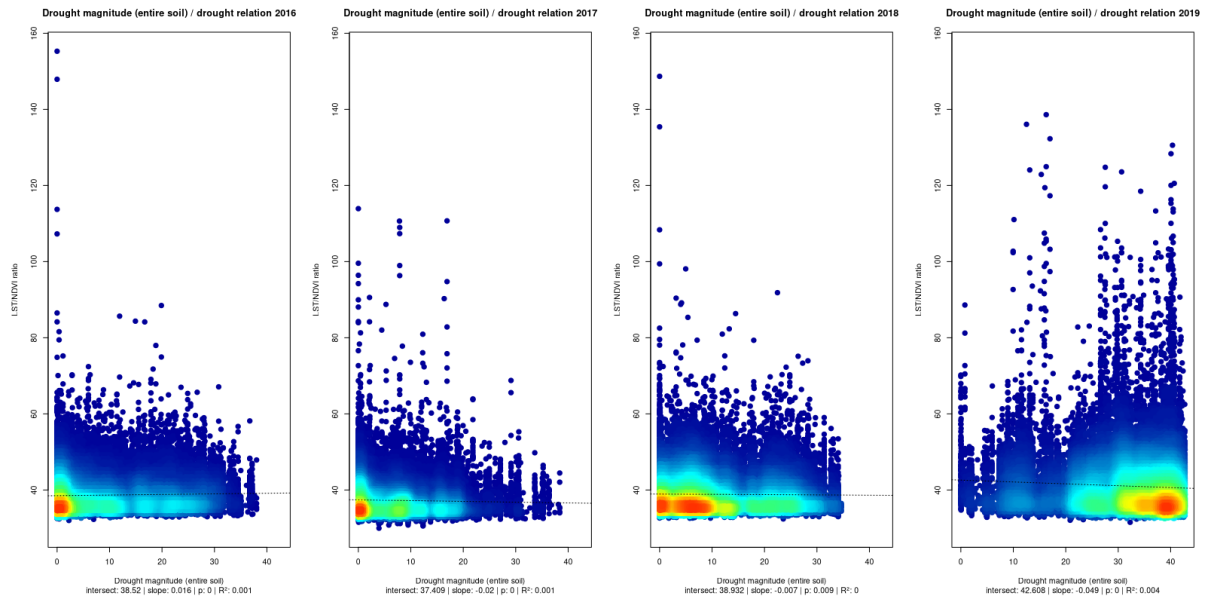


**Figure 28** Drought Magnitude (entire soil) / drought relation in 2016-2019 (left to right), colours indicating point density ranging from blue (low) via green (medium) to red (high)

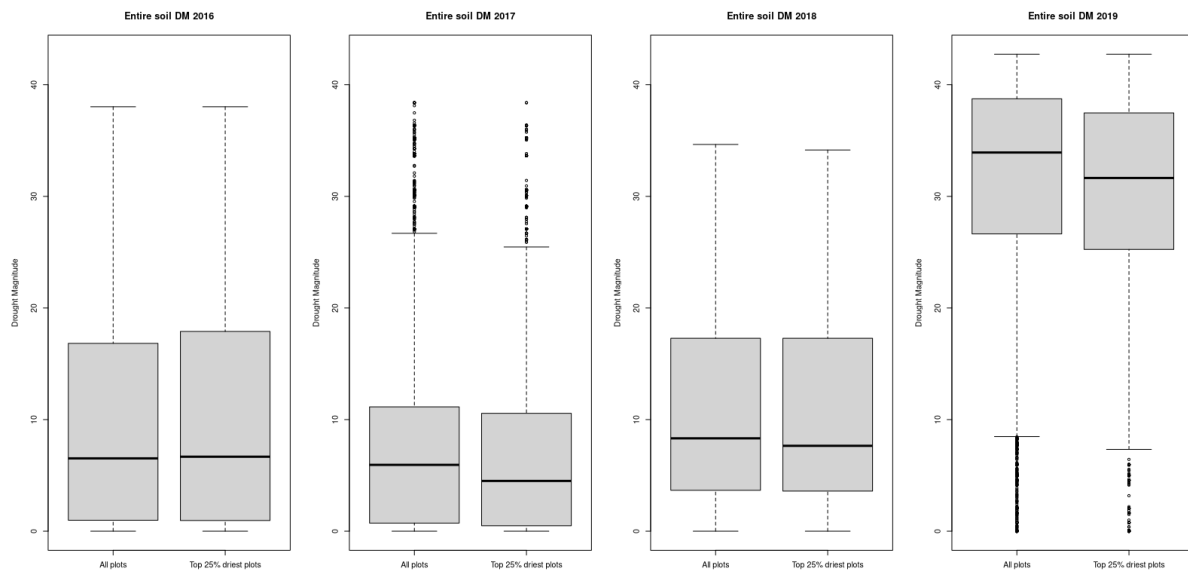


**Figure 29** Boxplots of entire soil Drought Magnitude across all plots (respectively left) and the plots with LST/NDVI ratios in the upper quartile thereof in the given year (respectively right), for 2016-2019 (left to right)

**Table 26** Percentiles of entire soil Drought Magnitude values across all plots and the plots with LST/NDVI ratios in the upper quartile thereof in the given year, maxima and minima excluding outliers (outside 1.5\*IQR)

Percentile	2016		2017		2018		2019	
	All plots	Top 25%	All plots	Top 25%	All plots	Top 25%	All plots	Top 25%
Maximum	38.03	38.03	26.69	25.47	34.65	34.16	42.73	42.73
75th	16.8	17.90	11.14	10.56	17.28	17.28	38.74	37.48
Median	6.53	6.67	5.94	4.50	8.32	7.65	33.93	31.65
25th	0.98	0.96	0.73	0.49	3.67	3.59	26.64	25.24
Minimum	0.00	0.00	0.00	0.00	0.00	0.00	8.48	7.33

## Discussion

The values of the Soil Moisture Index and Drought Magnitude match expectations based on government reports (DWD, 2019a, p. 20) and calculated drought severity in the years of interest (see section 3.1.), both for the topsoil and the entire soil.

For topsoil SMI (figure 22), 2016 exhibits average low- to mid-range values, with a hotspot at 0.3, the distribution drastically shifts to the upper end of the spectrum in 2017, with hotspots around 0.55 and 0.65, and then drops to values almost entirely between 0.1 and 0.3 for the drought years of 2018 and 2019, with hotspots in both years barely above SMIs of 0.1. A lagged pattern emerges for SMI values calculated for the entire soil (figure 24), with 2016 plots showing values between 0.1 and ca. 0.5, with hotspots at 0.1 and 0.2, indicating dry conditions in the entire soil. These slowly improved in 2017, exhibiting a range between 0.1 and 0.6, with hotspots at ca. 0.3, before overall decreasing in 2018, with the highest data point density around an SMI of 0.2, and a drastic reduction to values almost entirely between 0.0 (indicating unprecedented drought in the entire soil) and ca. 0.2.

In 2016, topsoil DM shows drought effects on some plots, albeit the data points for a hot spot around DM values of ca. 2, ranging up to 10 (figure 26). In 2017, topsoil DM values are predominantly 0, with some plots reaching values of up to 3-4, indicating almost no drought conditions in the topsoil. This changes in 2018, when the range shifts upwards, reaching values up to 20, with a hotspot at ca. 12, indicating prolonged drought conditions. This is exacerbated in 2019, with the hotspot shifting to ca. 14. When examining DM values for the entire soil (figure 28), a lagged pattern emerges. Whilst overall drought magnitudes exhibit much wider ranges from 0 up to the upper 30s, in 2016, the highest data point density is in the lower ranges, around 0, indicating that even in a year with average climatic conditions, such as 2016, drought effects in the entire soil are present, but limited. The density around the lower range of DM values further increases in 2017, as soil moisture conditions improve. In 2018, as the drought begins, DM values slowly increase, with the highest density hotspot now diffusely ranging from 0 to 10, indicating that some plots still had enough moisture in the soil not to diverge from the 20th percentile of the SMI in the reference period, whereas some were already diverging for some time. The distribution dramatically shifts in 2019. In the second year of the drought, DM values in the entire soil are densest between 20 and 40,



with the highest density found at a DM value of ca. 39, indicating prolonged drought-like conditions.

This lagged pattern appears plausible due to soil moisture first leaving the upper layers of the soil via evaporation and percolation into lower soil layers. Without precipitation providing sufficient replacement, the drought effects permeate through the entire soil, thus leading to extreme conditions in the entire soil to manifest later.

When visually inspecting the LST/NDVI ratio for relations to the SMI or DM, few concrete behaviours immediately stand out. Particularly high ratios cluster around the lowest topsoil SMI and the highest topsoil DM values in 2019. Linear regression, however, recognizes statistically significant relations between all four indices and the LST/NDVI ratio. With regards to SMI, the p-value of these is lowest at 0.01 for topsoil SMI and 0.02 for entire soil SMI in 2018, which could be considered insignificant depending on the threshold chosen. Similarly, for DM, the p-value of these detected relationships is lowest at  $3.6e-4$  for topsoil DM and 0.009 for entire soil DM in 2018.

Furthermore, the correlations detected between these indices and the LST/NDVI ratio are inconsistent. With regards to SMI, positive slopes were detected in 2017, implying rising LST/NDVI ratios with higher soil moisture. In 2019, negative slopes were detected with regards to DM, implying declining LST/NDVI ratios with increasing drought magnitude.

The inconsistency of these patterns warranted the comparison of the values of these indices across entire samples and the subset of plots exhibiting LST/NDVI ratios within the upper quartile thereof in each year, as shown in figures 23, 25, 27 and 29 respectively. No dramatic changes were visible, with the aforementioned exception of 2019, with noticeably lower topsoil SMI values (figure 23, table 23) and noticeably higher topsoil drought magnitudes (figure 27, table 25) on plots with most drought-like conditions. However, the opposite can be observed for entire soil DM values in 2019, which are, counterintuitively, noticeably lower on plots with most drought-like conditions (figure 29, table 26).

Whilst linear regression suggests partially significant relations between the LST/NDVI ratio and both the SMI and the drought magnitude, these relations are incoherent. Conditions modelled by mHM will likely only be weakly reflected by LST/NDVI values exhibited by agricultural plots throughout the study area, if at all. This however, might change with prolonged drought conditions, as clearer patterns emerged in the second year of the drought. Depletion of soil water reserves modelled by mHM could potentially be reflected by higher LST/NDVI values, albeit this would have to be studied over longer drought situations. Furthermore the greenest pixel NDVI composites used to calculate the LST/NDVI values likely contain signals affected by irrigation, which neither the SMI nor the DM derived thereof account for. Further distortions in potential relations between DM and the LST/NDVI ratio might be caused by the varying aggregation periods. Whereas drought magnitudes are aggregated for entire growing periods between April and October of each year, the LST and NDVI rasters used throughout this thesis were aggregated to the water-dependent growing period between May and September.

Nonetheless, as both the SMI and the DM are modelled indices, rather than site-related variables, they cannot be considered suitable to provide insight into drought hazard.

### 3.3. Categorical Data

#### 3.3.1. Crop and Agricultural Land Use Type

In each year of interest, an average of 130 individual crop or agricultural land use types could be found on the agricultural plots throughout the study area. The ten most common varieties on all plots, as well as the subset of plots with LST/NDVI ratios within the upper quartile thereof, were compared for each year. Furthermore, it was investigated which crop varieties or agricultural land use types exhibited the best and worst LST/NDVI ratios in each year.

#### Results

**Table 27** Ten most common agricultural land use types across all plots and the plots with LST/NDVI ratios in the upper quartile thereof in the given year, underscores indicate types more common in plots with more drought-like conditions, legend to IACS agricultural land use type codes in table 29

2016		2017		2018		2019									
All plots		Top 25%		All plots		Top 25%		All plots		Top 25%		All plots		Top 25%	
Type	Count	Type	Count	Type	Count	Type	Count	Type	Count	Type	Count	Type	Count	Type	Count
452	7627	<u>121</u>	1933	452	7845	<u>121</u>	2297	452	8006	<u>121</u>	1615	452	8308	<u>121</u>	1761
451	6736	<u>424</u>	1368	451	6897	<u>62</u>	1294	451	7043	<u>591</u>	1458	451	7254	<u>591</u>	1470
<u>121</u>	4927	<u>62</u>	1298	<u>121</u>	4574	<u>424</u>	1248	<u>121</u>	4596	<u>424</u>	1282	<u>121</u>	4954	<u>424</u>	1217
<u>424</u>	3652	452	620	<u>424</u>	3709	452	565	<u>424</u>	3695	<u>411</u>	632	<u>424</u>	3224	<u>411</u>	843
<u>62</u>	2333	451	568	<u>62</u>	2456	451	521	<u>591</u>	3377	452	571	<u>591</u>	2914	452	761
411	2224	<u>591</u>	410	411	1904	<u>115</u>	385	<u>411</u>	1605	451	498	<u>411</u>	2461	451	747
115	1425	411	407	<u>115</u>	1470	<u>143</u>	380	115	1439	<u>143</u>	412	115	1572	<u>422</u>	302
311	1125	<u>143</u>	371	131	1141	<u>156</u>	276	131	1157	<u>230</u>	252	131	1286	<u>143</u>	274
131	1093	<u>422</u>	275	311	1079	<u>230</u>	265	311	1103	115	242	<u>143</u>	810	115	253
156	863	115	274	<u>143</u>	815	<u>591</u>	243	<u>143</u>	811	<u>422</u>	207	<u>422</u>	784	131	242

**Table 28** Relative share of ten most common agricultural land use types across all plots and plots with LST/NDVI ratios in the upper quartile thereof in the given year, underscores indicate types more common in plots with more drought-like conditions, legend to IACS agricultural land use type codes in table 29

2016		2017		2018		2019									
All plots	Top 25%	All plots	Top 25%	All plots	Top 25%	All plots	Top 25%								
Type	%	Type	%	Type	%	Type	%								
452	18.5	<u>121</u>	18.7	452	18.7	<u>121</u>	22.0	452	18.8	<u>121</u>	15.2	452	19.4	<u>121</u>	16.5
451	16.3	<u>424</u>	13.2	451	16.5	<u>62</u>	12.4	451	16.6	<u>591</u>	13.7	451	17.0	<u>591</u>	13.8
<u>121</u>	11.9	<u>62</u>	12.6	<u>121</u>	10.9	<u>424</u>	11.9	<u>121</u>	10.8	<u>424</u>	12.1	<u>121</u>	11.6	<u>424</u>	11.4
<u>424</u>	8.9	452	6.0	<u>424</u>	8.9	452	5.4	<u>424</u>	8.7	<u>411</u>	6.0	<u>424</u>	7.5	<u>411</u>	7.9
<u>62</u>	5.7	451	5.5	<u>62</u>	5.9	451	5.0	<u>591</u>	7.9	452	5.4	<u>591</u>	6.8	452	7.1
411	5.4	<u>591</u>	4.0	411	4.6	<u>115</u>	3.7	<u>411</u>	3.8	451	4.7	<u>411</u>	5.8	451	7.0
115	3.5	411	4.0	<u>115</u>	3.5	<u>143</u>	3.6	115	3.4	<u>143</u>	3.9	115	3.7	<u>422</u>	2.8
311	2.7	<u>143</u>	3.6	131	2.7	<u>156</u>	2.6	131	2.7	<u>230</u>	2.4	131	3.0	<u>143</u>	2.6
131	2.6	<u>422</u>	2.7	311	2.6	<u>230</u>	2.5	311	2.6	115	2.8	<u>143</u>	1.9	115	2.4
156	2.1	115	2.7	<u>143</u>	2.0	<u>591</u>	2.3	<u>143</u>	1.9	<u>422</u>	2.0	<u>422</u>	1.8	131	2.3

**Table 29** Legend to IACS agricultural land use type codes in tables 27 and 28

Code	IACS land use type	Code	IACS land use type
62	Fallow	311	Winter rapeseed
115	Winter wheat	411	Silage maize
121	Winter rye	422	Clover grassland
131	Winter barley	424	Ley grassland
143	Winter oats	451	Meadows
156	Winter triticale	452	Mowing meadows
230	Lupinus	591	Non-active fields

**Table 30** Ranks of IACS agricultural land use types with regards to median LST/NDVI ratios, ranging from 1 (lowest ratio) to -1 (highest ratio) due to the unequal amount of categories in every year of interest

Rank	2016	2017	2018	2019
1	Conservation areas	Conservation areas	Conservation areas	Conservation areas
2	Sugar beets	Brassica rapa	Hemp	Hemp
3	Turf	Energy forestry	Turf	Turf
4	Cabbage	Mowing meadows	Mowing meadows	Mowing meadows
5	Sudan grass	Szarwasi grass	Meadows	Cabbage
...	...	...	...	...
-5	Winter emmer/ Einkorn wheat	Dry lawn, heath	Dry lawn, heath	Lentils
-4	Dry lawn, heath	Tobacco	Other stone fruit	Tomatoes
-3	Leek	Wine	Garden cress	Cichorium
-2	Energy forestry	Celery	Mustard	Wine
-1	Wine	Non-listed variety	Wine	Other vegetables

## Discussion

When observing the varieties of crops and agricultural land use types of all plots throughout the study area (tables 27, 28), the first thing to note is that the relative rank of each type remains comparable. Across all plots in each given year, mowing meadows always form the largest group, followed by meadows, winter rye, ley grassland and fallows or non-active fields on rank five. Ranks six and seven, silage maize and winter wheat, are also constant throughout the studied years. The eight through tenth most common crop or land use varieties include winter barley, winter oats, winter triticale, winter rapeseed and clover grassland.

This relatively stable pattern is overturned when examining only the crop and agricultural land use types of the plots whose LST/NDVI ratio falls within the upper quartile thereof. Their complex behaviour can be classified into three groups. First are crop varieties and agricultural land use types that are relatively more common in plots strongly affected by drought-like conditions as compared to the overall sample of the respective year. In tables 27 and 28, these are underscored. The opposite thereof forms the second group, crop varieties and agricultural land use types that are relatively less common in plots strongly affected by drought-like conditions as compared to the overall sample of the respective year. In tables 27 and 28, these are not underscored. The former group includes fallows, winter rye, winter oats, lupinus, clover grassland, ley grassland and non-active fields. The latter group includes winter barley, winter rapeseed, meadows and mowing meadows. Some crop types exhibit inconsistent behaviour. When compared to the respective total sample, the relative commonness in relation to plots with LST/NDVI ratios in the upper quartile thereof

decreases for winter wheat in 2016, 2018 and 2019, but increases in 2017, decreasing for winter triticale in 2016 but increasing in 2017, and decreases for silage maize in 2016 and 2017, but increases in 2018 and 2019. These inconsistent varieties constitute a third group.

This would indicate that crop varieties and agricultural land use types falling within the first group (relatively more common on plots with high LST/NDVI ratios), constitute a potential drought hazard, whereas varieties less common on plots with high LST/NDVI ratios appear more resilient.

However, it is notable that the upper half of most common crop types and agricultural land use types are never displaced from the top 10, nor do practices not represented in the overall top 10 enter the upper half of most common practices when examining the subset of plots most affected by drought-like conditions. This indicates statistical effects. The likelihood of types more common in the overall sample to appear in the subset of plots most affected by drought-like conditions is higher than that of less common types. Nonetheless, as the high shares of these practices in the overall sample do not prevent the order from changing when limited to the subset of plots in the upper quartile of LST/NDVI ratios, these statistical effects appear less pronounced than the relation between crop variety or agricultural land use type and the LST/NDVI ratio.

Of further interest is the observation that whilst their relative ranks changed, the constituents of the ten most common crop varieties and agricultural land use types remained the same in 2019, in contrast to all other years of interest. This might suggest that the initial shock of drought onset in 2018 only affected those types more vulnerable to it, but by the second drought year the effects had mounted to such a degree that the LST/NDVI ratio uniformly rose across all vegetation types on agricultural plots within the study area.

Furthermore, it is notable that the most common crop varieties and agricultural land use types include several winter varieties that are sown in autumn or winter, thus bolting in spring, where they exhibit their highest NDVI values. Whilst this state might have been captured in satellite imagery at the beginning of the growing period and therefore might still be reflected in the greenest pixel NDVI components, it is noteworthy that such plots might display high temperatures and low NDVI values when the crops are ripe or already harvested, leaving barren soil. This might further lead to the association of LST values to NDVI values measured on plants primarily grown during the year prior. This issue could be addressed by investigating when each pixel reached its maximum NDVI value during the respective growing period (greenest pixel), albeit the aggregation of these dates to plot level would pose further issues. Whereas the use of greenest pixel NDVI components somewhat mitigates the issue of individual plant phenology with regards to soil barrenness, restricting the observations to crops growing throughout the summer and commonly harvested in autumn might provide scientifically more robust results. Nonetheless, such varieties form a minority in the study area, wherefore results thereof might not provide insight into overall drought hazards in the study area.

In the same vein, agricultural plots containing fallows or non-active fields are more common throughout plots with LST/NDVI ratios within the upper quartile thereof as compared to the total yearly samples. This is likely due to self-intensifying feedback loops, i.e. the lack of vegetation on fallows leading to high land surface temperatures due to the lack of cover and

resulting in low NDVI values, thus causing high ratios. A similar process might be assumed for non-active fields, although prolonged lack of management might provide some leeway for the intrusion of wild vegetation.

Potential relations of interest might arise in the case of clover and ley grassland, which are often grown with the intent of high biomatter production, either for animal fodder or as energy crops (Hartmann, Stickse, 2010). Whereas one might assume that this practice would imply stronger irrigation and therefore lower LST/NDVI values, these two classes are relatively more common on plots with LST/NDVI ratios within the upper quartile thereof as compared to the total yearly samples. Reasons might include high mowing frequencies or low root depth. However, either case would rather imply common drought-like conditions due to intensive agricultural use, rather than a reduction in plant productivity due to drought-like conditions. This issue too, might be somewhat mitigated by the use of greenest pixel NDVI composites, which are more likely to depict photosynthetically active vegetation, thus lending more credence to the notion that the cultivation of clover or ley grassland might pose a drought hazard.

When ranking all crop varieties and agricultural land use types found within each year according to the median LST/NDVI ratio exhibited by plots they apply to, see table 30, regardless of their absolute count, some commonalities appear. In all four years, plots particularly designated as conservation areas are least affected by drought-like conditions. Likewise, the production of grasses is linked with low prevalence of drought-like conditions. This can likely be explained by deliberate irrigation to produce biomass (energy forestry), animal fodder (mowing meadows) or pasture (meadows), as well as for direct sale of grass in the form of turf. Sudan grass, notably, is a so-called cover crop, used in soil management. Hemp is one of the fastest-growing plants on Earth. All of these cultivation types would imply high biomass, and therefore high NDVI values (Rouse et al., 1973) and comparatively low LST/NDVI ratios. On the other end of the spectrum are extensively managed monocultures, such as tomatoes or wine, for the production of which soils are often weeded to prevent wild plants from syphoning nutrients away from the crops (Guerra, Steenwerth, 2012), resulting in barren soils between rows of e.g. grapevines.

Albeit this cursory overview of crops exhibiting low and high LST/NDVI ratios is insufficient to display any concrete trends with regard to drought hazard, it does serve to support the assumption that crop variety does have an impact on the value of LST/NDVI ratio itself. Plants that tend to produce high amounts of biomass, such as hemp, or that are deliberately grown to be as green as possible (turf), lower the LST/NDVI ratio by the nature of their being. On the other hand, however, cultivation types involving weeding, thereby exposing bare soil, exhibit high land surface temperatures and low NDVI values, thus leading to high LST/NDVI ratios.

### 3.3.2. Soil Type

In each year of interest, an average of 30 individual soil types could be found on the agricultural plots throughout the study area. The ten most common types found across all plots within the study area, as well as across the subset of plots with LST/NDVI ratios within the upper quartile thereof, were compared for each year.

#### Results

**Table 31** Ten most common soil types across all plots and the plots with LST/NDVI ratios in the upper quartile thereof in the given year, underscores indicate types more common in plots with more drought-like conditions, legend to soil type abbreviations in table 33

2016		2017		2018		2019									
All plots	Top 25%	All plots	Top 25%	All plots	Top 25%	All plots	Top 25%								
Type	Count	Type	Count	Type	Count	Type	Count								
S	154 50	S	671 8	S	157 67	S	672 5	S	159 96	S	679 3	S	160 19	S	695 2
SI	933 9	SI	228 1	SI	944 4	SI	229 2	SI	961 4	SI	226 9	SI	967 5	SI	223 1
IS	627 1	IS	631	IS	627 8	IS	647	IS	636 1	IS	702	IS	644 6	IS	665
Mo	493 1	<u>SL</u>	66	Mo	507 0	Mo/ S	99	Mo	511 8	<u>SL</u>	103	Mo	515 7	<u>Mo/ S</u>	102
Mo/ S	192 8	Mo/ S	50	<u>Mo/ S</u>	192 7	<u>SL</u>	94	Mo/ S	194 2	Mo/ S	87	<u>Mo/ S</u>	196 8	<u>SL</u>	75
<u>SL</u>	717	Mo	48	<u>SL</u>	718	Mo	60	<u>SL</u>	737	Mo	63	<u>SL</u>	751	Mo	73
L	365	<u>sL</u>	11	L	370	<u>sL</u>	18	L	374	<u>sL</u>	19	L	372	<u>sL</u>	16
LM o	298	L	10	LM o	306	L	10	LM o	305	L	11	LM o	314	L	9
Mo/ IS	155	<u>Mo/ S</u>	6	Mo/ IS	162	<u>Mo/ S</u>	3	Mo/ IS	162	<u>Mo/ S</u>	6	Mo/ IS	167	<u>Mo/ S</u>	9
S/ Mo	151	Mo/ IS	3	S/ Mo	154	S/ Mo	3	S/ Mo	153	<u>SM o</u>	4	S/ Mo	152	Mo/ IS	4

**Table 32** Relative share of ten most common soil types across all plots and the plots with LST/NDVI ratios in the upper quartile thereof in the given year, underscores indicate types more common in plots with more drought-like conditions, legend to soil type abbreviations in table 33

2016		2017		2018		2019									
All plots	Top 25%	All plots	Top 25%	All plots	Top 25%	All plots	Top 25%								
Type	%	Type	%	Type	%	Type	%								
<u>S</u>	37.4	<u>S</u>	65.2	<u>S</u>	37.7	<u>S</u>	64.3	<u>S</u>	37.6	<u>S</u>	63.9	<u>S</u>	37.4	<u>S</u>	65.0
SI	22.6	SI	22.1	SI	22.6	SI	22.0	SI	22.6	SI	21.6	SI	22.6	SI	20.9
IS	15.2	IS	6.1	IS	15.0	IS	6.2	IS	15.0	IS	6.6	IS	15.1	IS	6.2
Mo	12.0	<u>SL</u>	0.6	Mo	12.1	Mo/ <u>S</u>	0.9	Mo	12.0	<u>SL</u>	1.0	Mo	12.0	<u>Mo/S</u>	1.0
Mo/ <u>S</u>	4.7	Mo/ <u>S</u>	4.9	<u>Mo/S</u>	4.6	<u>SL</u>	0.9	Mo/ <u>S</u>	4.6	Mo/ <u>S</u>	0.8	<u>Mo/S</u>	4.6	<u>SL</u>	0.7
<u>SL</u>	1.7	Mo	0.6	<u>SL</u>	1.7	Mo	0.6	<u>SL</u>	1.7	Mo	0.6	<u>SL</u>	1.8	Mo	0.7
L	0.9	<u>sL</u>	0.1	L	0.9	<u>sL</u>	0.2	L	0.9	<u>sL</u>	0.2	L	0.9	<u>sL</u>	0.2
LMo	0.7	L	0.1	LMo	0.7	L	0.1	LMo	0.7	L	0.1	LMo	0.7	L	0.1
Mo/ <u>IS</u>	0.4	<u>Mo/S</u>	0.1	Mo/ <u>IS</u>	0.4	<u>Mo/S</u>	0.0	Mo/ <u>IS</u>	0.4	<u>Mo/S</u>	0.1	Mo/ <u>IS</u>	0.4	<u>Mo/S</u>	0.1
<u>S/Mo</u>	0.4	Mo/ <u>IS</u>	0.0	<u>S/Mo</u>	0.4	<u>S/Mo</u>	0.0	<u>S/Mo</u>	0.4	<u>SMo</u>	0.0	<u>S/Mo</u>	0.4	Mo/ <u>IS</u>	0.0

**Table 33** Legend to soil type abbreviations in tables 31 and 32

Code	IACS land use type	Code	IACS land use type
S	Sand	SMo	Sand, moor
SI	Slightly loamy sand	LMo	Loam, moor
IS	Loamy sand	MoS	Moor, sand
SL	Very loamy sand	S/Mo	Sand on moor
L	Loam	Mo/S	Moor on sand
sL	Sandy Loam	Mo/IS	Moor on loamy sand
Mo	Moor		



**Table 34** Ranks of soil types with regards to median LST/NDVI ratios, ranging from 1 (lowest ratio) to -1 (highest ratio) due to the unequal amount of categories in every year of interest

Rank	2016	2017	2018	2019
1	Moor on clay	Moor, loam	Moor on clay	Clay, moor
2	Moor, loam	Moor on clay	Moor on loam	Loam on sand
3	Moor on loam	Moor on loam	Loam, moor	Loam, moor
4	Loam, moor	Loam, moor	Clay	Moor on clay
5	Loam on moor	Loam on moor	Loam	Moor, loam
...	...	...	...	...
-5	Loamy sand on clay	Loamy sand on clay	Slightly loamy sand	Slightly loamy sand
-4	Slightly loamy sand	Sand on clay	Heavy loam on sand	Slightly loamy sand on heavy loam
-3	Sand on clay	Sand	Sand on heavy loam	Sand on clay
-2	Sand	Slightly loamy sand on heavy loam	Moor, clay	Sand
-1	Heavy loam on sand	Sand on heavy loam	Sand	Sand on heavy loam

## Discussion

As was to be expected, the overall shares of soil type remain unchanged relative to the years of interest when observing the total study area, with sand, slightly loamy sand and loamy sand dominating the soils of the study area, with moors constituting a further large group on place four (table 31). However, when observing only the upper quartile of plots with the highest LST/NDVI ratio, a threefold pattern emerges. Firstly, the three most common soil types maintain their relative rank regardless of whether all plots are examined or only the subset of plots with most drought-like conditions. This is likely due to their disproportionate commonness, as compared to other, less common soils. This leads to the soil types most common in the total sample also being the most common in all subsets. Second, when comparing the fourth-, fifth- and sixth-most common soils in the total sample and the subset, one can notice the respective soils changing ranks relative to each other. Moors, the fourth-most common soils in the total sample, drop to sixth place in all subsets of plots with most drought-like conditions. Very loamy sand, the sixth-most common soil type in the total sample, ascends to the fourth place when observing the subsets of most plots most affected by drought-like conditions, with the exception of 2019, where it ranks fifth behind moor on sand, which in the other years of interest maintained its fifth position regardless of set examined. This might suggest that very loamy sand posits a stronger drought hazard than moors on sand and moors. Lastly, beyond this point, all further soil types found within the subsets of plots with most drought-like conditions occur so rarely that ranking them hardly yields statistically significant results. With very loamy sand displacing moor-type soils in occurrences on plots with high LST/NDVI ratios, the examination of soil types suggests that

sandy substrate posits a stronger drought hazard than moors, conforming with the state of research (Huang, Hartemink, 2020).

This assumption is further reinforced by the changes observed in the relative shares of soil types on plots highly affected by drought-like conditions in comparison to the total samples, which are shown in table 32. Changes in relative distribution show that regardless of the year, plots in the upper quartile of high LST/NDVI values are much more likely to be on sandy terrain. Whereas in the total samples, sand (class S) forms the soil of, on average, 37.5% of plots, this figure increases to an average of 64.6% on plots with most drought-like conditions. Furthermore, when ranking all soil types according to the median LST/NDVI ratio of agricultural plots thereupon (table 34), sand consistently ranks among the soil types with the highest ratios, further supporting the suggestion of sandy terrain positing a drought hazard. Moors, clays and loams exhibit lower LST/NDVI values, albeit the statistical rarity of some types would warrant the further investigation of the significance of these results. This reinforces the suggestion that soil type does posit a drought hazard, particularly the more the substrate is characterised by sand.

### 3.3.3. Rooting Capacity

Rooting capacity is directly derivative of soil depth and delimited by bedrock or groundwater influenced horizons. The BGR divides maximum root depth into ten classes, ranging from 3m maximum root depth to 20m. The commonness of these types across all plots within the study area, as well as across the subset of plots with LST/NDVI ratios within the upper quartile thereof, were compared for each year.

### Results

**Table 35** Maximum root depth classes across all plots and the plots with LST/NDVI ratios in the upper quartile thereof in the given year, underscores indicate types more common in plots with more drought-like conditions, class names indicate maximum root depth in metres

2016		2017		2018		2019									
All plots		Top 25%		All plots		Top 25%		All plots		Top 25%					
Type	Count	Type	Count	Type	Count	Type	Count	Type	Count	Type	Count				
20	225 68	20	692 5	20	228 56	20	699 1	20	233 04	20	714 1	20	233 84	20	686 6
6	803 9	6	139 7	6	809 2	6	150 2	6	814 5	6	153 6	6	823 4	6	140 3
3	387 1	3	381	3	396 7	3	561	3	402 0	3	447	3	406 0	3	794
8	163 3	8	225	8	165 6	8	253	8	169 8	8	292	8	172 2	8	290
13	136 3	13	150	13	143 6	13	122	13	146 0	13	125	13	147 8	13	131
5.5	301	5.5	91	7	304	<u>5.5</u>	74	5.5	316	5.5	74	5.5	316	<u>12</u>	109
7	295	<u>7.5</u>	65	<u>5.5</u>	301	<u>12</u>	62	7	294	<u>12</u>	62	7	289	5.5	73
12	215	12	52	<u>12</u>	222	7	56	<u>12</u>	235	<u>7.5</u>	58	<u>12</u>	232	<u>7.5</u>	64
<u>7.5</u>	213	7	51	7.5	206	7.5	52	<u>7.5</u>	217	7	47	<u>7.5</u>	208	7	47
4	71	4	17	4	86	4	12	4	90	5	17	4	90	4	14

**Table 36** Relative share of maximum root depth classes across all plots and the plots with LST/NDVI ratios in the upper quartile thereof in the given year, class names indicate maximum root depth in metres

2016		2017		2018		2019							
All plots		Top 25%		All plots		Top 25%		All plots		Top 25%			
Type	%	Type	%	Type	%	Type	%	Type	%	Type	%		
20	58.9	20	74.0	20	58.4	20	72.2	20	58.6	20	58.4	20	70.1
6	21.9	6	14.9	6	20.1	6	15.5	6	20.5	6	20.1	6	14.3
3	10.1	3	4.1	3	10.1	3	5.8	3	10.1	3	10.1	3	8.1
8	4.3	8	2.4	8	4.2	8	2.6	8	4.3	8	4.3	8	3.0
13	3.6	13	1.6	13	3.7	13	1.6	13	3.8	13	3.7	13	1.3
5.5	0.8	5.5	1.0	7	0.8	5.5	0.8	5.5	0.8	5.5	0.8	12	0.1
7	0.8	7.5	0.7	5.5	0.8	12	0.6	7	0.7	12	0.6	7	0.7
12	0.6	12	0.6	12	0.6	7	0.6	12	0.6	7.5	0.6	12	0.6
7.5	0.6	7	0.5	7.5	0.5	7.5	0.5	7.5	0.5	7	0.5	7.5	0.5
4	0.2	4	0.2	4	0.2	4	0.1	4	0.2	5	0.2	4	0.1

## Discussion

In the case of maximum rooting capacity, the geographical distribution of soil depth throughout the study area is strongly reflected in both the yearly total samples and the subset of plots in the upper quartile of high LST/NDVI ratios, as changes in the ranking only start occurring in the five least common classes, with the exception of the least common class, whose rank is also stable (table 35). As the observation of total counts alone appears to lack any discernible pattern, changes in the relative share were also analysed (table 36). When examining the latter, it becomes noticeable that the most common class in the total samples, a depth of 20 m, is significantly more common in the subsets of plots with high LST/NDVI ratios. Whereas, on average, 58.6% of all agricultural plots lie on 20m deep soil, this figure rises to, on average, 72.3% for plots with high LST/NDVI ratios, at the detriment of most other classes. Albeit no coherent pattern emerges with regards to the other soil depth classes, this might suggest that water reserves in particularly deep soils might be too far below the surface to be available for agriculturally cultivated crops or that leaching has deposited nutrients necessary for plant health into depths unavailable to crops. Soil depth might therefore be considered a drought hazard. Interdependence between rooting capacity, soil type, percolation rates and field value would warrant further research, as e.g. water could quickly percolate through deep sand layers into depths inaccessible to vegetation thereupon (Huang, Hartemink, 2020, p. 7).

### 3.3.4. Erosion Potential (Wind)

The BGR classifies agricultural plots in Germany into six categories with regards to wind-based erosion potential.

**Table 37** BGR wind erosion classes

Type	Danger of wind erosion
0	None
1	Very little
2	Little
3	Medium
4	High
5	Very High

To evaluate whether wind erosion potential has an influence on the distribution of LST/NDVI ratio, the occurrence of wind erosion classes was analysed for all plots throughout the study area and plots with LST/NDVI ratios within the upper quartile thereof in each year of interest.

### Results

**Table 38** Most common wind erosion classes across all plots and the plots with LST/NDVI ratios in the upper quartile thereof in the given year

2016		2017		2018		2019									
All plots	Top 25%	All plots	Top 25%	All plots	Top 25%	All plots	Top 25%								
Type	Count	Type	Count	Type	Count	Type	Count								
3	21788	3	6100	3	21991	3	63100	3	22426	3	6302	3	22565	3	6392
2	2662	2	1092	2	2727	2	1135	2	2772	2	1110	2	2789	2	1116
5	1739	5	394	5	1767	5	425	5	1781	5	427	5	1761	5	339
1	814	1	167	1	800	1	183	1	797	1	222	1	788	1	218
0	127	4	33	0	138	0	45	0	146	0	53	0	138	0	33
4	105	0	30	4	107	4	32	4	109	4	30	4	106	4	27

**Table 39** Relative share of wind erosion classes across all plots and the plots with LST/NDVI ratios in the upper quartile thereof in the given year

2016		2017		2018		2019	
All plots		Top 25%		All plots		Top 25%	
Type	%	Type	%	Type	%	Type	%
3	80.0	3	78.0	3	80.0	3	77.6
2	9.8	2	14.0	2	10.0	2	13.6
5	6.4	5	5.0	5	6.4	5	5.2
1	3.0	1	2.1	1	2.9	1	2.3
0	0.5	4	0.4	0	0.5	0	0.6
4	0.4	0	0.4	4	0.4	4	0.4

## Discussion

The ranking of wind erosion classes across agricultural plots based on absolute numbers (table 38) does not change when comparing all plots of a given year to those with LST/NDVI ratios within the upper quartile, with the exception of the least common classes, 0 (no danger) and 4 (high danger) switching ranks in 2016. This likely reflects the overall geographical distribution, with class 3 (medium danger) being the largest group by an order of magnitude, followed by classes 2 (little danger), 5 (very high danger) and 1 (very little danger). Relative shares (table 39) were calculated to analyse whether any wind erosion class appears more often relative to the subset, thus being more common in plots with more pronounced drought-like conditions than in the total sample. The most drastic change in relative shares can be seen for class 2 (little danger), which is moderately more common on high LST/NDVI ratio plots in all four years of interest, at the detriment of most other classes, increasing from an average of 9.9% of the total samples to an average of 13.8% of plots with high LST/NDVI ratios.

As no clear pattern emerges from the distribution of wind erosion classes across agricultural plots in the study area, it is assumed that the danger of wind erosion does not have a direct influence on drought hazard on agricultural plots throughout the study area. Furthermore, as previously stated, surface erosion and drought are interdependent (Thurow, Taylor, 1999, p. 1), with prolonged droughts accelerating erosion. Relations between the LST/NDVI ratio and the total amount of soil eroded per plot per year might yield clearer results, albeit the latter would likely also be dependent on other site-based variables such as soil type, e.g. sand, agricultural practices, such as weeding, and soil moisture (Operstein, Frydman, 2000).

### **3.4. Discussion**

The thesis attempted to answer the following research questions via exploratory data analysis:

- Which data sets provide valuable insight into agricultural drought hazards in the study area?
- Which, if any, patterns can be found in the spatial distribution of drought hazards in the study area?
- How is drought hazard intensity distributed and/or stratified across agricultural plots?
- Which, if any, processes and/or phenomena can be identified?

Out of the ten data sets investigated for relationships to the LST/NDVI ratio as a drought indicator, six were identified to provide insight into agricultural drought hazard. Statistically significant relationships were found with regards to field value, soil water exchange frequency and percolation rate. Particular crop and agricultural land use types, soil types and rooting capacity classes were identified to be more common on plots highly affected by drought-like conditions. No clear relation could be found between the LST/NDVI ratio and the Soil Quality Rating, as well as water- and wind-based erosion potential. Field capacity potentially relates to the LST/NDVI ratio, albeit the relationship is likely nonlinear and interdependent with other site-related factors, such as soil type and rooting capacity.

Plots exhibiting LST/NDVI ratios within the upper quartile of the respective year's values, consistently had lower field values, higher soil water exchange frequencies and higher percolation rates than the overall samples in each year. Furthermore, these plots most affected by drought-like conditions, were more commonly found on sandy terrain and deep soil layers, whereas agricultural plots on moors, clays and loams exhibited lower median LST/NDVI ratios. Cultivation of crops with significant pruning or monocultures with commonly exposed ground, such as tomatoes or wine, was found to exhibit high median LST/NDVI ratios, whereas conservation areas, commonly irrigated grasses intended for high biomass production and cover crops exhibited particularly low median LST/NDVI ratios.

The analyses succeeded in identifying data sets which provide valuable insight into agricultural drought hazards in the study area and found stratification of drought hazard across agricultural plots with regards to crop and soil type, as well as soil depth. However, the viability of further investigation of potential spatial patterns and identifiable processes was overestimated. The intended scope of the thesis was too ambitious, considering both the time constraints and the capabilities of the author. In retrospect, before attempting an analysis of the intended scope, several, thorough studies should first have been conducted on the interdependencies of site-related variables throughout the study area. For example, soil water exchange frequency, percolation rate, field capacity and soil depth might form an inter-related complex of local variables, which would warrant its own investigation. Another relation of interest might be the soil types and soil water exchange frequencies of particularly deep soils. After the relations between such variables by themselves was sufficiently understood, knowledge gained thereby could have been applied to potential relations to drought indices, such as the LST/NDVI ratio, or used to identify potential spatial patterns and multi-dimensional clusters indicating particular processes or phenomena.

## 4. Opportunities & Limitations

This thesis posits an attempt at investigating the relation between site-based hydrological and pedological variables, agricultural practices and agricultural drought intensity. The methods employed succeeded in highlighting several site-based variables influencing the LST/NDVI ratio of affected plots. Furthermore, the investigation of categorical variables, such as agricultural practices and soil types, revealed the potential of their use for drought hazard stratification. However, the overambitious scope of this thesis resulted in a lack of results regarding identification of spatial patterns, processes and phenomena. The following suggestions might serve to facilitate more conclusive analyses in the future.

Insight regarding individual site-based variables and their interdependence was lacking. Before attempting the identification of spatial patterns with regards to drought hazards, the local distribution of site-based variables must first be properly studied and understood.

Furthermore, individual variables display a wide range of values across study areas as spatially extensive as river catchments. The more such variables are investigated at once, the more permutations are possible per areal unit. Thematic clusters of variable interdependence should be identified, e.g. common per-plot combinations of specific soil type, -depth and soil water exchange frequencies. Drought indices could be investigated on a per-cluster basis. Furthermore, more scientifically founded selection of data sets chosen for investigation might increase the reliability of potential relations discovered and help curtail the scope of the analysis. The more environmental variables are chosen, the higher the number of possible combinations of value ranges per unit of analysis (clusters), thus complicating investigation. Alternatively, study areas could be restricted to ecologically distinct areas, such as the Spree Forest, which is already visually identifiable as a spatial cluster of low LST/NDVI values in the middle of the lower half of the study area (figure 4).

Whilst the restriction to fewer site-related factors might prove beneficial, it should also be noted that a variety of other data sets might also be available. In the case of the study area of this thesis, or any other study area in Germany, for example, the BGR soil atlas provides multiple data sets not yet investigated for correlation to the LST/NDVI indicator. Thematic categories of these data sets might provide a solid basis for the investigation of interdependencies thereof.

Some data sets, however, have not covered all plots within the target area. Missing values were not interpolated to reduce the amount of approximated data, albeit the benefits and disadvantages of doing so in further analyses could and should be deliberated.

Furthermore, the analysis did not consider vegetation phenology, hoping to circumvent this issue through the use of greenest pixel NDVI composites. Nonetheless, different types of vegetation exhibit different phenological behaviour. For example, winter crops should be excluded from the analysis of mid growing season agricultural droughts. This also extends to agricultural use classes not directly involved in production, such as fallows and barren fields. In future studies, crop types within the study area should be grouped by similar phenology, and the relation of site-based variables investigated on the LST/NDVI ratios of plots growing phenologically similar plants, or even specific crop types only. This could also include further



limiting the time frames investigated to the periods in which said crop types usually exhibit the most photosynthetically active biomass. This would further legitimise the use of mean NDVI rasters over greenest pixel composites, mitigating the chance of masking generally poor conditions with individual maximum value pixels, and wrongfully associating LST values to NDVI values measured on plants primarily grown during the year prior (see 3.3.1.).

Further potential for criticism arises from the fact that the LST/NDVI ratio as a drought indicator is aggregated yearly, but compared to environmental variables with no temporal resolution, i.e. effectively unchanging ones, such as soil type. Alternatively, the investigation of potential relations between these temporally constant variables and the LST/NDVI ratio slopes exhibited by individual plots might prove more fruitful. However, this would necessitate the consideration of varying significance of the plot level temporal regressions of the drought indicator. Relations between local variables and the non-homogenous correlation of LST and NDVI on each plot (compare Karnieli et al., 2010, p. 626) could also be included in such investigations. In this vein, plots investigated could be restricted to subsets exhibiting ranges of statistically significant temporal slopes only. By doing so, plots exhibiting drought conditions improving or largely unchanging despite anthropogenic climate change could be investigated and the environmental variables characterising them identified. The opposite would contribute to vulnerability detection.

Whilst agricultural practices or crop types might imply irrigation intensity, the actual frequency of irrigation events could also influence NDVI values, especially with regards to greenest pixel composites. Consideration of irrigation frequencies could further refine the scientific soundness of potential study results.

Furthermore, when comparing the situations of different growing seasons, the selection of the respective years could be conducted in a scientifically sounder way. Whilst the concept of ranking years with regards to individual indicators and indices has merit, the use of aggregated mean ranks for the selection of years of interest is suboptimal. In this case, indicators later disregarded, such as mean NDVI and the ratio of LST and mean NDVI, had an influence on the selection of the years of interest. This should either be avoided or properly justified. Alternatively, the selection of years of interest based on aggregated mean ranks could be discarded in favour of selecting years based on individual characteristics, such as the years with highest, lowest or most average LST or NDVI. Should resources suffice, analyses could also be conducted for the entire temporal range of available data.

Penultimately, whilst the LST/NDVI ratio is a well-established index for agricultural drought monitoring across wide areas, both its components are only proxies for the core problem of insufficient soil moisture. Investigating the relations between site-based variables and directly measured soil moisture could form the basis for more scientifically sound drought hazard analyses. Whilst there are many ways of direct soil moisture measurement (Babaeian et al., 2019, p. 535), such approaches would likely imply smaller sample sizes (fewer plots) and resource-intensive field work.

Lastly, after the establishment of ranges of site-based variables as drought hazards, spatially aggregating cumulative hazard to spatially conjunct areal units might foster the identification of autocorrelating drought hazard patterns. Suitable areal units could be equivalent in spatial extent to average agricultural plots throughout the given study area.

## 5. Conclusions

This thesis analysed several hydrological, pedological and agricultural land uses for potential relations to the LST/NDVI ratio as a drought indicator throughout agricultural plots in the Spree river catchment, Brandenburg, Germany, within the context of the 2018 European heat wave.

Field value, a measure of soil quality, was found to significantly and consistently influence the value of the LST/NDVI ratio on agricultural plots, with plots with higher field values tending to exhibit lower LST/NDVI ratios. Further continuous site-based variables found to have relationships with the drought indicator include soil water exchange frequency and percolation rates, with an increase in either significantly and consistently correlated with higher LST/NDVI ratios. Field capacity, water-based erosion potential and the Soil Quality Rating were not found to exert consistent influence over the LST/NDVI ratio. Furthermore, it has been found that crop varieties or agricultural land use types, soil types as well as rooting capacity can be used to stratify drought hazard. The most common crop types on plots exhibiting high LST/NDVI ratios differed from the overall most common varieties, with fallows, winter rye, winter oats, lupinus, clover and ley grassland and non active fields increasing in relative commonness. Furthermore, conservation areas, turfs and meadows were found to exhibit particularly low median LST/NDVI ratios, with dry lawns and crop cultivation associated with extensive weeding exhibiting high LST/NDVI ratios. With regards to soil type, fields on combinations of moor, loam and clay consistently exhibited low LST/NDVI ratios, with sandy substrates being strongly associated with high LST/NDVI ratios. Furthermore, deep soils, with a theoretical rooting capacity of 20 metres, were found to be more common on plots with high LST/NDVI ratios as compared to the total samples. No concrete relations could be found with regards to wind-based erosion potential.

The study concludes that field value, soil water exchange frequency and percolation rates provide valuable insight into agricultural drought hazard throughout the study area. Drought intensity can be stratified using crop or agricultural land use type, soil type and rooting capacity. Depending on their values, these indicators pose likely drought hazards.

Several potential approaches of improving the research design of future analyses were identified. First, clusters of site-based variable ranges should be identified, due to their interdependence. Once clusters exhibiting similar ranges with regards to selected variables have been identified, these could then be analysed with regards to drought hazard. For example, clusters of similar soil types, depths and soil water exchange frequencies might be of particular interest. Second, the number of variables considered should be limited to a necessary minimum or specific variables of interest to curtail scope. Third, analyses should be limited to agricultural plots cultivating phenologically similar crop types or single crop types only, to enable the use of growing season NDVI means instead of greenest pixel composites. Likewise, inactive plots or crops primarily growing outside the periods of interest should be excluded from the analysis. Further potential for improved research design includes consideration of irrigation, different selection of years of interest and the choice of a different drought indicator. Further research potential includes aggregating identified drought hazards to spatially conjunct areal units for autocorrelation analysis and investigating the influence of site-based variables on plot-level temporal drought indicator trajectories.

## Sources

**AUTHOR UNKNOWN** (1968): Remote Sensing. *Nature*, 218(5140), 419-420. URL: <https://link.springer.com/content/pdf/10.1038/218419b0.pdf> [last access on: 10.10.2022]

**BABAEIAN, E., SADEGHI, M., JONES, S. B., MONTZKA, C., VEREECKEN, H., TULLER, M.** (2019): Ground, proximal, and satellite remote sensing of soil moisture. *Review of Geophysics*, 57, 530-616. doi: 10.1029/2018RG000618

**BANNARI, A. A., HUETE, A.** (1996): A review of vegetation indices. *Remote Sensing Reviews*, 13(1), 95-120. doi: 10.1080/02757259509532298

**BURAS, A., RAMMIG, A., ZANG, C. S.** (2020): Quantifying impacts of the 2018 drought on European ecosystems in comparison to 2003. *Biogeosciences*, 17, 1655-1672. doi: 10.5194/bg-17-1655-2020

**BGR** (2014): Ackerbaulichews Ertragspotential der Böden in Deutschland. URL: [https://www.lgi.geographie.uni-kiel.de/de/media/ws\\_13\\_14/handzettel-soil-quality-rating-hennings-et-al.pdf](https://www.lgi.geographie.uni-kiel.de/de/media/ws_13_14/handzettel-soil-quality-rating-hennings-et-al.pdf) [last access on: 10.10.2022]

**CHERLINKA, V.** (2019): NDVI FAQ: All You Need To Know About NDVI. *EOS Data Analytics*. URL: <https://eos.com/blog/ndvi-faq-all-you-need-to-know-about-ndvi/> [last access on: 10.10.2022]

**CHUKWUDI, U. P., KUTU, F. R., MAVENGAHAMA, S.** (2021): Influence of Heat Stress, Variations in Soil Type, and Soil Amendment on the Growth of Three Drought-Tolerant Maize Varieties. *Agronomy*, 11, 1485. doi: 10.3390/agronomy11081485

**CLIWAC** (2022): The Model Region Berlin-Brandenburg. URL: <https://www.cliwac.de/en/casestudy/index.html> [last access on: 10.10.2022]

**CROCETTI, L., FORKEL, M., FISCHER, M., JUREČKA, F., GRLJ, A., SALENTINIG, A., TRNKA, M., ANDERSON, M., NG, W.-T., KOKALJ, Ž, BUCUR, A., DORIGO, W.** (2020): Earth Observation for agricultural drought monitoring in the Pannonian Basin (southeastern Europe): current state and future directions. *Regional Environmental Change*, 20, 123. doi: 10.1007/s10113-020-01710-w

**DUJNISVELD, W.** (2016a): Mittlere jährliche Sickerwasserrate aus dem Boden in Deutschland. Metadaten. Available via: <https://www.bodenatlas.de> [last access on: 10.10.2022]

**DUJNISVELD, W.** (2016b): Nutzbare Feldkapazität im effektiven Wurzelraum in Deutschland. Metadaten. Available via: <https://www.bodenatlas.de> [last access on: 10.10.2022]

**DWD** (2019a): Klimareport Brandenburg. URL:  
[https://www.dwd.de/DE/leistungen/klimareport\\_bb/klimareport\\_bb\\_2019\\_download.pdf?\\_\\_blob=publicationFile&v=5](https://www.dwd.de/DE/leistungen/klimareport_bb/klimareport_bb_2019_download.pdf?__blob=publicationFile&v=5) [last access on: 10.10.2022]

**DWD** (2019b): Ursachen und Folgen der Trockenheit in Deutschland und Europa ab Juni 2019. URL:  
[https://www.dwd.de/DE/leistungen/besondereereignisse/duerre/20190712\\_trockenheit\\_juni\\_juli\\_2019.pdf?\\_\\_blob=publicationFile&v=1](https://www.dwd.de/DE/leistungen/besondereereignisse/duerre/20190712_trockenheit_juni_juli_2019.pdf?__blob=publicationFile&v=1) [last access on: 10.10.2022]

**FUKAI, S., COOPER, M.** (1995): Development of drought-resistant cultivars using pysiomorphological traits in rice. *Field Crops Research*, 40, 67-86. doi: 10.1016/0378-4290(94)00096-U

**GORELICK, N., HANCHER, M., DIXON, M., ILYUSHCHENKO, S., THAU, D., MOORE, R.** (2017): Google Earth Engine: Planetary-scale geospatial analysis for everyone. *Remote Sensing of Environment*, 202, 18-27. doi: 10.1016/j.rse.2017.06.031

**GREUNER-PÖNICKE, S., WALTER, S., PETEAUX, K., STRAßENBURG, J., BIEGANSKY, F.** (2014): Antragsunterlagen Raumordnungsverfahren für den Neubau einer Mono-Deponie. URL:  
[http://www.landkreis-wesermarsch.de/uploads/files/antragsunterlagen\\_bericht\\_final\\_2014-11-15\\_komplett\\_teil\\_1-bericht\\_und\\_anlagen.pdf](http://www.landkreis-wesermarsch.de/uploads/files/antragsunterlagen_bericht_final_2014-11-15_komplett_teil_1-bericht_und_anlagen.pdf) [last access on: 10.10.2022]

**GUERRA, B., STEENWERTH, K.** (2012): Influence of Floor Management Technique on Grapewine Growth, Disease Pressure, and Juice and Wine Composition: A Review. *American Journal of Enology and Viticulture*, 63(2), 149-164. doi: 10.5344/ajev.2011.10001

**HARTMANN, S., STICKSEL, E.** (2010): Kleegras als Biogassubstrat. *Biogas Forum Bayern*, 8. URL:  
[https://www.lfl.bayern.de/mam/cms07/ipz/dateien/leitfaden\\_2010-08\\_biogasforum.pdf](https://www.lfl.bayern.de/mam/cms07/ipz/dateien/leitfaden_2010-08_biogasforum.pdf) [last access on: 10.10.2022]

**HUANG, J., HARTEMINK, A. E.** (2020): Soil and environmental issues in sandy soils. *Earth-Science Reviews*, 208, 103295. doi: 10.1016/j.earscirev.2020.103295

**HÜWE, R., ROUBITSCHKE, W.** (2004): Landwirtschaftliche Bodennutzung. *Nationalatlas Bundesrepublik Deutschland*, 8, 28-29. URL:  
[http://archiv.nationalatlas.de/wp-content/art\\_pdf/Band8\\_28-29\\_archiv.pdf](http://archiv.nationalatlas.de/wp-content/art_pdf/Band8_28-29_archiv.pdf) [last access on: 10.10.2022]

**IHINEGBU, C., OGUNWUMI, T.** (2021): Multi-criteria modelling of drought: a study of Brandenburg Federal State, Germany. *Modeling Earth Systems and Environment*, 8, 2035-2049. doi: 10.1007/s40808-021-01197-2

**IPCC** (2018): Global Warming of 1.5 C; An IPCC Special Report on the Impacts of Global Warming of 1.5°C above Pre-Industrial Levels and Related Global Greenhouse Gas Emission Pathways, in the Context of Strengthening the Global Response to the Threat of Climate Change, Sustainable Development, and Efforts to Eradicate Poverty. URL: <https://www.ipcc.ch/sr15/> [last access on: 10.10.2022]

**JÄNICKE, C., GODDARD, A., STEIN, S., STEINMANN, H.-H., LAKES, T., NENDEL, C., MÜLLER, D.** (2022): Field-level land-use data reveal heterogeneous crop sequences with distinct regional differences in Germany. *European Journal of Agronomy*, 141, 126632. doi: 10.1016/j.eja.2022.126632

**KARNIELI, A., AGAM, N., PINKER, R. T., ANDERSON, M., IMHOFF, M. L., GUTMAN, G. G., PANOV, N., GOLDBERG, A.** (2010): Use of NDVI and Land Surface Temperature for Drought Assessment: Merits and Limitations. *Journal of Climate*, 23(3), 618-633. doi: 10.1175/2009JCLI2900.1

**KAYE, J. P., QUEMADA, M.** (2017): Using cover crops to mitigate and adapt to climate change. A review. *Agronomy for Sustainable Development*, 37(1), 1-17. doi: 10.1007/s13593-016-0410-x

**KNIPLING, E. B.** (1970): Physical and Physiological Basis for the Reflectance of Visible and Near-Infrared Radiation from Vegetation. *Remote Sensing of Environment*, 1, 155-159. doi: 10.1016/S0034-4257(70)80021-9

**KNOBLAUCH, S., ROTH, D., PFLEGER, I.** (1999): Beziehungen zwischen N-Saldo,  $N_{\min}$  im Boden, Nitratgehalt im Sickerwasser und N-Austrag bei unterschiedlichen Ackerstandorten Thüringens. 8. *Gumpensteiner Lysimetertagung*. URL: [https://raumberg-gumpenstein.at/jdownloads/Tagungen/Lysimetertagung/Lysimetertagung\\_1999/2l\\_1999\\_knoblauch.pdf](https://raumberg-gumpenstein.at/jdownloads/Tagungen/Lysimetertagung/Lysimetertagung_1999/2l_1999_knoblauch.pdf) [last access on: 10.10.2022]

**KOGAN, F. N.** (1997): Global Drought Watch from Space. *Bulletin of the American Meteorological Society*, 78(4), 621-636. URL: [https://journals.ametsoc.org/downloadpdf/journals/bams/78/4/1520-0477\\_1997\\_078\\_0621\\_gdwfs\\_2\\_0\\_co\\_2.pdf](https://journals.ametsoc.org/downloadpdf/journals/bams/78/4/1520-0477_1997_078_0621_gdwfs_2_0_co_2.pdf) [last access on: 10.10.2022]

**KOWALSKI, K., OKUJENI, A., BRELL, M., HOSTERT, P.** (2022): Quantifying drought effects in Central European grasslands through regression-based unmixing of intra-annual Sentinel-2 time series. *Remote Sensing of Environment*, 268, 112781. doi: 10.1016/j.rse.2021.112781

**KUMAR, R., SAMANIEGO, L., ATTINGER, S.** (2013): Implications of distributed hydrologic model parametrization on water flexes at multiple scales and locations. *Water Resources Research*, 49, 360-379. doi: 10.1029/2012WR012195

**KUNKEL, R., WENDLAND, F.** (2003): Auswirkung von Bodenbedeckungsszenarien auf den Wasserhaushalt im Elbeinzugsgebiet. In: Stein, G., Umwelt und Technik im Gleichklang. Springer Berlin Heidelberg. doi: 10.1007/978-3-642-55681-4\_18

**KÖHN, J., MEIBNER, R., RUPP, F., REINSTORF, F.** (year): Langzeituntersuchungen zum Sickerwasser- und Stickstoffaustrag in Abhängigkeit von Bodenart, Nutzung und Mineraldüngung. 18. *Gumpensteiner Lysimetertagung*. URL: [https://raumberg-gumpenstein.at/jdownloads/Tagungen/Lysimetertagung/Lysimetertagung\\_2019/2l\\_2019\\_koehn.pdf](https://raumberg-gumpenstein.at/jdownloads/Tagungen/Lysimetertagung/Lysimetertagung_2019/2l_2019_koehn.pdf) [last access on: 10.10.2022]

**MARX, A., SAMANIEGO, L., KUMAR, R., THOBER, S., MAI, J., ZINK, M.** (2016): Der Dürremonitor – Aktuelle Information zur Bodenfeuchte in Deutschland. *Forum für Hydrologie und Wasserbewirtschaftung*, 37(16), 131-142. URL: [https://www.ufz.de/export/data/2/248360\\_111650\\_D%C3%BCrremonitor\\_Marx\\_etal\\_TdH\\_2016.pdf](https://www.ufz.de/export/data/2/248360_111650_D%C3%BCrremonitor_Marx_etal_TdH_2016.pdf) [last access on: 10.10.2022]

**MAZDIYASNI, O., AGHAKOUCHAK, A.** (2015): Substantial increase in concurrent droughts and heatwaves in the United States. *Proceedings of the National Academy of Sciences*, 112(37), 11484-11489. doi: 10.1073/pnas.1422945112

**MCVICAR, T. R., BIERWIRTH, P. N.** (2001): Rapidly assessing the 1997 drought in Papua New Guinea using composite AVHRR imagery. *International Journal of Remote Sensing*, 22(11), 2109-2128. doi: 10.1080/01431160120728

**MIRALLES, D. G., GENTINE, P., SENEVIRATNE, S. I., TEULING, A. J.** (2019): Land–atmospheric feedbacks during droughts and heatwaves: state of the science and current challenges. *Annals of the New York Academy of Sciences*, 1436(1), 19-35. doi: 10.1111/nyas.13912

**MISHRA, A. K., SINGH, V. P.** (2010): A review of drought concepts. *Journal of Hydrology*, 319, 202-216. doi: 10.1016/j.jhydrol.2010.07.012

**MLUK** (2020a): Klima und Boden; Steckbriefe Brandenburger Böden. URL: <https://mluk.brandenburg.de/Steckbriefe-BB-Boeden/SB-13-2-Klima-Boden.pdf> [last access on: 10.10.2022]

**MLUK** (2020b): Steckbriefe Brandenburger Böden; Sammelmappe. URL: <https://mluk.brandenburg.de/sixcms/media.php/9/Steckbriefe-BB-Boeden-Textteil.pdf> [last access on: 10.10.2022]

**NOAA** (2021): State of the Climate: Monthly Global Climate Report for Annual 2020. URL: <https://www.ncei.noaa.gov/access/monitoring/monthly-report/global/202013> [last access on: 10.10.2022]

**OPERSTEIN, V., FRYDMAN, S.** (2000): The influence of vegetation on soil strength. *Ground Improvement*, 4, 81-89. doi: 10.1680/grim.2000.4.2.81

**RATZKE, U., MOHR, H.J.** (2005): Böden in Mecklenburg-Vorpommern; Abriss ihrer Entstehung, Verbreitung und Nutzung. 2. URL: <https://www.lung.mv-regierung.de/dateien/boedenmv.pdf> [last access on: 10.10.2022]

**REBETEZ, M., MAYER, H., DUPONT, O., SCHINDLER, D., GARTNER, K., KROPP, J. P., MENZEL, A.** (2006): Heat and drought 2003 in Europe: a climate synthesis. *Annals of Forest Science*, 63(3), 569-577. doi: 10.1051/forest:2006043

**REBETEZ, M., DUPONT, O., GIROUD, M.** (2009): An analysis of the July 2006 heatwave extent in Europe compared to the record year of 2003. *Theoretical and Applied Climatology*, 95, 1-7. doi: 10.1007/s00704-007-0370-9

**ROUSE, J. W., HAAS, R. H., SCHELL, J. A., DEERING, D. W.** (1973): Monitoring Vegetation Systems in the Great Plains with ERTS. *Third Earth Resources Technology Satellite-1 Symposium: The Proceedings of a Symposium Held by Goddard Space Flight Center at Washington, DC*, 351, 309-317. URL: <https://books.google.de/books?hl=de&lr=&id=s4KOAAAAIAAJ&oi=fnd&pg=PA309&dq=MONITORING+VEGETATION+SYSTEMS+IN+THE+GREAT+PLAINS+WITH+ERTS&ots=G6cXXeR2nu&sig=UiAycMhAnc3f7Dr3swVFfmvaegk#v=onepage&q=MONITORING%20VEGETATION%20SYSTEMS%20IN%20THE%20GREAT%20PLAINS%20WITH%20ERTS&f=false> [last access on: 10.10.2022]

**SAMANIEGO, L., KUMAR, R., ATTINGER, S.** (2010): Multiscale parameter regionalization of a grid-based hydrologic model at the mesoscale. *Water Resources Research*, 46, W05523. doi: 10.1029/2008WR007327

**SAMARAH, N. H.** (2005): Effects of drought stress on growth and yield of barley. *Agronomy for Sustainable Development*, 25(1), 145-149. doi: 10.1051/agro:2004064

**SPINONI, J., VOGT, J. V., NAUMANN, G., BARBOSA, P., DOSIO, A.** (2018): Will drought events become more frequent and severe in Europe? *International Journal of Climatology*, 38, 1718-1736. doi: 10.1002/joc.5291

**STEGGER, U.** (2016): Austauschhäufigkeit des Bodenwassers in landwirtschaftlich genutzten Böden Deutschlands. Metadaten. Available via: <https://www.bodenatlas.de> [last access on: 10.10.2022]

**SUN, D., KAFATOS, M.** (2007): Note on the NDVI-LST relationship and the use of temperature-related drought indices over North America. *Geophysical Research Letters*, 34, L24406. doi: 10.1029/2007GL031485

**THUROW, T. L., TAYLOR, C. A.** (1999): Viewpoint: The role of drought in range management. *Journal of Range Management*, 52(5), 413-419. URL: <https://journals.uair.arizona.edu/index.php/jrm/article/download/9436/9048> [last access on: 10.10.2022]

**WILHELMI, O. V., WILHITE, D. A.** (2002): Assessing Vulnerability to Agricultural Drought: A Nebraska Case Study. *Natural Hazards*, 25, 37-58. URL: <https://link.springer.com/content/pdf/10.1023/A:1013388814894.pdf> [last access on: 10.10.2022]

**WILHITE, D. A., GLANTZ, M. H.** (1985): Understanding: the Drought Phenomenon: The Role of Definitions. *Water International*, 10(3), 111-120. doi: 10.1080/02508068508686328

## **Software**

**HIJMANS, R. J., BIVAND, R., FORNER, K., OOMS, J., PEBESMA, E., SUMNER, M. D.** (2022): Package 'terra'. URL: <https://CRAN.R-project.org/package=terra> [last access on: 10.10.2022]

**PEBESMA, E.** (2018): Simple Features for R: Standardized Support for Spatial Vector Data. *The R Journal*, 10(1), 439-446. URL: <http://pebesma.staff.ifgi.de/RJwrapper.pdf> [last access on: 10.10.2022]

**QGIS.ORG** (2022): QGIS Geographic Information System. Release 3.26 Buenos Aires. Open Source Geospatial Foundation Project. URL: <http://www.qgis.org> [last access on: 10.10.2022]

**R CORE TEAM** (2022): R: A language and environment for statistical computing. R Foundation for Statistical Computing, Vienna, Austria. URL: <https://www.R-project.org> [last access on: 10.10.2022]

**RSTUDIO TEAM** (2022): RStudio: Integrated Development Environment for R. RStudio, PBC, Boston, MA. URL: <https://www.rstudio.com> [last access on: 10.10.2022]



Thomas Hoffmann  
Möllendorffstraße 114 A  
10367 Berlin  
Telephone: +49 1573 519 0089  
E-mail: hoffmatho@hu-berlin.de

## **Declaration of Authenticity**

I declare that I have not submitted this thesis or parts thereof for other examinations or study projects, that I have prepared it independently and only using the literature and aids indicated. All external sources, including internet sources, graphics, tables and pictures, which I have reproduced unchanged or modified, have been marked as such. I am aware that violations of these principles will be prosecuted as deception or attempted deception.

Berlin, 10.12.2022



Signature

---

Thomas Hoffmann  
Möllendorffstraße 114 A  
10367 Berlin  
Telefon: +49 1573 519 0089  
E-mail: hoffmatho@hu-berlin.de

## **Eidesstattliche Erklärung**

Ich erkläre, dass ich die vorliegende Arbeit oder Teile davon nicht für andere Prüfungs- und Studienleistungen eingereicht, selbstständig und nur unter Verwendung der angegebenen Literatur und Hilfsmittel angefertigt habe. Sämtliche fremde Quellen, inklusive Internetquellen, Grafiken, Tabellen und Bilder, die ich unverändert oder abgewandelt wiedergegeben habe, habe ich als solche kenntlich gemacht. Mir ist bekannt, dass Verstöße gegen diese Grundsätze als Täuschungsversuch bzw. Täuschung geahndet werden.

Berlin, den 12.10.2022



Unterschrift

# Appendix

## Plots

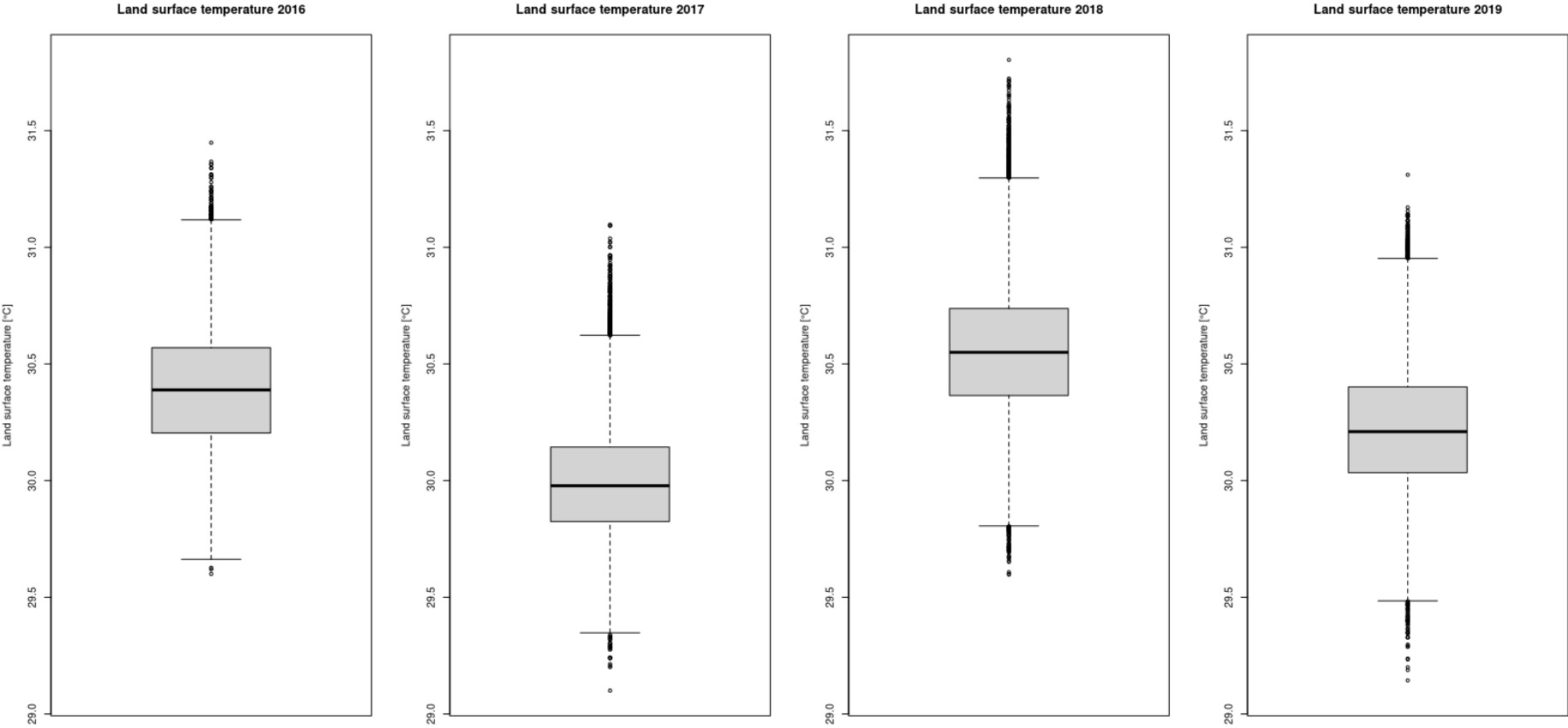


**Figure 6** Boxplots of land surface temperature across all plots 2016-2019 (left to right)

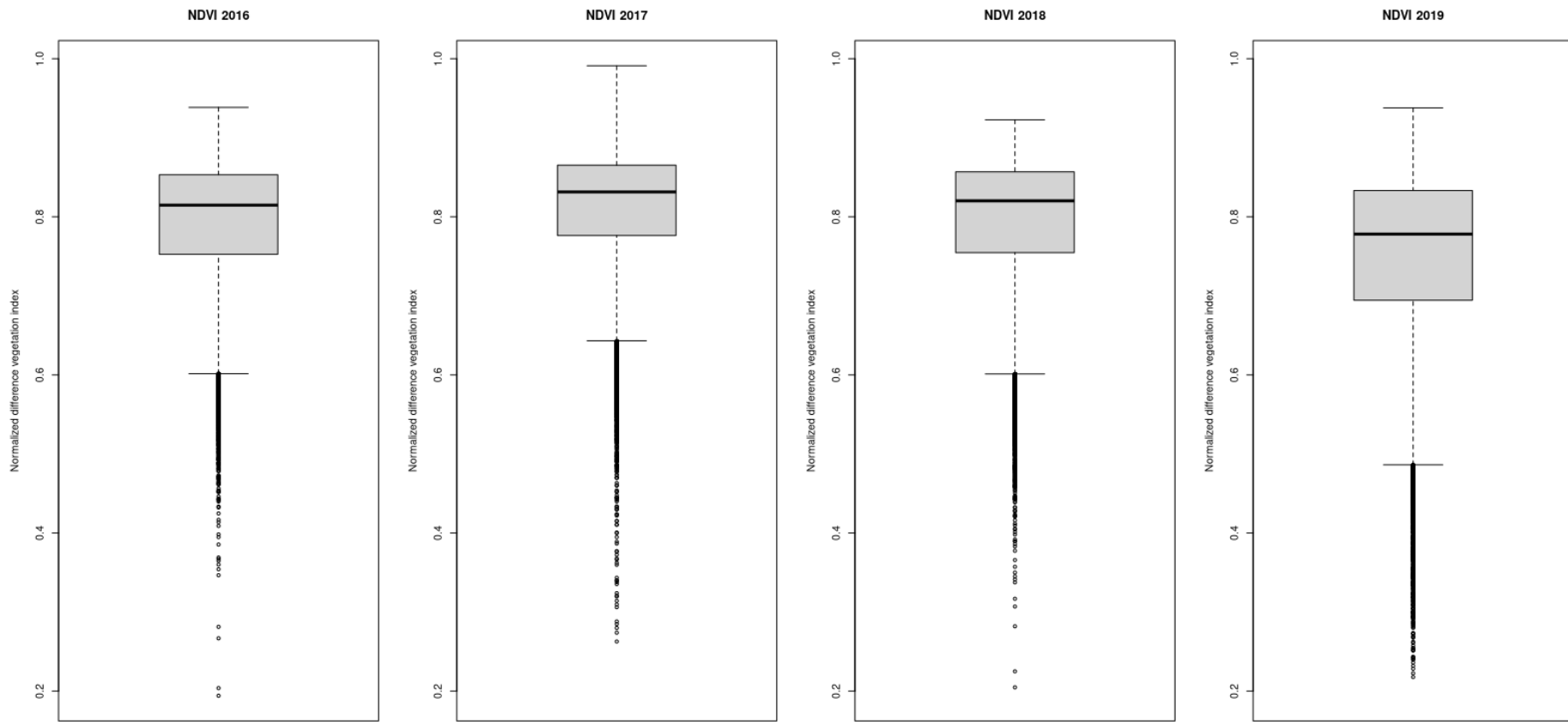


**Figure 7** Boxplots of NDVI across all plots 2016-2019 (left to right)

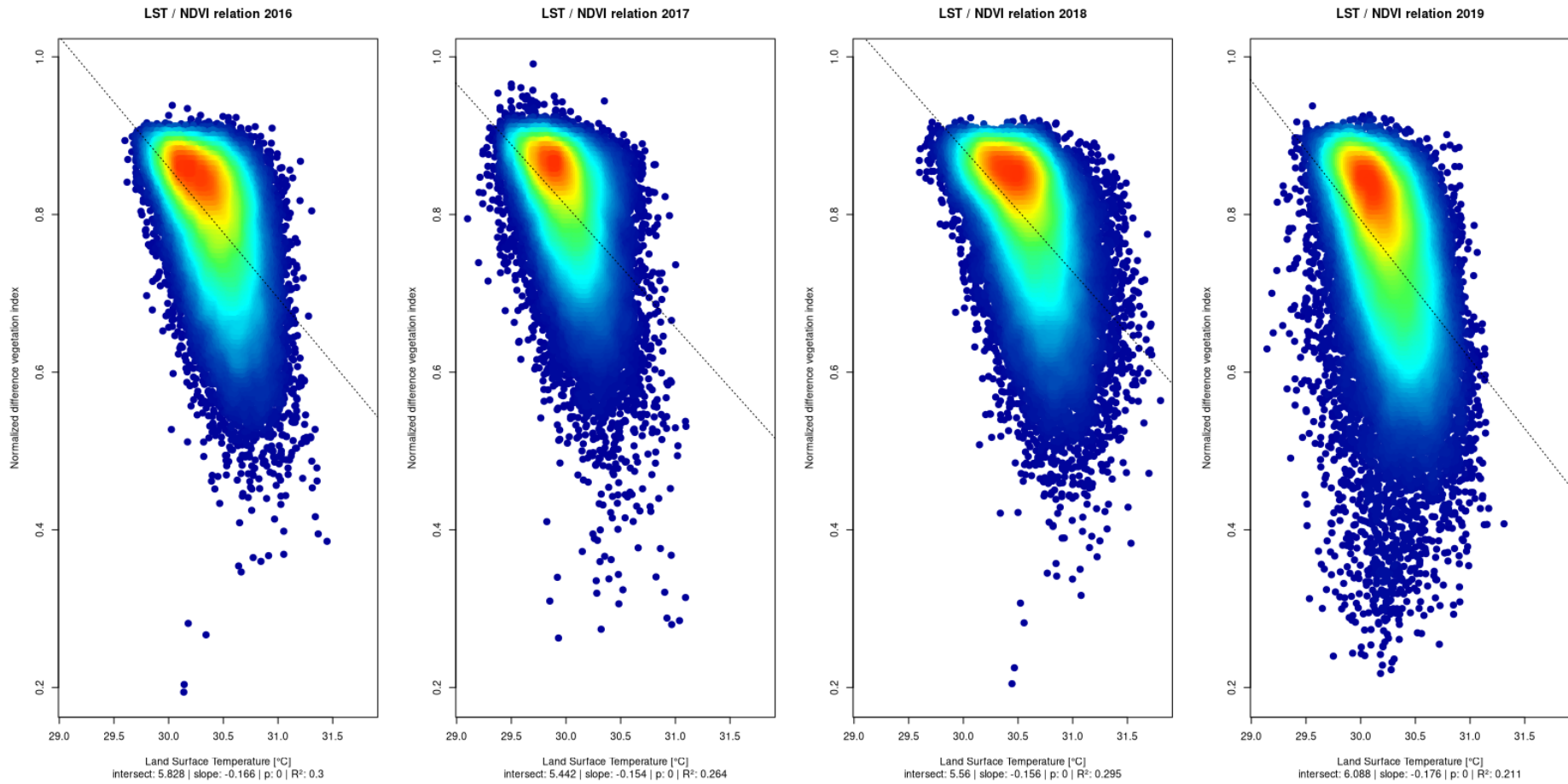


**Figure 8** LST / NDVI relation in 2016-2019 (left to right), colours indicating point density ranging from blue (low) via green (medium) to red (high)

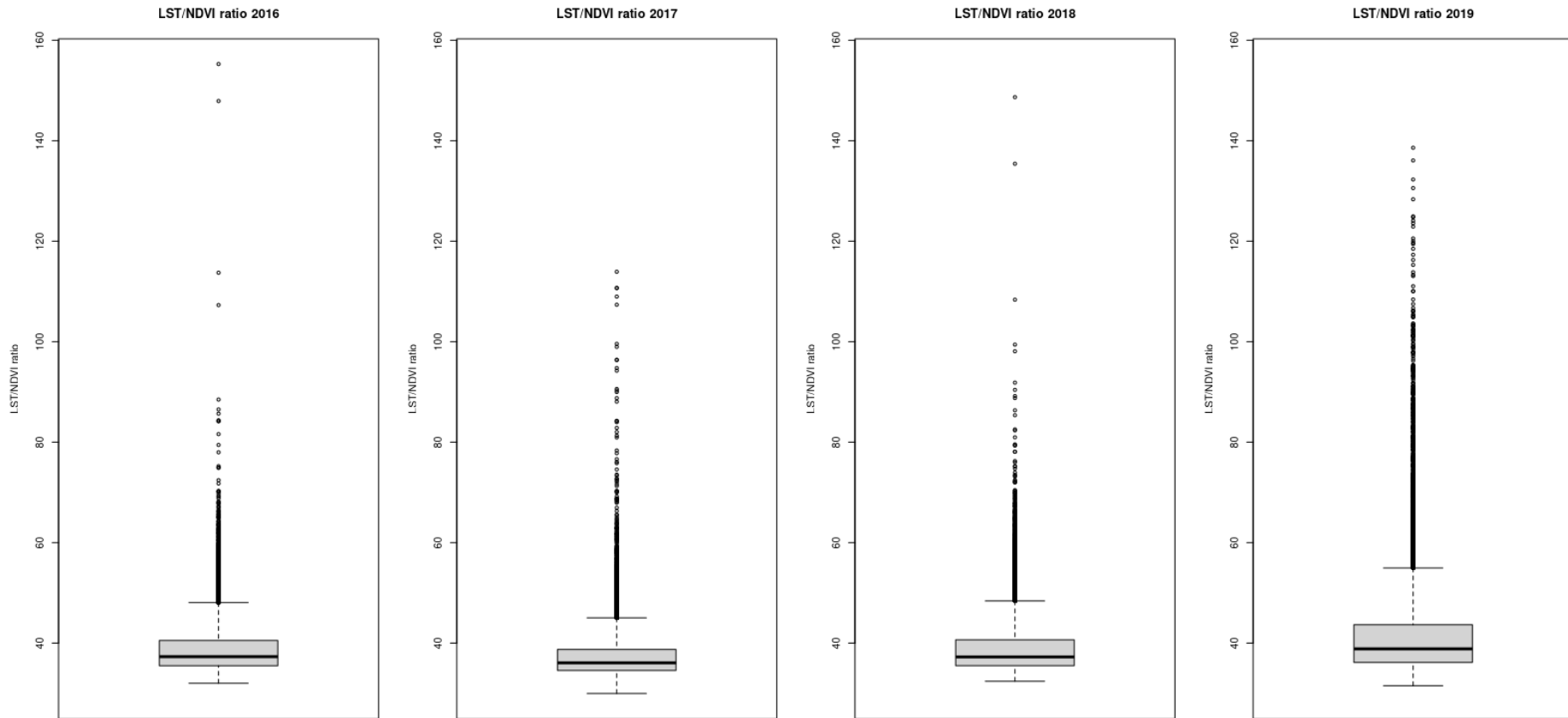


**Figure 9** Boxplots of LST/NDVI ratio across all plots 2016-2019 (left to right)

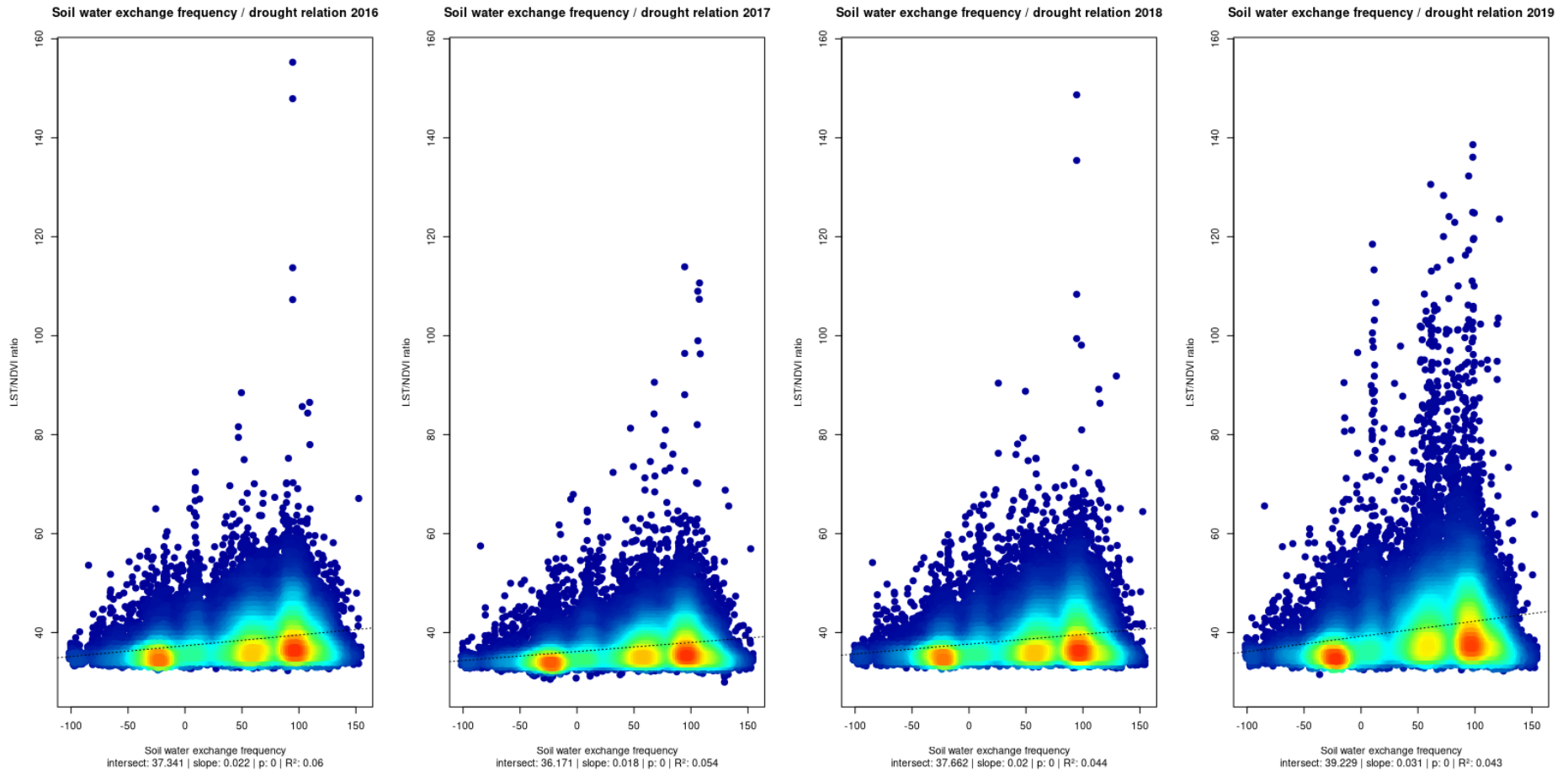


**Figure 10** Soil water exchange frequency / drought relation in 2016-2019 (left to right), colours indicating point density ranging from blue (low) via green (medium) to red (high)

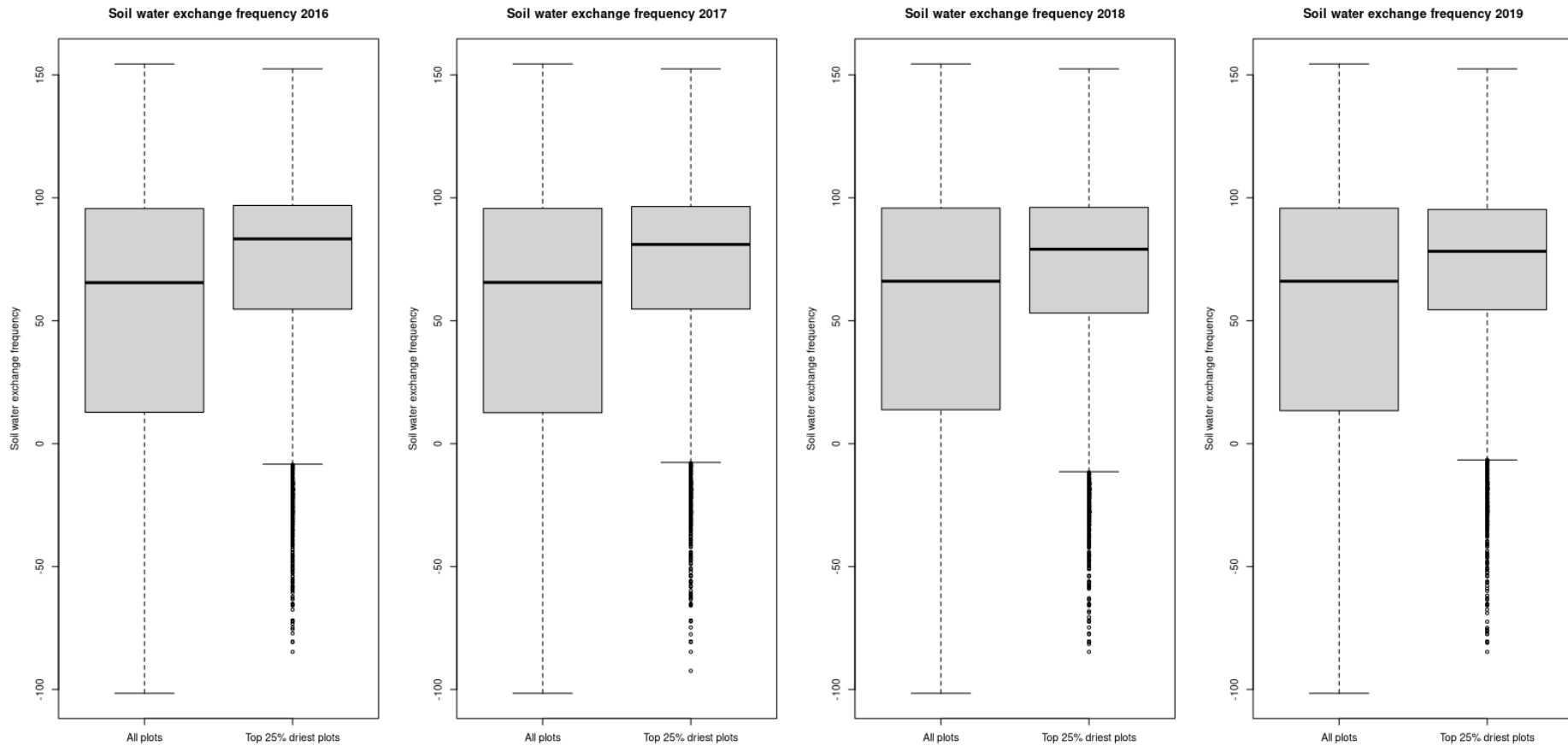


**Figure 11** Boxplots of soil water exchange frequency across all plots (respectively left) and the plots with LST/NDVI ratios in the upper quartile thereof in the given year (respectively right), for 2016-2019 (left to right)

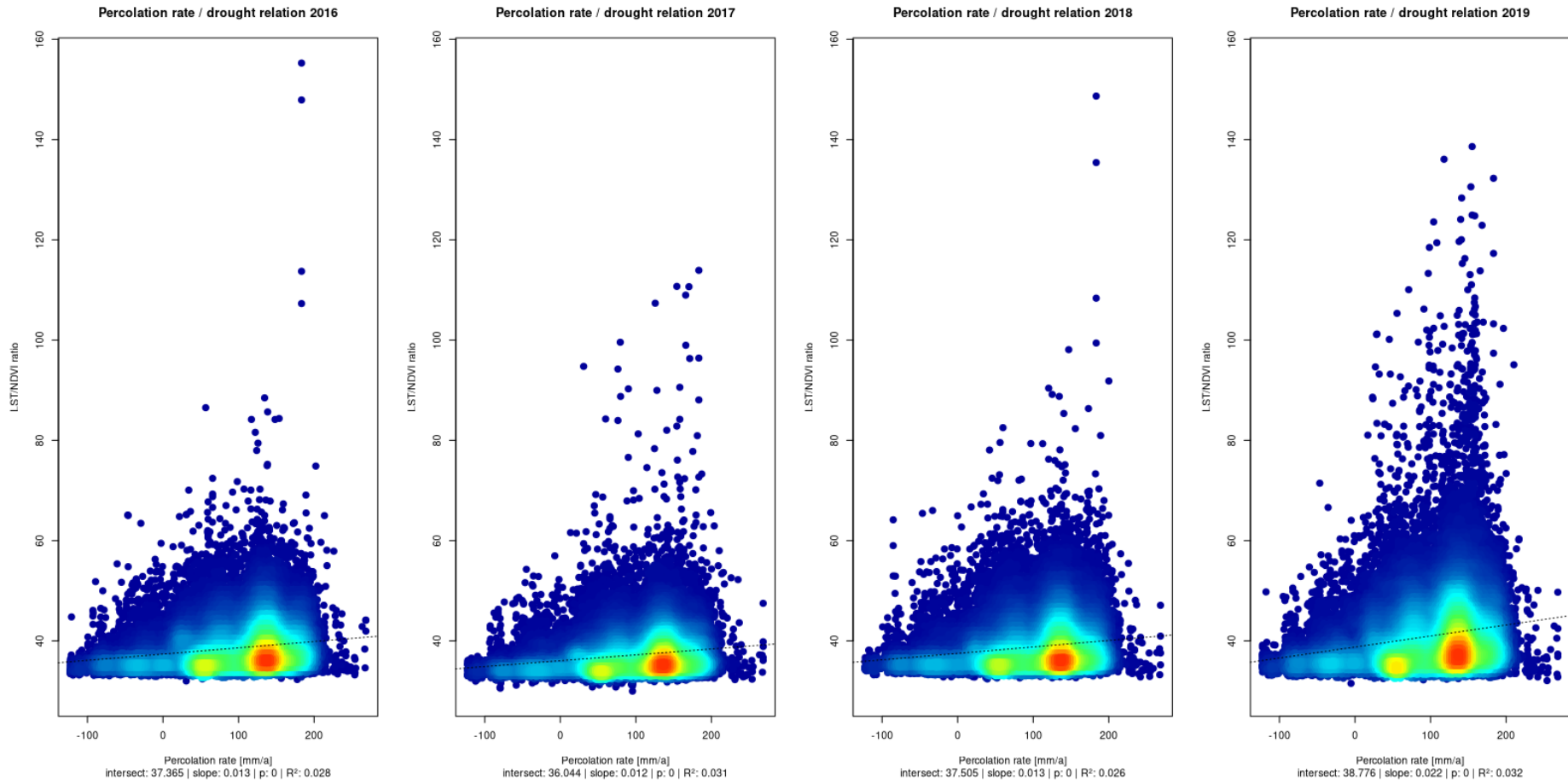


**Figure 12** Percolation rate / drought relation in 2016-2019 (left to right), colours indicating point density ranging from blue (low) via green (medium) to red (high)



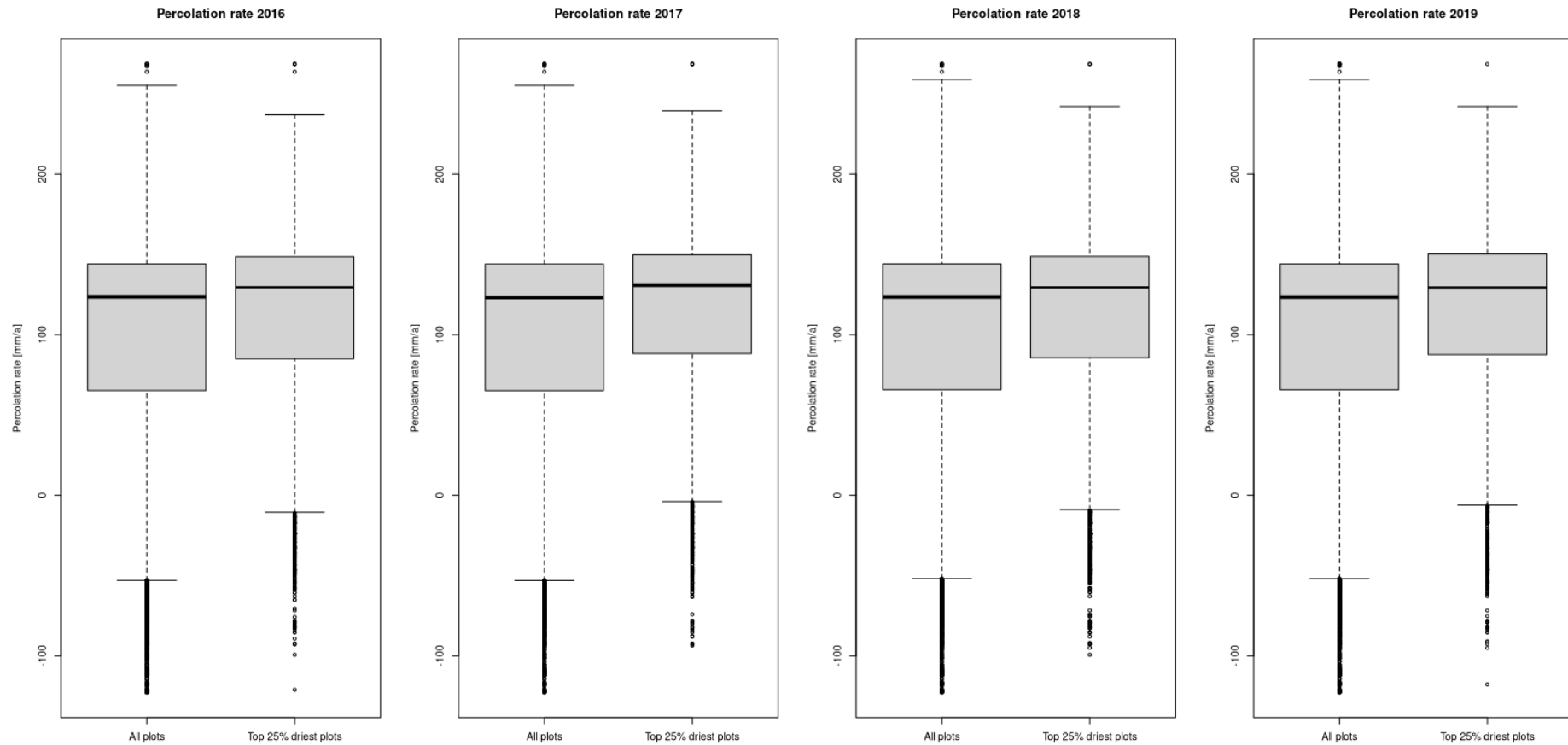


**Figure 13** Boxplots of percolation rates across all plots (respectively left) and the plots with LST/NDVI ratios in the upper quartile thereof in the given year (respectively right), for 2016-2019 (left to right)

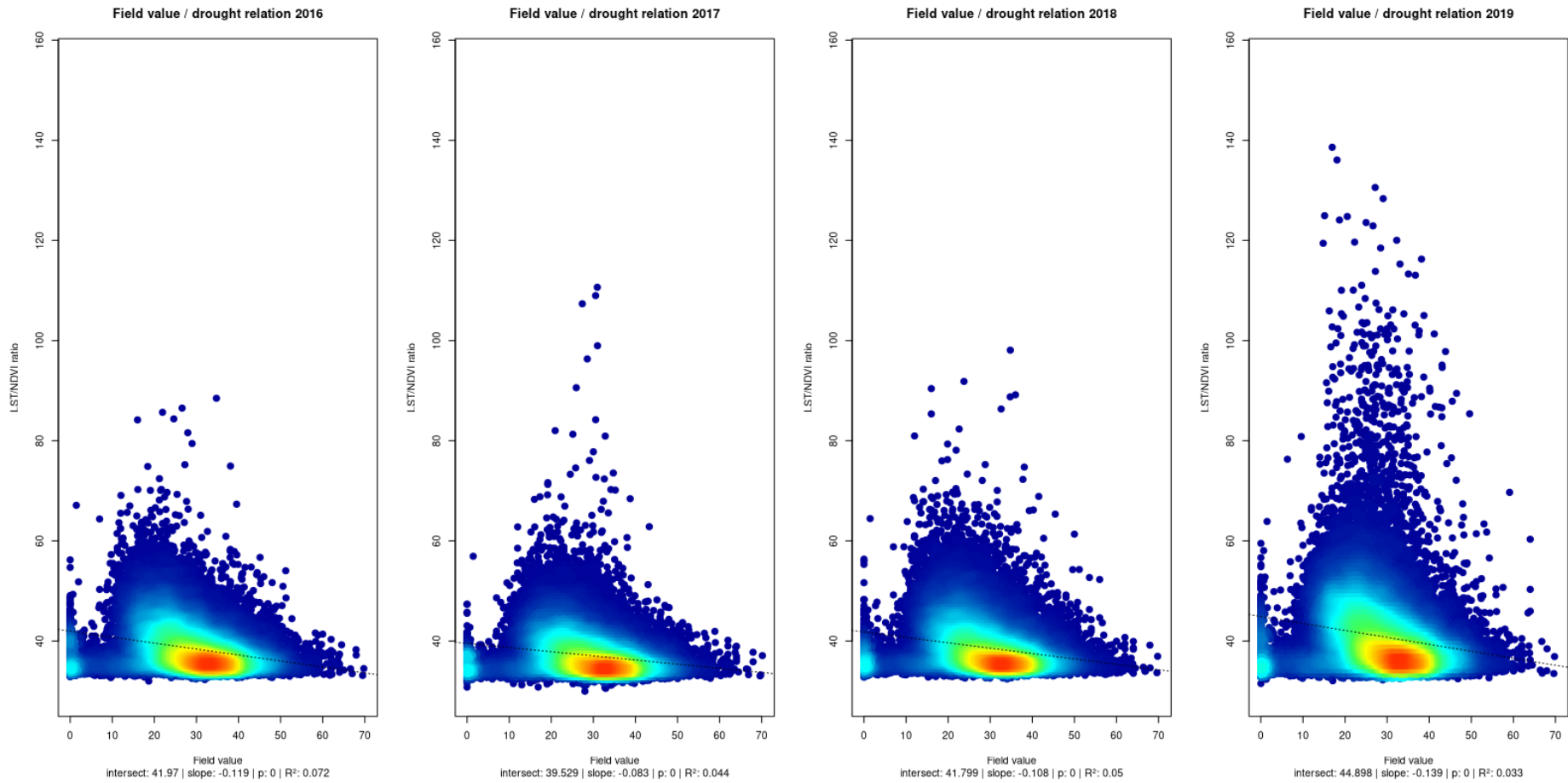


**Figure 14** Field value / drought relation in 2016-2019 (left to right), colours indicating point density ranging from blue (low) via green (medium) to red (high)

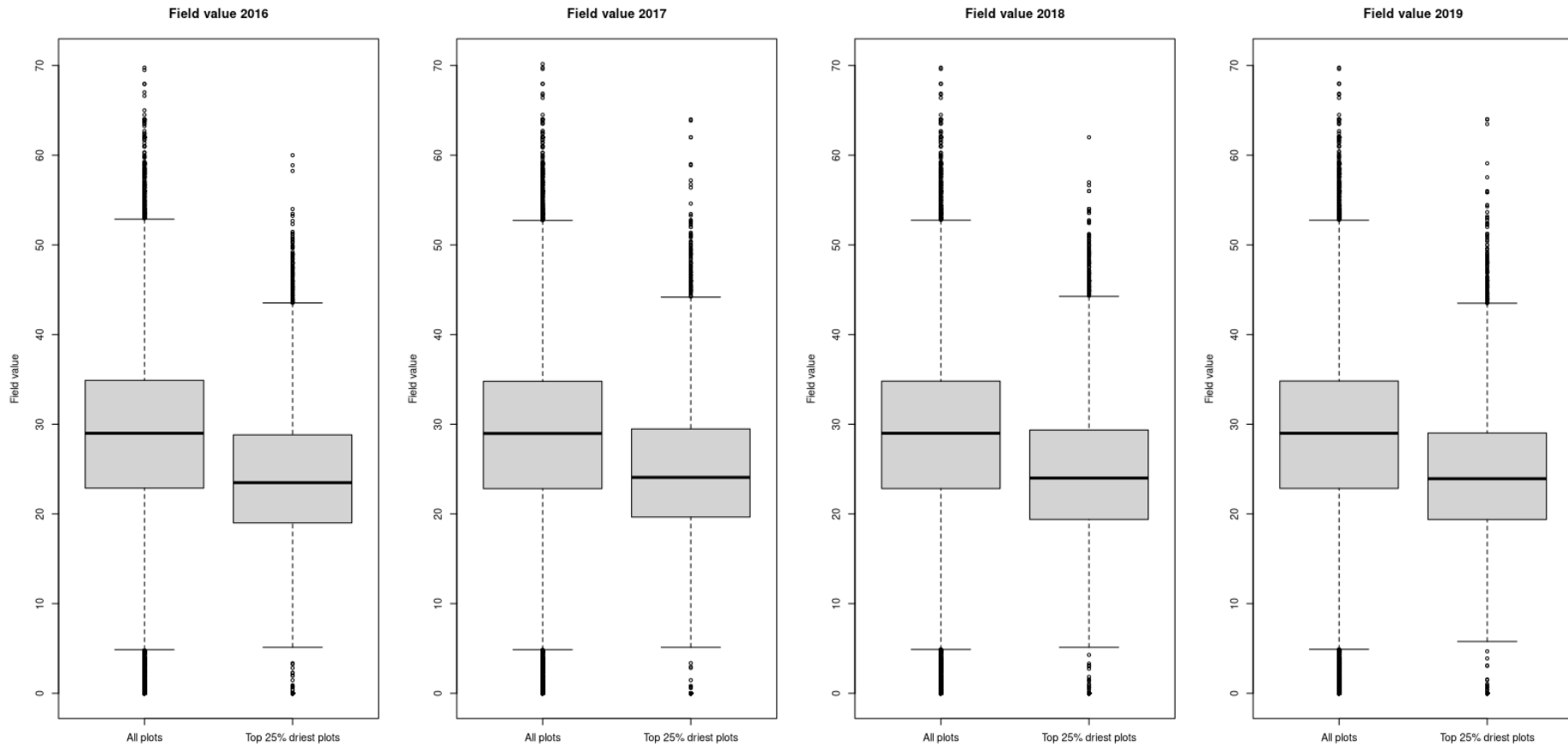


**Figure 15** Boxplots of field values across all plots (respectively left) and the plots with LST/NDVI ratios in the upper quartile thereof in the given year (respectively right), for 2016-2019 (left to right)

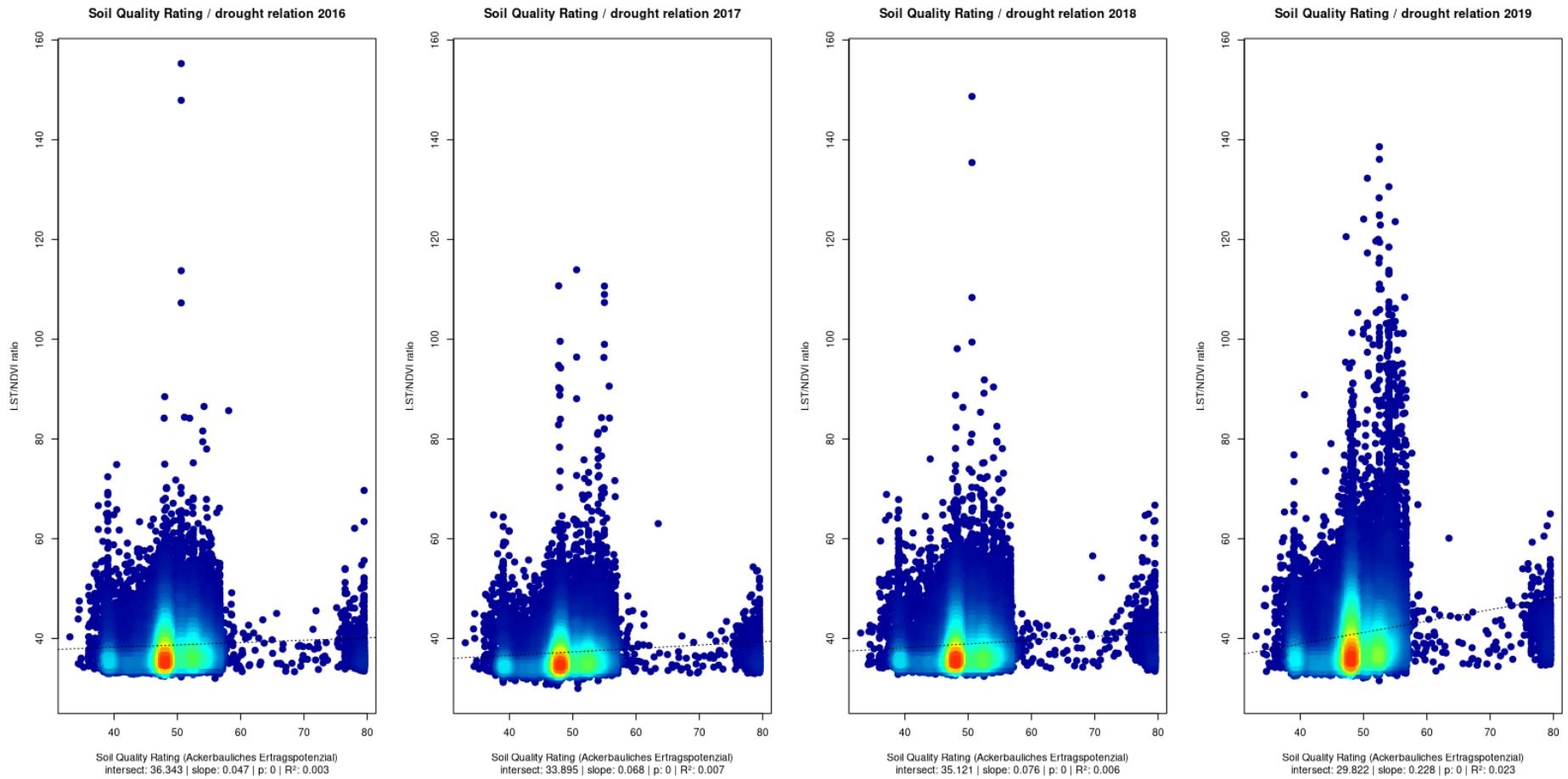


**Figure 16** Soil Quality Rating / drought relation in 2016-2019 (left to right), colours indicating point density ranging from blue (low) via green (medium) to red (high)

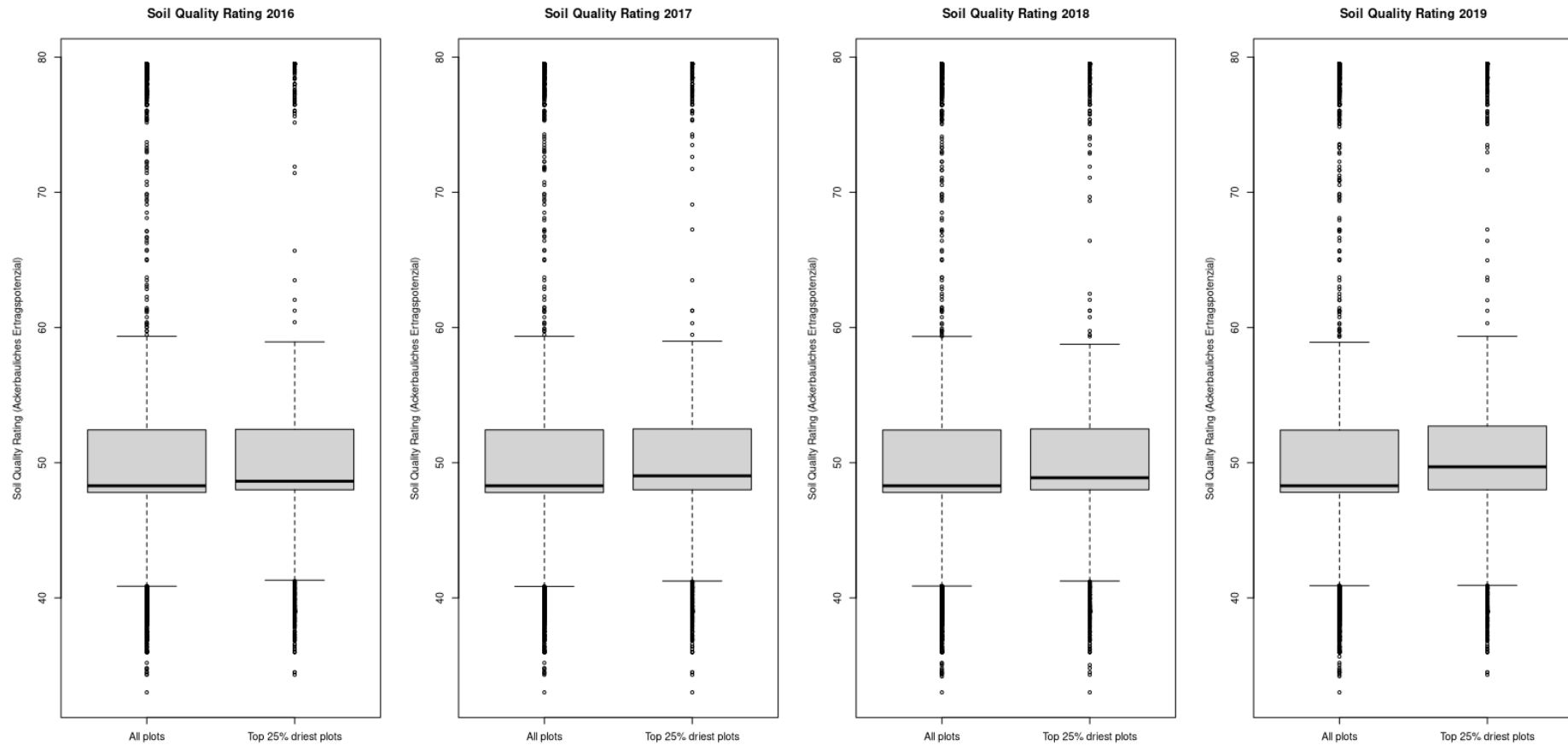


**Figure 17** Boxplots of SQR scores across all plots (respectively left) and the plots with LST/NDVI ratios in the upper quartile thereof in the given year (respectively right), for 2016-2019 (left to right)

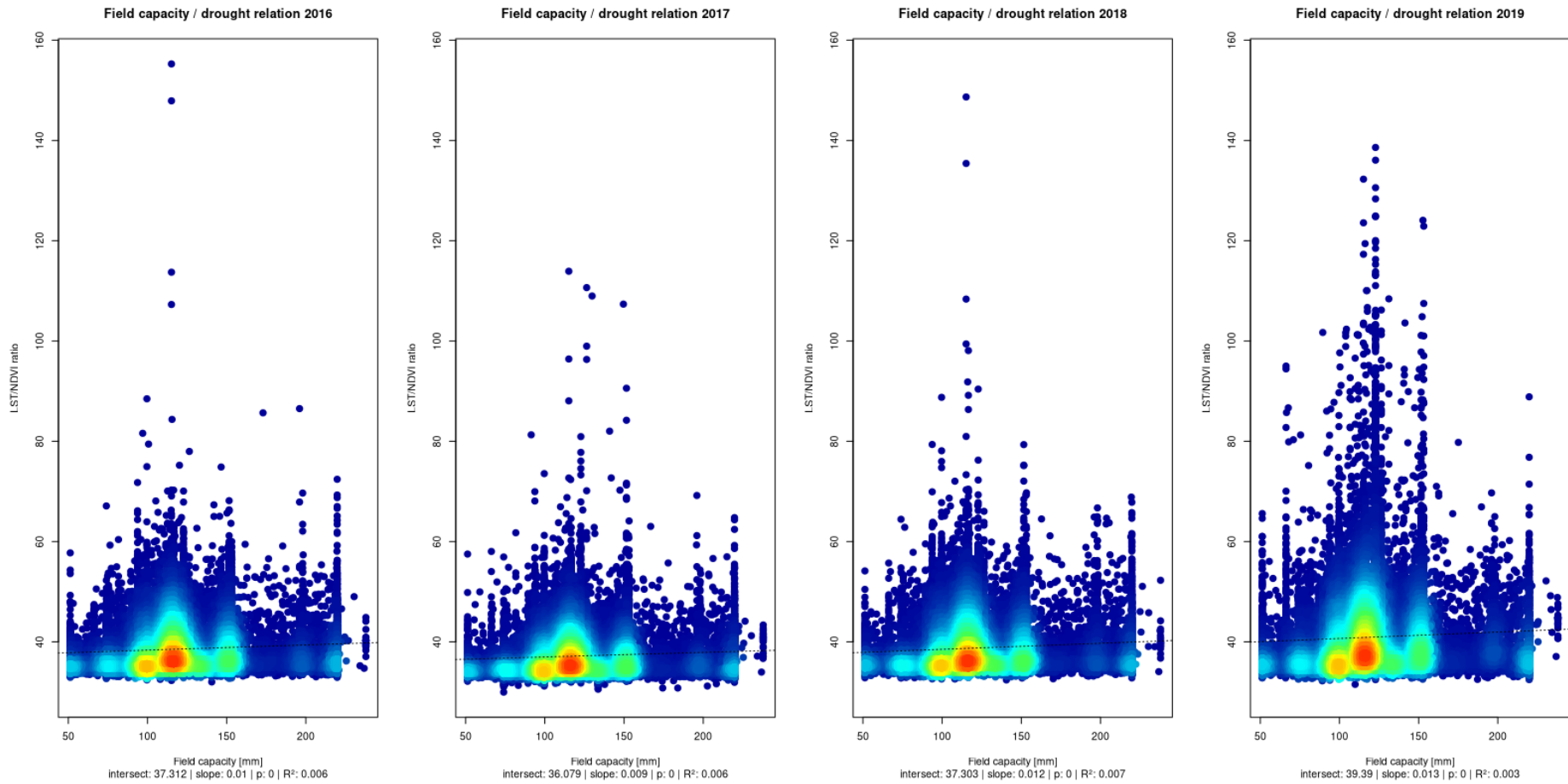


**Figure 18** Field capacity / drought relation in 2016-2019 (left to right), colours indicating point density ranging from blue (low) via green (medium) to red (high)

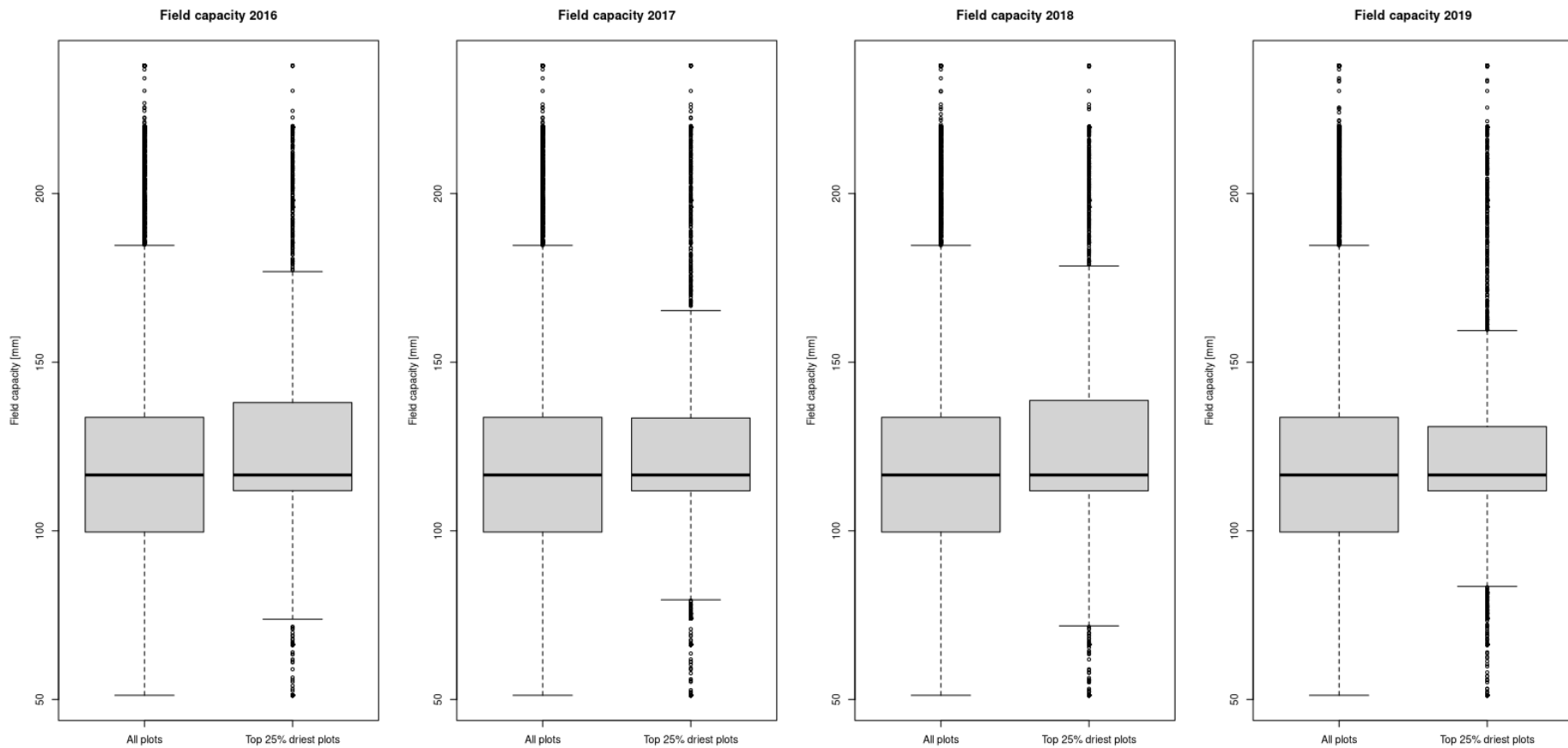


**Figure 19** Boxplots of field capacity across all plots (respectively left) and the plots with LST/NDVI ratios in the upper quartile thereof in the given year (respectively right), for 2016-2019 (left to right)

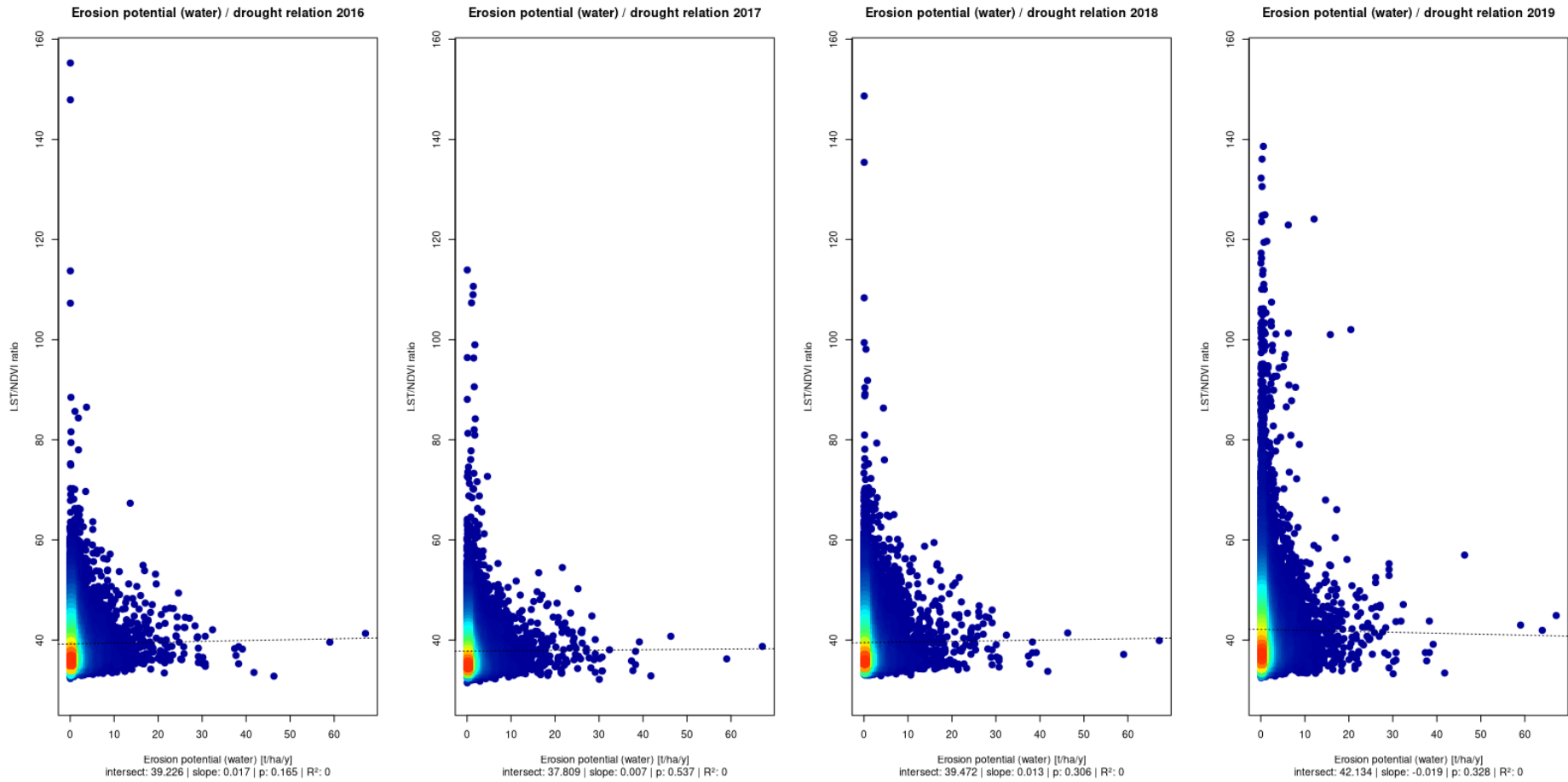


**Figure 20** Potential erosion (water) / drought relation in 2016-2019 (left to right), colours indicating point density ranging from blue (low) via green (medium) to red (high)



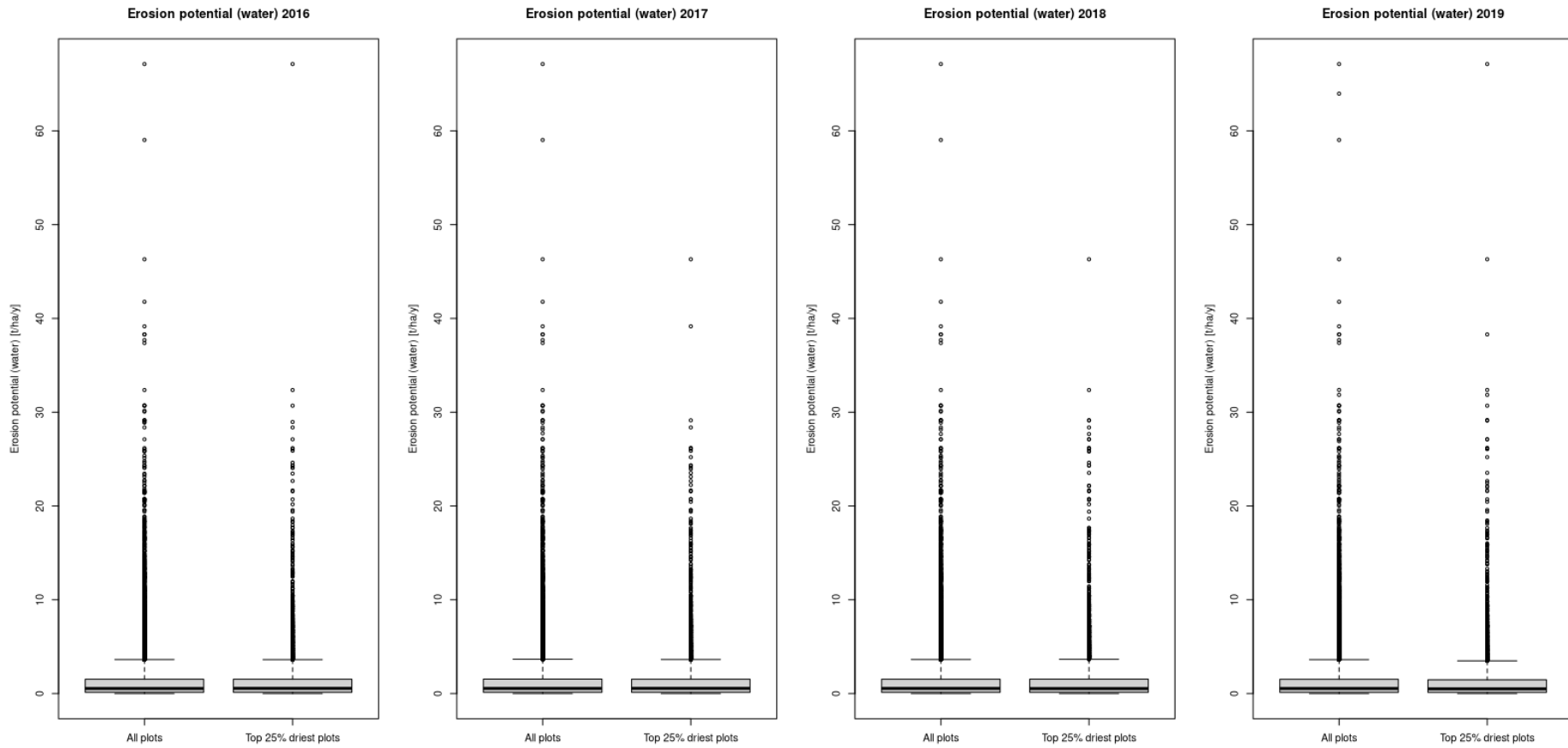


**Figure 21** Boxplots of potential erosion (water) across all plots (respectively left) and the plots with LST/NDVI ratios in the upper quartile thereof in the given year (respectively right), for 2016-2019 (left to right)

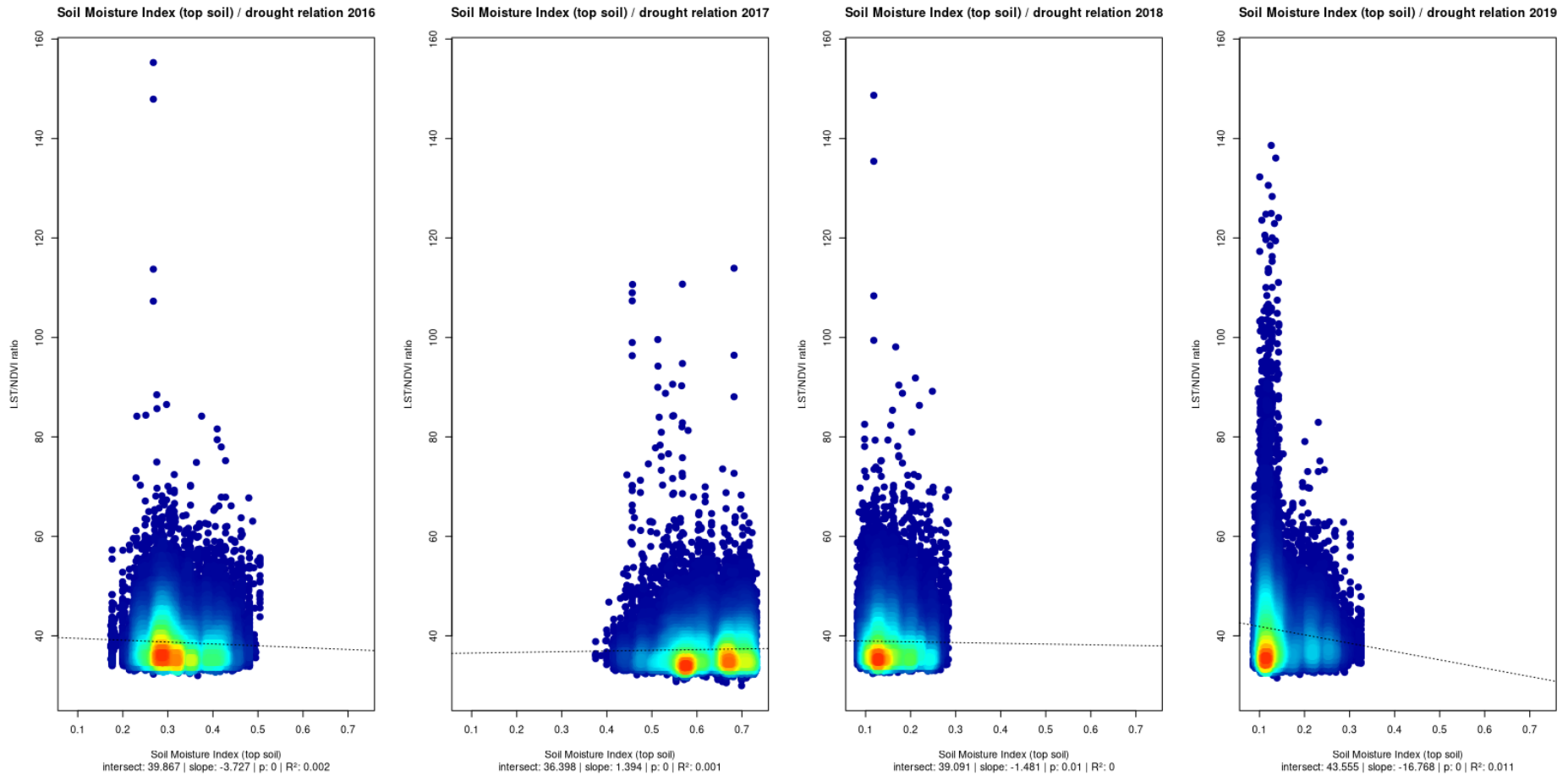


**Figure 22** Soil Moisture Index (top soil) / drought relation in 2016-2019 (left to right), colours indicating point density ranging from blue (low) via green (medium) to red (high)

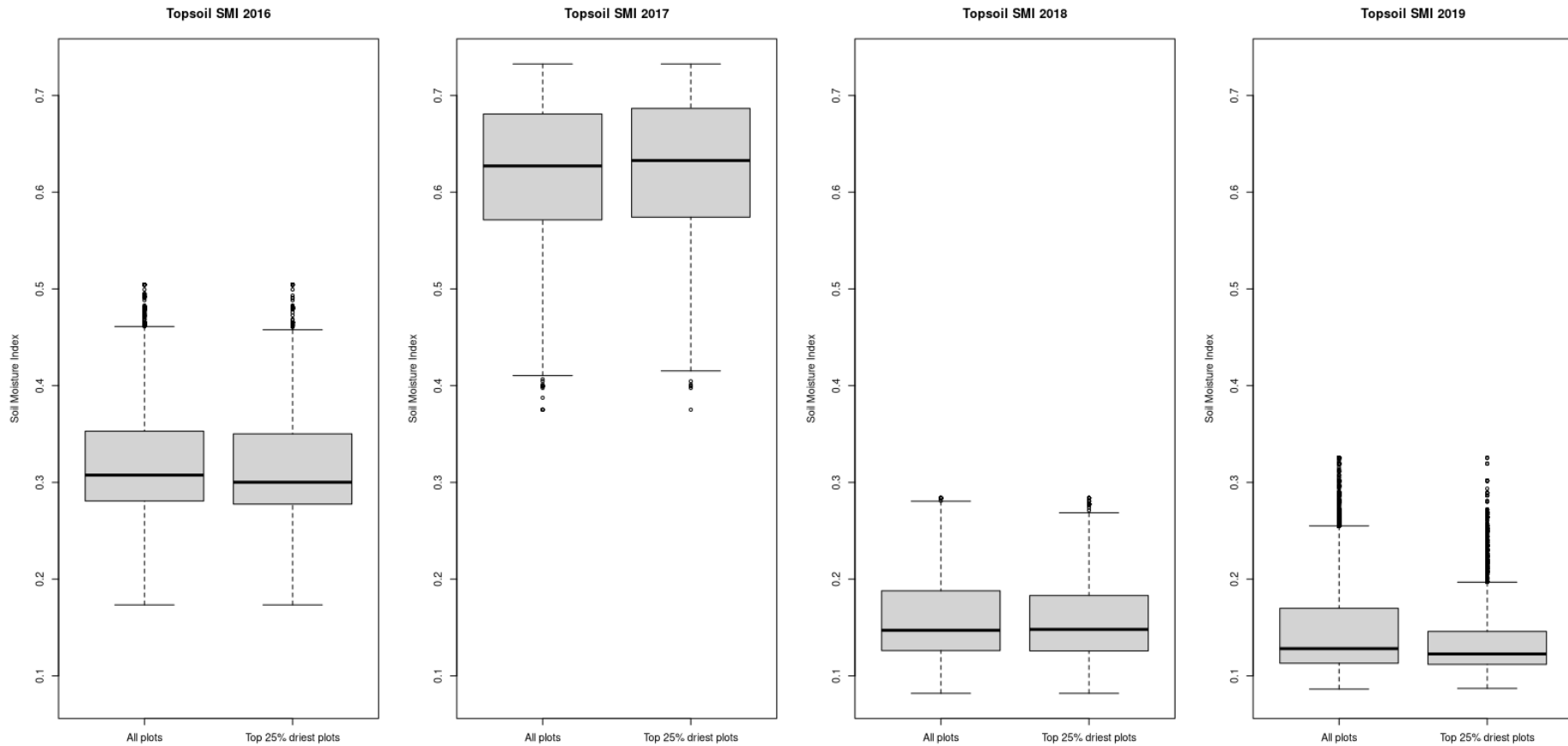


**Figure 23** Boxplots of topsoil Soil Moisture Index across all plots (respectively left) and the plots with LST/NDVI ratios in the upper quartile thereof in the given year (respectively right), for 2016-2019 (left to right)

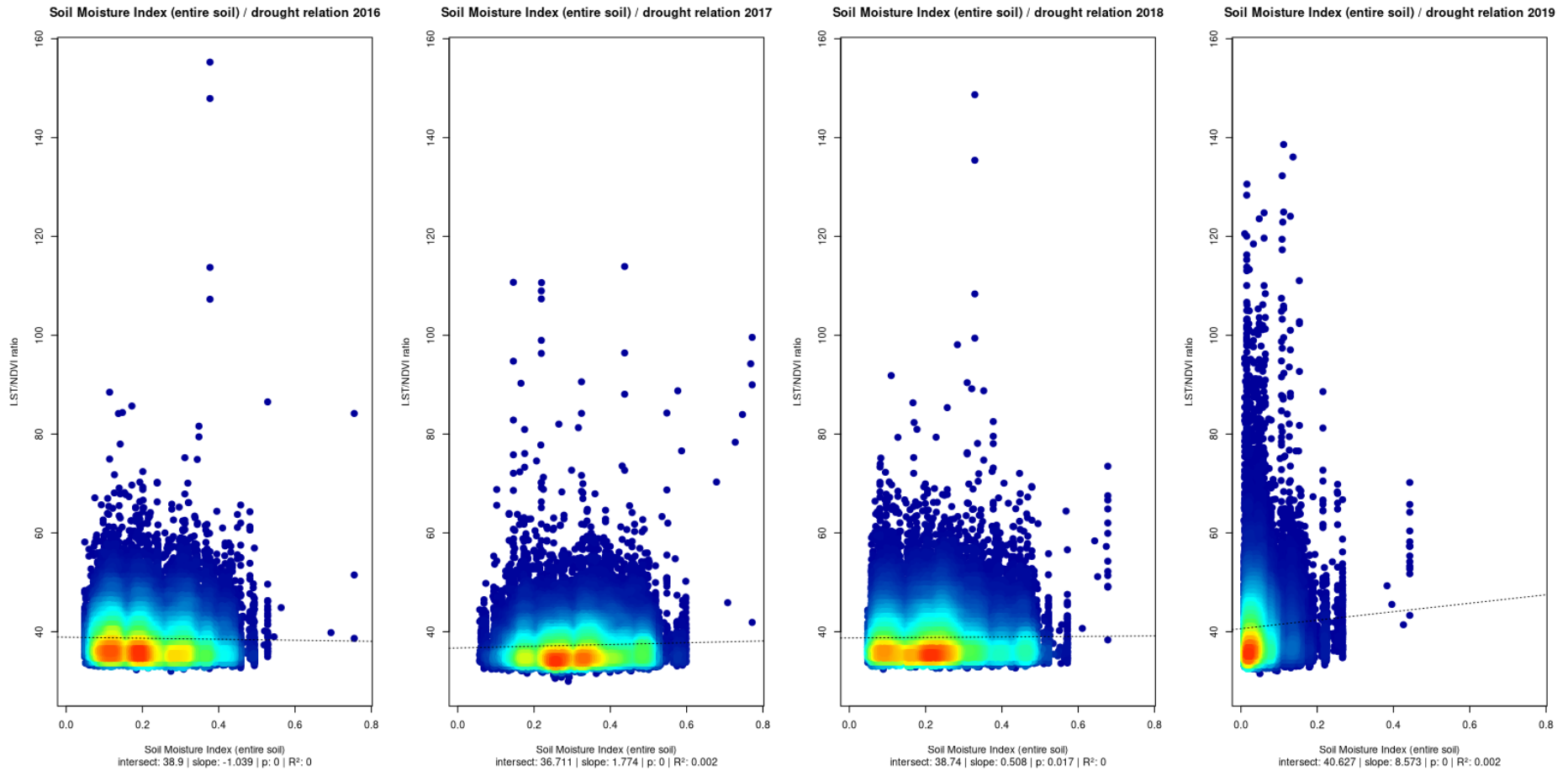


**Figure 24** Soil Moisture Index (entire soil) / drought relation in 2016-2019 (left to right), colours indicating point density ranging from blue (low) via green (medium) to red (high)

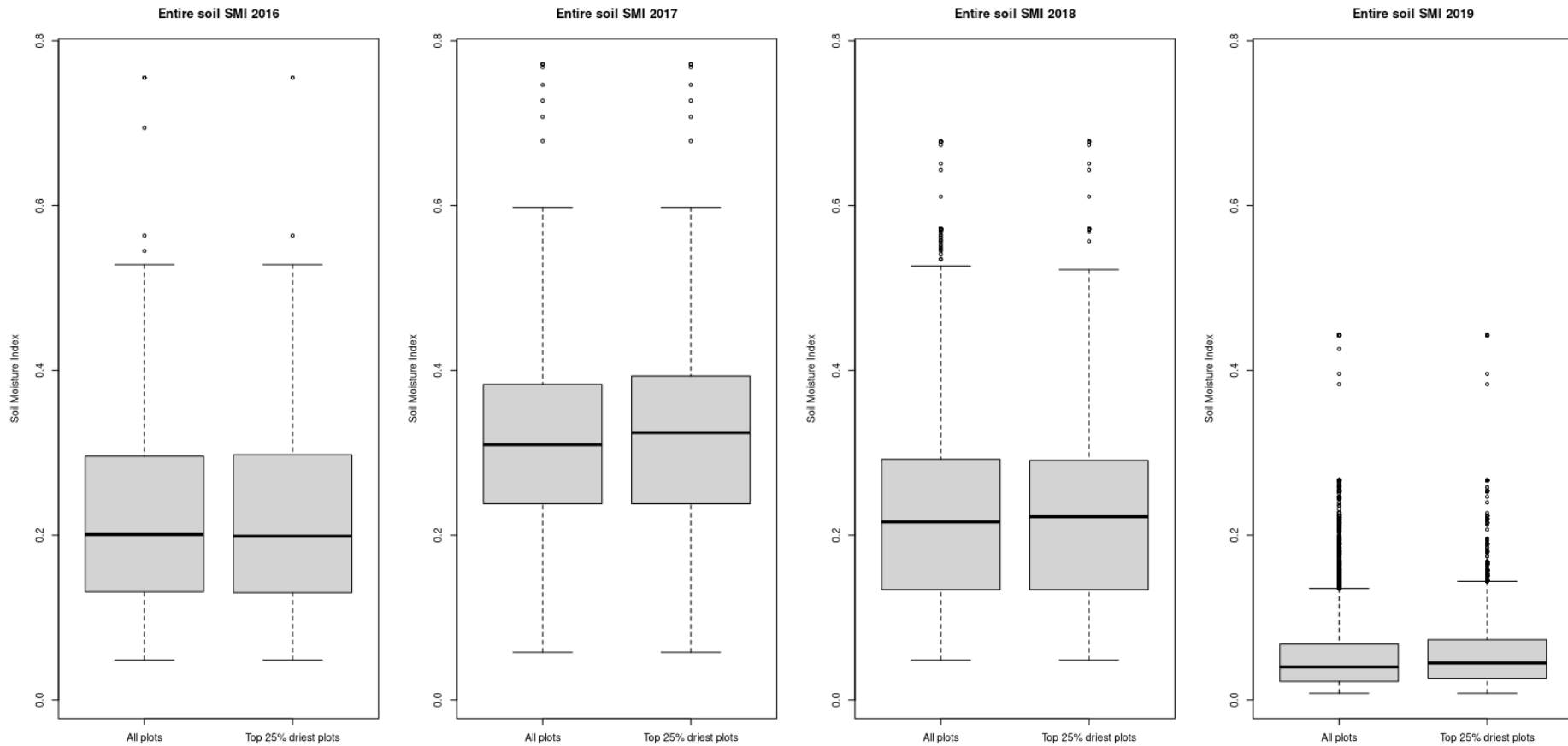


**Figure 25** Boxplots of entire soil Soil Moisture Index across all plots (respectively left) and the plots with LST/NDVI ratios in the upper quartile thereof in the given year (respectively right), for 2016-2019 (left to right)

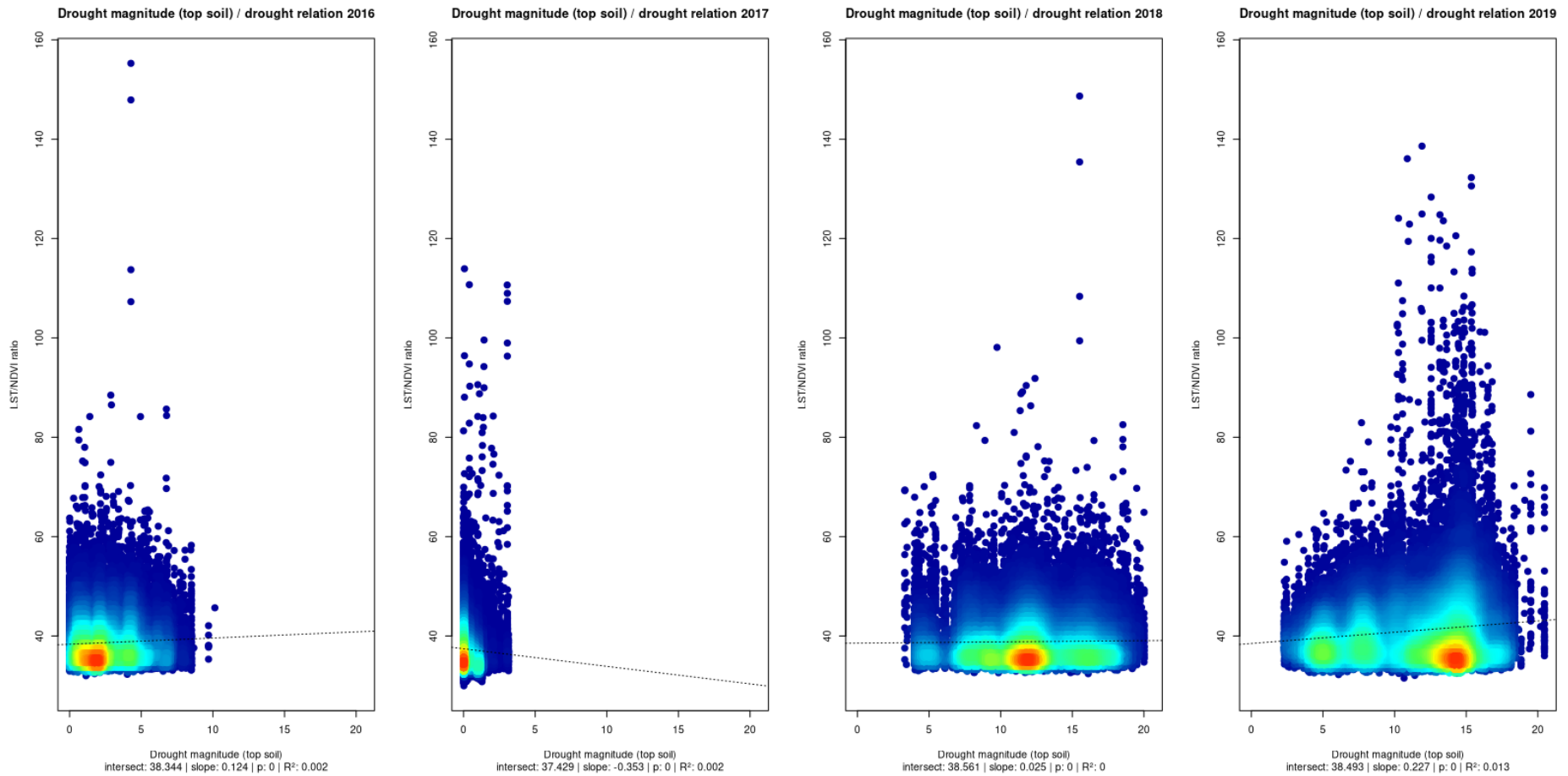


**Figure 26** Drought Magnitude (top soil) / drought relation in 2016-2019 (left to right), colours indicating point density ranging from blue (low) via green (medium) to red (high)

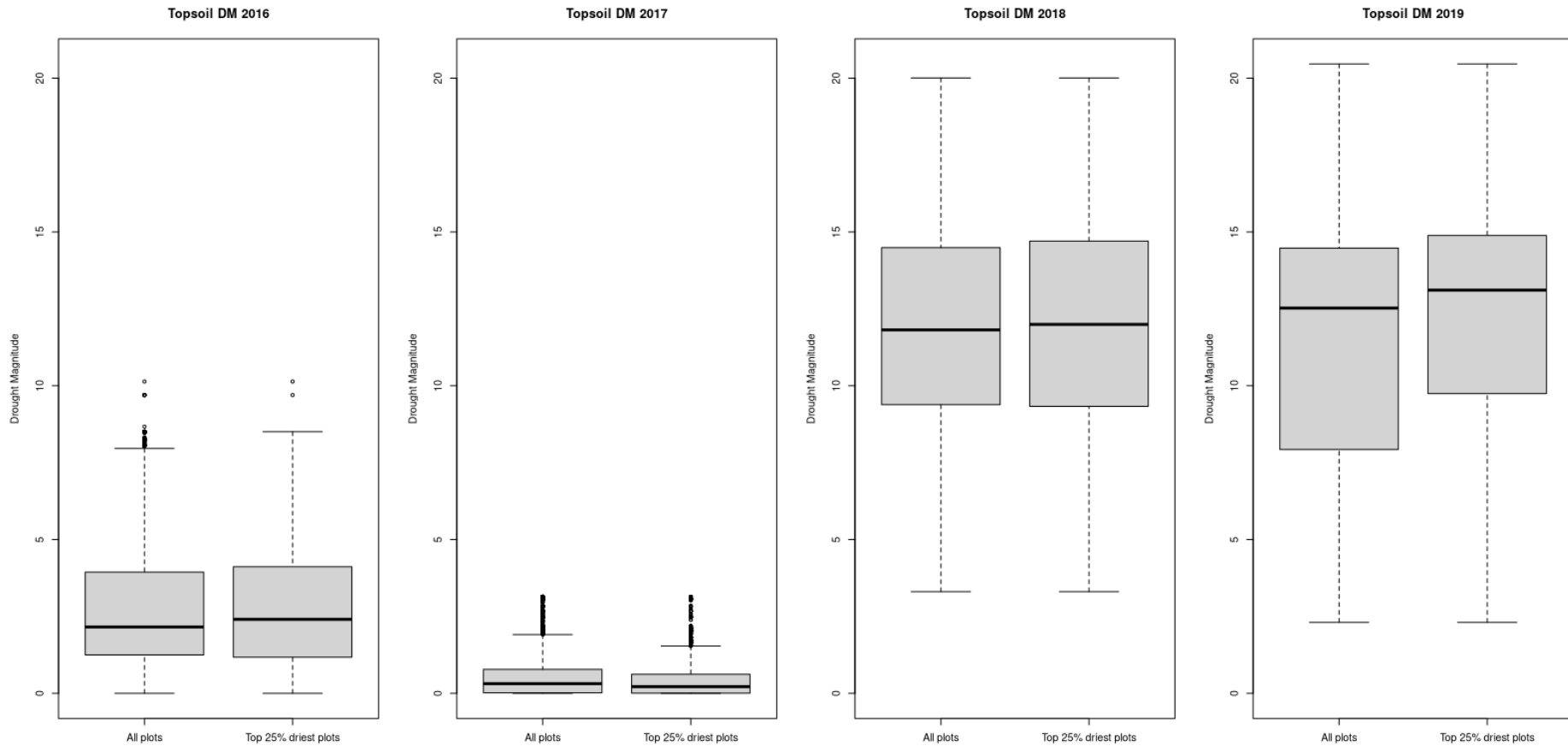


**Figure 27** Boxplots of topsoil Drought Magnitude across all plots (respectively left) and the plots with LST/NDVI ratios in the upper quartile thereof in the given year (respectively right), for 2016-2019 (left to right)

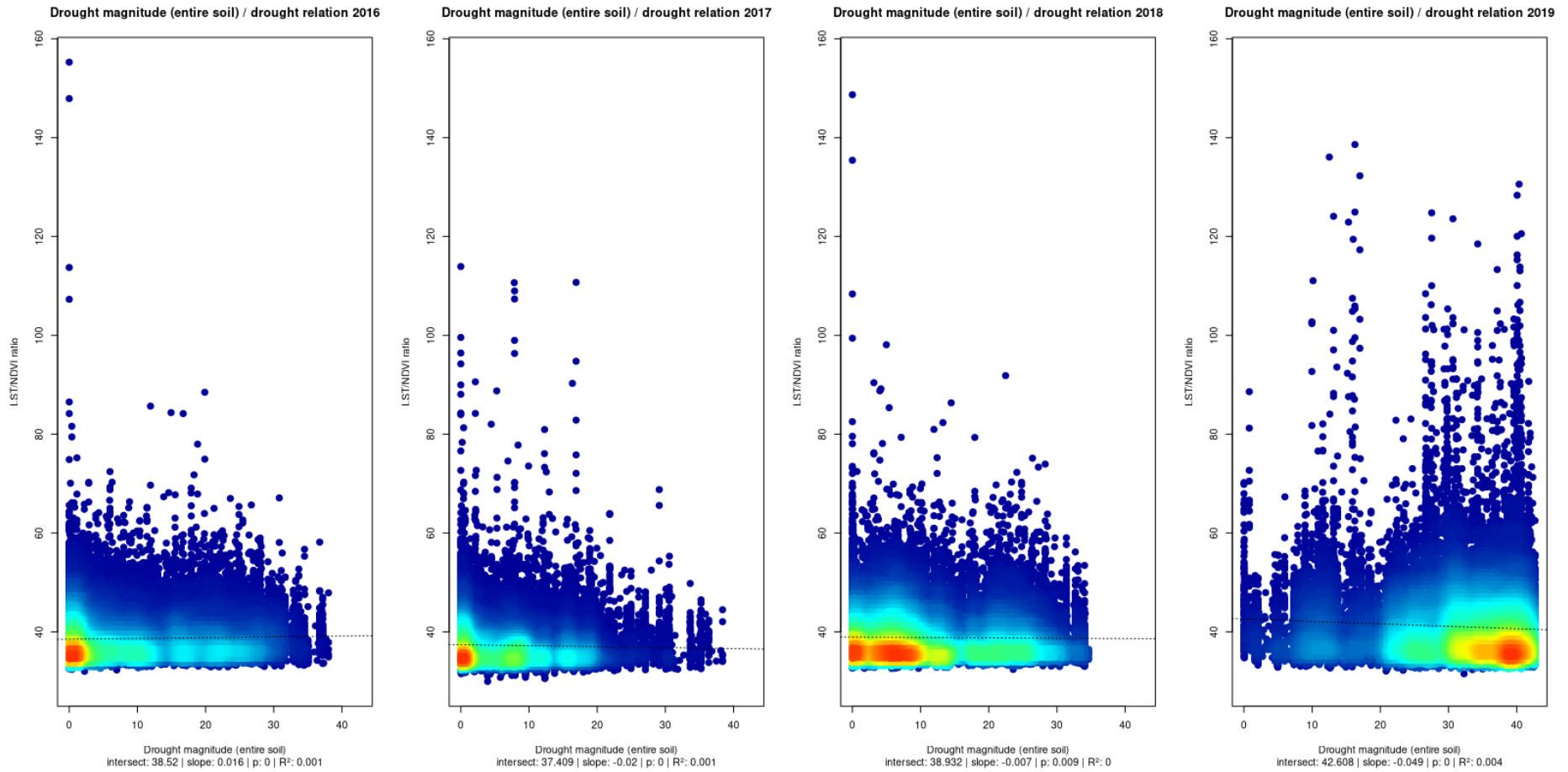


**Figure 28** Drought Magnitude (entire soil) / drought relation in 2016-2019 (left to right), colours indicating point density ranging from blue (low) via green (medium) to red (high)



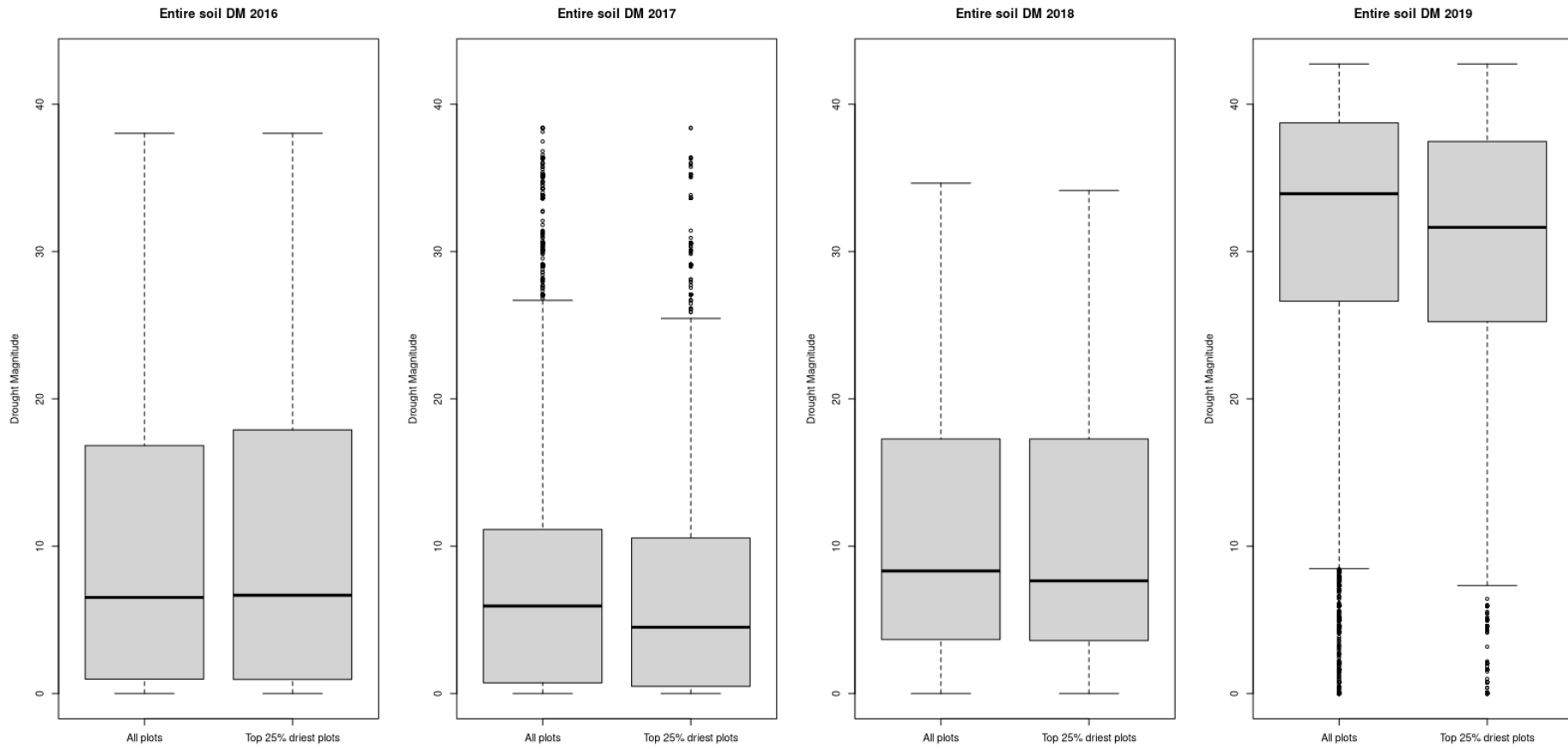


**Figure 29** Boxplots of entire soil Drought Magnitude across all plots (respectively left) and the plots with LST/NDVI ratios in the upper quartile thereof in the given year (respectively right), for 2016-2019 (left to right)

## **Code**

Google Earth Engine (Code courtesy of Dr. Fabio Brill):

<https://code.earthengine.google.com/6f5e38918abc96feb8252e10f9280da1>

Time Series Calculation: <https://box.hu-berlin.de/f/63266404edfd435ca926/?dl=1>

Extraction to IACS: <https://box.hu-berlin.de/f/c056c97fb2fb497f9208/?dl=1>

Visualisation: <https://box.hu-berlin.de/f/1f84221f130f47bda69b/?dl=1>

Multivariate Linear Regression: <https://box.hu-berlin.de/f/c9214c96e1ff4c13809d/?dl=1>

Categorical Analysis: <https://box.hu-berlin.de/f/b178e3c4a47845f2939e/?dl=1>